UNIVERSIDADE ESTADUAL PAULISTA
"JÚLIO DE MESQUITA FILHO"
CAMPUS DE BOTUCATU – INSTITUTO DE BIOCIÊNCIAS

BIOSUSCEPTOMETRIA DE CORRENTE ALTERNADA APLICADA AO TRATO GASTRINTESTINAL: GASTRECTOMIA VERTICAL, IMAGENS E PROBLEMA INVERSO

LEONARDO ANTONIO PINTO

Botucatu
2021

UNIVERSIDADE ESTADUAL PAULISTA
"JÚLIO DE MESQUITA FILHO"
CAMPUS DE BOTUCATU – INSTITUTO DE BIOCIÊNCIAS

BIOSUSCEPTOMETRIA DE CORRENTE ALTERNADA APLICADA AO TRATO GASTRINTESTINAL: GASTRECTOMIA VERTICAL, IMAGENS E PROBLEMA INVERSO

LEONARDO ANTONIO PINTO

Orientador: Prof. Dr. José Ricardo de Arruda Miranda

Coorientador: Dr. André Gonçalves Próspero

Tese de doutorado apresentada ao Instituto de Biociências, Universidade Estadual Paulista "Júlio de Mesquita Filho", Câmpus de Botucatu para obtenção do título de Doutor em Farmacologia e Biotecnologia.

Botucatu
2021

FICHA CATALOGRÁFICA ELABORADA PELA SEÇÃO TÉC. AQUIS. TRATAMENTO DA INFORM.
DIVISÃO TÉCNICA DE BIBLIOTECA E DOCUMENTAÇÃO - CÂMPUS DE BOTUCATU - UNESP

BIBLIOTECÁRIA RESPONSÁVEL: ROSEMEIRE APARECIDA VICENTE-CRB 8/5651

Pinto, Leonardo Antonio.
Biosusceptometria de corrente alternada aplicada ao trato gastrintestinal : gastrectomia vertical, imagens e problema inverso / Leonardo Antonio Pinto. - Botucatu, 2021

Tese (doutorado) - Universidade Estadual Paulista "Júlio de Mesquita Filho", Instituto de Biociências de Botucatu
Orientador: José Ricardo de Arruda Miranda
Coorientador: André Gonçalves Próspero
Capes: 20903006

1. Biosusceptometria de corrente alternada. 2. Sistema gastrointestinal - Motilidade. 3. Nanopartículas. 4. Trânsito gastrointestinal.

Palavras-chave: Motilidade gastrintestinal; Nanopartículas magnéticas; Técnicas magnéticas; Trânsito intestinal.

AGRADECIMENTOS

Agradeço em primeiro lugar aos meus pais, Luiz Antonio Pinto e Ana Lúcia Gaiotto Pinto, por sempre terem apoiado minhas decisões, e por todos os valores transmitidos com amor e carinho. Sem o apoio e a ajuda de vocês eu nada seria, e é o amor de vocês que me motiva a sempre querer chegar mais longe. Agradeço também à toda minha família, por me dar forças e servir de exemplo para seguir em frente, mesmo em momentos difíceis.

À minha companheira Gabriela Nogueira Bittencourt, que me acompanha há quase quatro anos em todos os momentos da minha vida, por ser meu porto seguro em momentos difíceis e um exemplo de pessoa com valores incríveis. Agradeço também à sua família, em especial à Edna Ramos Nogueira Bittencourt e Elson Bittencourt, que me acolheram como parte de sua família.

Ao professor José Ricardo de Arruda Miranda, meu orientador, que através do seu conhecimento e dedicação sempre me mostrou as melhores oportunidades e caminhos a serem tomados, além de todos os valores transmitidos durante todo meu período como seu aluno. Agradeço por me fazer acreditar ser capaz de realizar sonhos, e me proporcionar uma série de oportunidades na carreira acadêmica, como meu período de doutorado sanduíche no exterior, o qual sem sua ajuda não teria sido possível. Além de um pesquisador e professor brilhante, seu modo de trabalhar com pessoas é inspirador.

À todos os integrantes do Laboratório de Biomagnetismo por todo o crescimento profissional e pessoal que me proporcionaram. Agradeço especialmente ao Dr. André Gonçalves Próspero e ao Dr. Marcos Felipe Calabresi, os quais levo como mentores tanto na vida acadêmica quanto profissional.

Agradeço à Universidade Estadual Paulista "Júlio de Mesquita Filho", ao Instituto de Biociências, ao Departamento de Biofísica e Farmacologia e todos os professores, pela infraestrutura, formação e todas as oportunidades.

Aos pesquisadores do Physikalisch-Technische Bundesanstalt e grandes amigos, em especial Dr. Frank Wiekhorst, Dr. Maik Liebl e Patricia Radon, que me receberam de braços abertos na Alemanha e me proporcionaram meses de um incrível crescimento profissional e pessoal.

Aos meus amigos, Guilherme Augusto Soares, Lucas Faconi, João Victor Carneiro Faria, Gustavo Serafim Rodrigues, Davi Santos Souza, Roberto Galante, Erick Stoppa, Gabriel Serafim e Thamara Coelho e Gustavo Morlin Moretto pela convivência, grande amizade e todos os momentos compartilhados. Cada qual com seu momento de maior proximidade, mas todos grandes amigos que irei levar para o resto da vida.

Agradeço a todos da república Bagudos, a qual tive o prazer de morar durante meus oitos anos em Botucatu. Devo à Bagudos muitos ensinamentos e momentos que me fizeram ser quem eu sou. Serei eternamente grato por ter sido moldado pelos valores da república, além de poder transmitir valores íntegros para os ingressantes. Agradeço em especial aos membros que me acolheram quando cheguei em Botucatu: Nilo Martin, Marcos Felipe Calabresi, André Gonçalves Próspero, Guilherme Martelini, Gustavo Morlin Moretto, Bruno Brenga, Fernando Bacchim, Guilherme Giacomini e Fábio Perez.

Além disso, agradeço a todos os membros da república Jagdcorps Masovia zu Berlin, que apesar do choque cultural de início, me acolheram de braços abertos. Tenho orgulho de fazer parte da história centenária da república e da amizade de vocês. Em especial, agradeço à Ingo Grebe, Philipp Dehn, Carl Hagemeier, Hendrik Heimbruch, Ferdinand Gopfert, Dan Trölitzsch, Lucas Wiehofsky, Maximilian Brosche, Thibaut Mohr, Caro Westphal e Bennet Westphal.

O presente trabalho foi realizado com apoio da Coordenação de Aperfeiçoamento de Pessoal de Nível Superior - Brasil (CAPES) - Código de Financiamento 001.

RESUMO

A proposta deste trabalho consiste na aplicação da técnica de Biosusceptometria de Corrente Alternada (BAC) associada ao trato gastrintestinal, com o intuito de estabelecer uma nova metodologia que possibilite estudos do efeito de doenças e alterações fisiológicas na motilidade gastrintestinal. Foram realizados experimentos com ratos para a avaliação dos efeitos da cirurgia de gastrectomia vertical na motilidade gastrintestinal, e, de forma inédita, analisar o trânsito gastrintestinal regional através de imagens obtidas com o sistema BAC. Além disso, este trabalho apresenta a implementação de modelos matemáticos e computacionais para a resolução do problema inverso dos sistemas BAC mono e multi canal para reconstruções quantitativas de distribuições 2D de nanopartículas magnéticas (MNPs). No estudo da gastrectomia vertical, avaliamos os efeitos do procedimento cirúrgico na motilidade gastrintestinal (esvaziamento gástrico, trânsito orocecal e contratilidade gástrica), parâmetros nutricionais, morfometria e histopatologia do estômago, perfil lipídico e percentual de gordura. O trabalho acerca do trânsito gastrintestinal regional através de imagens é uma aplicação inédita da técnica BAC para a avaliação de parâmetros gastrintestinais em ratos através do escaneamento de amostras, fato que permite a análise da distribuição intrasegmentar de traçadores magnéticos. A metodologia proposta foi validada com a técnica de vermelho de fenol, considerada padrão ouro em ratos. Por fim, a resolução do problema inverso para sistemas BAC contendo uma e múltiplas bobinas detectoras é aplicada para reconstruir imagens quantitativas de fantomas contendo MNPs. As imagens quantitativas apresentam os pixels na unidade de massa de nanopartículas, possibilitando o uso da técnica BAC em diversas aplicações biomédicas envolvendo o uso de MNPs e também para o estudo do trato gastrintestinal. Os resultados desse trabalho demonstram a aplicação da técnica BAC para o estudo do trato gastrintestinal através de distintas metodologias, o que proporcionará o desenvolvimento de trabalhos inovadores nas áreas de motilidade gastrintestinal, engenharia biomédica e nanopartículas magnéticas.

ABSTRACT

This work consists in the application of the Alternate Current Biosusceptometry (ACB) technique associated with the gastrointestinal tract, aiming to establish a new tool to study the effects of diseases and physiological alterations in gastrointestinal motility. We performed studies to evaluate the effects of sleeve gastrectomy in gastrointestinal motility and a novel ACB application to assess the regional gastrointestinal transit through images. Also, this study presents the implementation of mathematical and computational models to solve the inverse problems of the single and multi-channel ACB systems to reconstruct quantitative images of 2D distributions of magnetic nanoparticles (MNPs). In the sleeve gastrectomy study, we assessed the effects of the surgical procedure in gastrointestinal motility (gastric emptying, orocecal transit, and gastric contractility), nutritional parameters, gastric morphometry and histopathology, lipid profile, and adiposity index. The study regarding regional gastrointestinal transit through images is a novel application of the ACB system to evaluate gastrointestinal parameters in rats through the scanning of samples, which enables an intrasegmental analysis of magnetic tracers. The proposed methodology was validated with phenol red, considered the gold standard technique to assess gastrointestinal transit in rats. We also solved the inverse problem for ACB systems containing one and multiple detection coils to reconstruct quantitative images of phantoms containing MNPs. The quantitative images result in pixels intensity in MNPs mass, which enables the application of the ACB technique for several biomedical applications, and also for the study of the gastrointestinal tract. Our results show the application of ACB to study gastrointestinal transit through distinct methodologies, which will enable the development of future studies in the area of gastrointestinal motility, biomedical engineering, and MNPs.

Sumário

Capítulo 1

Introdução geral

Revisão de Literatura

A motilidade gástrica é essencial para que o processamento e o esvaziamento de refeições ingeridas ocorram adequadamente. Em humanos, a região anatômica do fundo e do corpo proximal do estômago atuam como reservatório, proporcionando o processo de acomodação gástrica. Enquanto que as regiões de corpo distal e do antro proximal são responsáveis pelas contrações fásicas, misturando os alimentos ingeridos, o antro distal e o esfíncter pilórico possuem a função de triturar e filtrar os alimentos [1, 2].

A acomodação gástrica consiste em um reflexo pós-prandial que controla o tônus do estômago, de maneira que o aumento do volume gástrico proveniente da ingestão de alimentos não resulta em um aumento da pressão intragástrica [3]. O reflexo da acomodação possui dois componentes: a relaxação receptiva e a relaxação adaptativa. A relaxação receptiva ocorre alguns segundos após a ingestão do alimento, e é provocada pela estimulação orofaríngea e gástrica, tendo como resultado, a relaxação do esfíncter esofágico inferior e do estômago proximal. A relaxação adaptativa é um processo mais lento, o qual é iniciado pela distensão gástrica e duodenal, além de ser modulada por macronutrientes, volume ingerido e densidade calórica [4, 5]. O reflexo da acomodação é mediado pelo nervo vago [6] e pela ativação de mecanorreceptores e quimiorreceptores localizados no estômago e no duodeno [7].

O esvaziamento gástrico reflete uma coordenação motora entre o fundo, corpo, antro, piloro e o duodeno [8, 9]. Tal coordenação é regulada pela atividade elétrica do trato gastrintestinal (GI) através das células intersticiais de Cajal (ICCs) e do sistema nervoso entérico [2]. As ICCs são células marcapasso localizadas em maior densidade na grande curvatura do estômago, gerar as ondas lentas (do inglês *slow waves*) [10]. Os picos de atividade das ondas lentas dão início as contrações mecânicas do estômago, de maneira que a frequência de contração mecânica é modulada pela frequência das ondas lentas. Contrações gástricas iniciadas no antro (fásicas), de aproximadamente 3 ciclos por minutos em humanos, são responsáveis por triturar os alimentos ingeridos em partículas menores (entre 2 e 3 mm), para que atinjam um tamanho apropriado para serem esvaziadas através do piloro e digeridas no intestino [11]. Enquanto os líquidos são esvaziados do estômago em um perfil mono exponencial, pelo fato de depender apenas do gradiente de pressão entre estômago e duodeno, as partículas

sólidas necessitam atingir um tamanho específico para que sejam esvaziadas [8]. O tempo entre a ingestão do alimento até o início do esvaziamento gástrico de sólidos é definido como lag-phase, o qual inclui o tempo de acomodação e o início da trituração dos alimentos [12]. A regulação da taxa de esvaziamento gástrico é determinante para a digestão e absorção de nutrientes, a qual é alcançada através do intestino por uma variedade de hormônios. Enquanto que um esvaziamento gástrico retardado pode resultar em hipoglicemia, uma condição de hiperglicemia pode ser alcançada por um esvaziamento gástrico acelerado [1].

De maneira geral, distúrbios não apenas no funcionamento do estômago, mas da motilidade GI em si, como gastroparesia, dispepsia, síndrome do intestino irritável e constipação, afetam um grande número da população mundial, resultando em impactos na qualidade de vida e em um custo considerável para os sistemas de saúde [13]. Como resultado, a avaliação da motilidade GI é de extrema importância tanto na clínica quanto em laboratórios de pesquisa. Atualmente existem inúmeras metodologias que possibilitam o estudo de processos como o esvaziamento e a contratilidade gástrica [14], as quais são baseadas em princípios físicos distintos para a obtenção de seus resultados, apresentando vantagens e desvantagens de acordo com a aplicação proposta.

A cintilografia é a técnica considerada padrão ouro para a análise da motilidade gástrica em humanos, possuindo protocolos bem estabelecidos para a realização de medidas de esvaziamento gástrico [15]. Essa técnica consiste na ingestão de uma refeição teste contendo um radiofármaco, sendo o mais comumente utilizado o ^{99m}Tc [16]. De acordo com a instrumentação utilizada na cintilografia, uma ou mais gama câmaras podem ser utilizadas para detectar a radiação proveniente do radiofármaco, de forma que a variação na quantidade de refeição teste no estômago possa ser analisada. Além de humanos, a cintilografia também é aplicada para a avaliação do esvaziamento gástrico em ratos [17]. Em uma medida padrão, imagens são obtidas imediatamente após a ingestão, e 1, 2, e 4 horas após a ingestão [18]. A avaliação do esvaziamento gástrico é realizada através da seleção de regiões de interesse nas imagens para segmentar o estômago, obtendo-se a porcentagem de radiofármaco presente no estômago em cada um dos tempos determinados, após a ingestão do alimento [14]. Uma vantagem das imagens de cintilografia é a possibilidade de dividir o estômago de acordo com sua anatomia ou funções fisiológicas, de modo que a distribuição intragástrica de alimentos,

a acomodação fúndica e a contratilidade gástrica possam ser avaliadas de forma simultânea. Como resultado, é possível relacionar sintomas clínicos com distúrbios no funcionamento do estômago [19]. Entretanto, o baixo índice de adesão aos protocolos estabelecidos para medidas de cintilografia, principalmente em relação a composição da refeição teste, posicionamento de pacientes, tempo de aquisição das imagens e ausência de valores de referência, contribuem para a dificuldade na padronização dos resultados em diferentes centros de medicina nuclear. Além disso, o uso de radiação ionizante e o alto custo na implementação e manutenção dos equipamentos limitam a aplicação da técnica, principalmente para fins de pesquisa.

Portanto, a utilização de técnicas não invasivas para a avaliação da motilidade gástrica mostra-se relevante. Nesse contexto, a imagem por ressonância magnética (MRI, do inglês *magnetic resonance imaging*) permite a análise do esvaziamento gástrico, do volume gástrico e da contratilidade mecânica do estômago sem o uso de radiação ionizante [20–22]. De maneira análoga a cintilografia, a medida é realizada através da administração de uma refeição teste contendo material para contraste (não radioativo), geralmente à base de gadolínio, seguido por imagens repetidas em um intervalo pré-definido. O esvaziamento gástrico é quantificado através de regiões de interesse nas imagens [23]. Para a avaliação da contratilidade gástrica, as dobras no estômago provenientes das ondas de contração são analisadas visualmente para a determinação da frequência de contração [24]. Apesar da alta qualidade das imagens de MRI em comparação a cintilografia, ainda existem poucos estudos comparativos na literatura, entretanto, a MRI possui um alto potencial para se tornar a principal técnica para estudos envolvendo a motilidade gástrica. Atualmente, a limitação da técnica é o alto custo para aquisição das imagens e manutenção dos equipamentos, além da necessidade de ambiente blindado [14].

Através de características intrínsecas que proporcionam a redução de custos e complexidade técnica em relação a cintilografia e a MRI, o teste respiratório com isótopos estáveis do carbono permite a análise do esvaziamento gástrico sem o uso de radiação ionizante em humanos a ratos [25, 26]. Testes respiratório utilizando isótopos do ^{13}C misturado em refeições sólidas ou líquidas foram validados com a cintilografia para medir o esvaziamento gástrico [27, 28]. Após a ingestão e esvaziamento gástrico da refeição teste, o isótopo estável (*e.g.*,

^{13}C-ácido octanoico), é absorvido no intestino e metabolizado, formando $^{13}CO_2$, o qual é expelido pelo pulmão durante a respiração. A diferença entre razão dos isótopos $^{13}CO_2$ e $^{14}CO_2$ detectado são utilizados para estimar a taxa de esvaziamento gástrico [29]. As principais vantagens da técnica consistem na ausência de radiação ionizante, não dependência de operadores experientes para realização das medidas, além de sua versatilidade, uma vez que amostras podem ser transportadas para análises em outros laboratórios. Entretanto, as medidas de esvaziamento gástrico podem apresentar baixa acurácia em pacientes com doenças envolvendo o trato GI, pâncreas, fígado e o sistema respiratório, uma vez que os resultados dependem da metabolização do isótopo estável [14], e portanto, resultam em uma medida indireta do processo de esvaziamento gástrico.

Outra vertente para estudos envolvendo a motilidade GI é o uso de cápsulas de motilidade wireless, uma cápsula indigestível capaz de medir o pH, pressão e temperatura através de um sensor wireless, na medida que a cápsula é transportada ao longo do trato GI [30]. Nessa técnica, o tempo de esvaziamento gástrico é detectado através da variação abrupta de pH entre o estômago e duodeno. Além disso, os perfis de pressão permitem avaliar a motilidade do estômago, intestino delgado e cólon [31]. Estudos de validação demonstraram uma correlação satisfatória com medidas de cintilografia para o esvaziamento gástrico [32]. Uma vez que, a cápsula age como um alimento indigestível, não é possível analisar a dinâmica do esvaziamento gástrico, impossibilitando a realização de estudos envolvendo doenças que alteram a distribuição intragástrica de alimentos [15].

Com exceção do teste respiratório com isótopos estáveis do carbono, as técnicas citadas possuem limitações em relação a aplicação para experimentação animal, como o alto custo e necessidade de ambientes específicos para realização das medidas. No caso de estudos pré-clínicos, envolvendo ratos e camundongos, marcadores não absorvíveis, como o vermelho de fenol e o carvão ativado são as técnicas mais indicadas. Para tal, os marcadores são misturados em uma refeição teste, e após um tempo pré-determinado, os animais são eutanasiados para a quantificação do marcador em diversos segmentos do trato GI. Na técnica do vermelho de fenol, considerada padrão ouro para estudos envolvendo o trânsito GI em animais, o trato GI é dividido em vários segmentos distintos, os quais são processados e a quantidade do marcador em cada segmento é quantificada através da espectroscopia ultravioleta [33, 34].

A técnica do carvão ativado é amplamente utilizada para análise do esvaziamento gástrico e trânsito intestinal. A medida consiste em administrar uma refeição líquida contendo o marcador, seguido pela eutanásia do animal, de modo que a distância percorrida pelo marcador no intestino é analisada visualmente [35, 36]. Entretanto, ambas as técnicas apresentam alto índice de invasividade, resultando no aumento do número de animais necessários para os estudos, além de inviabilizar medidas repetidas.

Embora técnicas como a cintilografia, MRI e cápsula de motilidade permitirem a avaliação da contratilidade gástrica, denominadas contrações fásicas, a análise do perfil de contração elétrica (ondas lentas) é essencial para se obter uma avaliação completa da motilidade gástrica. A eletrogastrografia cutânea (EGG) é a técnica padrão para tal análise, e consiste na fixação de eletrodos na região do estômago para a aquisição do sinal elétrico proveniente das ondas lentas em humanos a animais [37, 38]. O EGG permite a quantificação da frequência dominante e do perfil elétrico contrátil do estômago de maneira indireta, detectando possíveis arritmias e irregularidades do perfil elétrico [8]. Utilizando-se o EGG, disritmias da contração gástrica e alterações na amplitude de contração foram detectadas em pacientes com diabetes e diversos sintomas GI, como vômito, enjoo e náusea [16]. De maneira geral, anormalidades no perfil de sinal do EGG estão presentes em até 75% de pacientes com gastroparesia [37]. Avanços na instrumentação do EGG resultaram no desenvolvimento da técnica de mapeamento elétrico de alta resolução (do inglês *high-resolution electrical mapping*). A técnica consiste no uso simultâneo de diferentes canais para detecção, podendo conter até 192 eletrodos distintos para mapear o sinal elétrico em uma área de até 12 cm^2 [39]. Tal técnica já foi aplicada para o estudo de pacientes com gastroparesia e submetidos a cirurgias bariátricas [40, 41]. Entretanto, a técnica de mapeamento elétrico de alta resolução é utilizada somente na sala de cirurgia, uma vez que os eletrodos são posicionados diretamente sob o órgão, fato que limita sua utilização [39]. A técnica do EGG pode ser considerada como complementar a avaliação do esvaziamento gástrico em pacientes com sintomas no trato GI, entretanto, sua utilização é limitada devido a uma baixa relação sinal ruído, presença de artefatos de movimento e dificuldades na interpretação dos dados [14].

Neste contexto, a biosusceptometria de corrente alternada (BAC) apresenta-se como uma técnica alternativa para a avaliação da motilidade GI. Os princípios físicos de funciona-

mento são descritos pela lei de indução de Faraday, e em relação as técnicas citadas, a BAC possui vantagens como a ausência de radiação ionizante, portabilidade, baixo custo e não-invasividade. O sensor BAC é composto por dois pares de bobinas coaxiais separados por uma distância fixa (linha de base), de modo que cada par consiste em uma bobina de indução (externas) e outra de detecção (internas). O par de bobinas mais próximo da amostra é atua como sistema de medida, enquanto que o par mais distante atua como sistema de referência. Amplificadores *lock-in* e de potência são utilizados para gerar uma tensão alternada com fase e frequência específica, a qual é aplicada nas bobinas de indução para gerar um campo magnético alternado, que é detectado em tempo real pelas bobinas de detecção. No sensor BAC, as bobinas de detecção são conectadas em configuração gradiométrica de primeira ordem, ou seja, o sinal detectado no sistema de referência é subtraído do sinal registrado no sistema de medida, de modo que o ruído ambiental seja reduzido. A presença de materiais com uma alta susceptibilidade magnética próximo ao sistema de medida resulta em um desbalanceamento no fluxo magnético total do sistema, gerando um sinal elétrico nas bobinas de detecção que é registrado pelo amplificador *lock-in*. O sinal analógico é convertido em sinal digital através de uma placa A/D, e os sinais são armazenados em computador para processamento e análise. A figura 1 demonstra os componentes que constituem o sistema BAC.

No sistema BAC, a intensidade de sinal obtida é proporcional à quantidade de material magnético e inversamente proporcional à distância entre o sensor e o material magnético. A proporcionalidade entre a quantidade de material magnético e a intensidade de sinal permite a determinação do trânsito de traçadores magnéticos em diversos segmentos do trato GI, como estômago, intestino e ceco. Além disso, a atividade contrátil dos segmentos GI é rítmica, com ciclos de contração e relaxamento ao longo do tempo, de modo que movimentos da parede de determinados segmentos (*e.g.*, estômago e cólon), gerados por contrações musculares, alteram a distância entre o sensor e o material magnético, promovendo modulações no sinal registrado pelo sistema BAC. Tais características do sistema viabilizam medidas do trânsito GI e da contratilidade de órgãos do trato GI in vivo em humanos e animais.

Diversos estudos utilizaram a técnica BAC para a avaliação de parâmetros envolvendo o

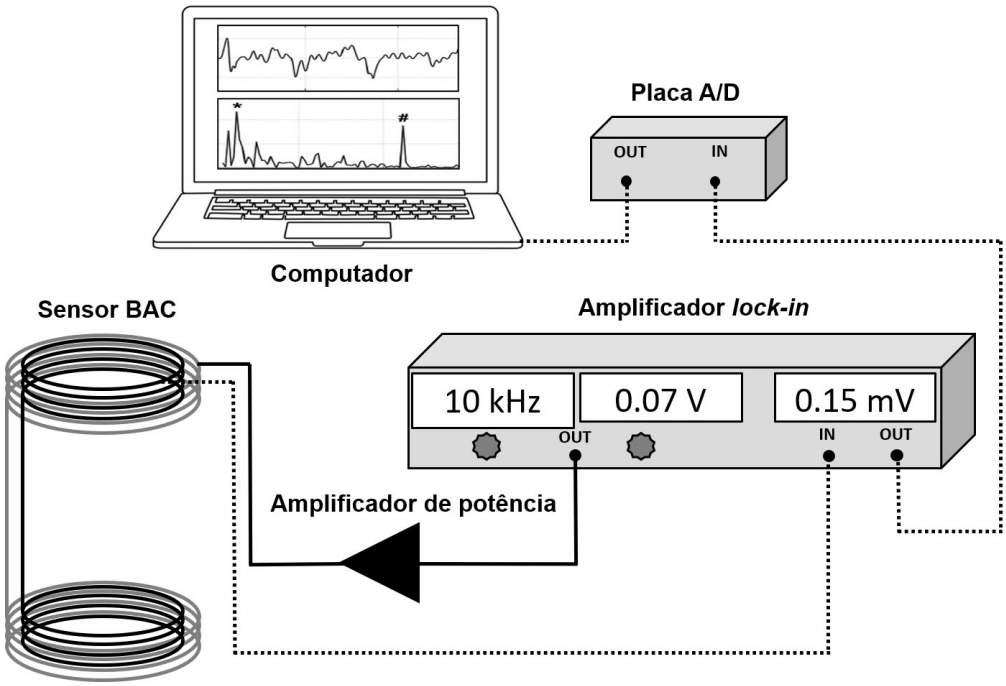

Figura 1. Componentes do sistema BAC. O amplificador *lock-in* e de potência aplicam uma tensão alternada nas bobinas de excitação (preto). A presença de materiais magnéticos gera um sinal elétrico, o qual é detectado pelas bobinas de detecção (cinza). O sinal é convertido através de uma placa A/D e armazenado em computador.

trato GI em humanos e animais, como o esvaziamento gástrico e trânsito intestinal [42–44], contratilidade gástrica e colônica [45–47], além de efeitos causados por patologias ou intervenções cirúrgicas em tais parâmetros [48, 49]. Além de aplicações envolvendo a motilidade GI, a BAC é amplamente utilizada para estudos farmacotécnicos [50, 51], apresentando-se como uma metodologia alternativa para a análise de farmacomagnetografia [52]. Em estudos envolvendo a motilidade GI e farmacotécnica, micropartículas de ferrita de manganês ($MnFe_2O_4$ - 50 a 100 μm) não absorvíveis e inertes em qualquer pH são utilizadas como marcadores ou traçadores magnéticos. Entretanto, Quini et al. [43] propôs a utilização de nanopartículas magnéticas (MNPs, do inglês *magnetic nanoparticles*) para estudar a motilidade GI de refeições líquidas. Como resultado, a técnica BAC vem sendo atualmente utilizada em estudos envolvendo a detecção de MNPs *in vivo* [53–56]. Recentemente, a técnica BAC foi aplicada de forma inédita para mapear a biodistribuição de MNPs em ratos através de imagens [57], possibilitando uma nova abordagem para estudos em animais.

Embora diversas aplicações da técnica BAC envolvam a aquisição de imagens para estudos de farmacotécnica em humanos [46, 51, 52], ainda não há relatos da utilização de imagens BAC para a avaliação da motilidade GI em animais. Até o momento, as imagens obtidas consistiam em projeções bidimensionais da intensidade do sinal adquirido, ou seja, as imagens apresentam intensidade de *pixels* correspondentes a valores de tensão, o que não possibilita a quantificação, de modo que os *pixels* da imagem possuam unidade de massa de do material magnético utilizado. Para tanto, é necessário o desenvolvimento de modelos matemáticos para aprimorar a BAC, viabilizando a reconstrução quantitativa de materiais magnéticos.

Desta forma, a presente tese de doutorado engloba a aplicação da BAC para a avaliação de parâmetros da motilidade GI em ratos, além da implementação de modelos matemáticos e computacionais para a obtenção de imagens quantitativas visando aplicações futuras na área de gastroenterologia. Primeiramente será apresentada a utilização da BAC no estudo dos efeitos causados pela cirurgia bariátrica chamada gastrectomia vertical na motilidade GI de ratos como um todo. A gastrectomia vertical é atualmente a cirurgia bariátrica mais realizada no mundo, e seus impactos na motilidade GI possuem relevância, uma vez que a anatomia do estômago é alterada de forma significativa. Além disso, estudamos de maneira inédita o trânsito GI regional ex vivo em ratos através de imagens (não quantitativas) obtidas com a técnica BAC. Os dados foram comparados com a técnica padrão ouro, o vermelho de fenol, demonstrando resultados satisfatórios e apresentando diversas vantagens, como a possibilidade de visualizar a distribuição de alimentos dentro de um segmento. Por último, o terceiro capítulo apresenta a obtenção de imagens quantitativas BAC utilizando MNPs como material magnético, além de comparar dois sistemas BAC distintos. Os resultados apresentados aqui demonstram o atual estado da arte da BAC para estudos envolvendo a gastroenterologia em ratos, o qual contempla novas aplicações para metodologias já utilizadas em nosso laboratório, além de propor a implementação de novas metodologias e desenvolvê-las para aplicações futuras.

Referências

[1] R. K. Goyal, Y. Guo, and H. Mashimo, "Advances in the physiology of gastric emptying," *Neurogastroenterology & Motility*, vol. 31, p. e13546, Feb. 2019.

[2] L. Johnson, *Encyclopedia of Gastroenterology*. Academic Press, 2004.

[3] W. B. Cannon and C. W. Lieb, "The receptive relaxation of the stomach," *American Journal of Physiology-Legacy Content*, vol. 29, pp. 267–273, Dec. 1911.

[4] N. Villanova, F. Azpiroz, and J. R. Malagelada, "Gastrogastric reflexes regulating gastric tone and their relationship to perception," *American Journal of Physiology-Gastrointestinal and Liver Physiology*, vol. 273, pp. G464–G469, Aug. 1997.

[5] T. Jahnberg, J. Martinson, L. Hultén, and S. Fasth, "Dynamic gastric response to expansion before and after vagotomy," *Scandinavian Journal of Gastroenterology*, vol. 10, pp. 593–598, Sept. 1975.

[6] S. Kindt and J. Tack, "Impaired gastric accommodation and its role in dyspepsia," *Gut*, vol. 55, pp. 1685–1691, Dec. 2006.

[7] C. Feinle, D. Grundy, and M. Fried, "Modulation of gastric distension-induced sensations by small intestinal receptors," *American Journal of Physiology-Gastrointestinal and Liver Physiology*, vol. 280, pp. G51–G57, Jan. 2001.

[8] M. Camilleri, W. L. Hasler, H. P. Parkman, E. M. Quigley, and E. Soffer, "Measurement of gastrointestinal motility in the GI laboratory," *Gastroenterology*, vol. 115, pp. 747–762, Sept. 1998.

[9] H. Parkman, A. Harris, B. Krevsky, J. Urbain, A. Maurer, and R. Fisher, "Gastroduodenal motility and dysmotility: an update on techniques available for evaluation," *The American journal of gastroenterology*, vol. 90, p. 869—892, June 1995.

[10] P. Janssen, P. V. Berghe, S. Verschueren, A. Lehmann, I. Depoortere, and J. Tack, "Review article: the role of gastric motility in the control of food intake," *Alimentary Pharmacology & Therapeutics*, vol. 33, pp. 880–894, Feb. 2011.

[11] N. Q. Nguyen, R. J. Fraser, L. K. Bryant, and R. H. Holloway, "Functional association between proximal and distal gastric motility during fasting and duodenal nutrient stimulation in humans," *Neurogastroenterology & Motility*, vol. 19, pp. 638–645, Aug. 2007.

[12] J. A. Siegel, B. Krevsky, A. H. Maurer, N. D. Charkes, R. S. Fisher, and L. S. Malmud, "Scintigraphic evaluation of gastric emptying: Are radiolabeled solids necessary?," *Clinical Nuclear Medicine*, vol. 14, pp. 40–46, Jan. 1989.

[13] V. Stanghellini, F. K. Chan, W. L. Hasler, J. R. Malagelada, H. Suzuki, J. Tack, and N. J. Talley, "Gastroduodenal disorders," *Gastroenterology*, vol. 150, pp. 1380–1392, May 2016.

[14] L. A. Szarka and M. Camilleri, "Methods for measurement of gastric motility," *American Journal of Physiology-Gastrointestinal and Liver Physiology*, vol. 296, pp. G461–G475, Mar. 2009.

[15] T. L. Abell, M. Camilleri, K. Donohoe, W. L. Hasler, H. C. Lin, A. H. Maurer, R. W. McCallum, T. Nowak, M. L. Nusynowitz, H. P. Parkman, P. Shreve, L. A. Szarka, W. J. Snape, and H. A. Ziessman, "Consensus recommendations for gastric emptying scintigraphy: A joint report of the american neurogastroenterology and motility society and the society of nuclear medicine," *Journal of Nuclear Medicine Technology*, vol. 36, pp. 44–54, Mar. 2008.

[16] H. P. Parkman, W. L. Hasler, J. L. Barnett, and E. Y. Eaker, "Electrogastrography: a document prepared by the gastric section of the american motility society clinical GI motility testing task force," *Neurogastroenterology and Motility*, vol. 15, pp. 89–102, Apr. 2003.

[17] R. J. Bennink, W. J. de Jonge, E. L. Symonds, R. M. van den Wijngaard, A. L. Spijkerboer, M. A. Benninga, and G. E. Boeckxstaens, "Validation of gastric-emptying scintigraphy of solids and liquids in mice using dedicated animal pinhole scintigraphy," *Journal of Nuclear Medicine*, vol. 44, no. 7, pp. 1099–1104, 2003.

[18] G. Tougas, E. Y. Eaker, T. L. Abell, H. Abrahamsson, M. Boivin, J. Chen, M. P. Hocking, E. M. Quigley, K. L. Koch, A. Z. Tokayer, V. Stanghellini, Y. Chen, J. D. Huizinga, J. Ryden, I. Bourgeois, and R. W. McCallum, "Assessment of gastric emptying using a low fat meal: establishment of international control values," *The American Journal of Gastroenterology*, vol. 95, pp. 1456–1462, June 2000.

[19] S. Gonlachanvit, A. H. Maurer, R. S. Fisher, and H. P. Parkman, "Regional gastric emptying abnormalities in functional dyspepsia and gastro-oesophageal reflux disease," *Neurogastroenterology and Motility*, vol. 18, pp. 894–904, Oct. 2006.

[20] P. Kunz, G. R. Crelier, W. Schwizer, J. Borovicka, C. Kreiss, M. Fried, and P. Boesiger, "Gastric emptying and motility: assessment with MR imaging–preliminary observations.," *Radiology*, vol. 207, pp. 33–40, Apr. 1998.

[21] P. Kunz, C. Feinle-Bisset, H. Faas, P. Boesiger, M. Fried, A. Steingötter, and W. Schwizer, "Effect of ingestion order of the fat component of a solid meal on intragastric fat distribution and gastric emptying assessed by MRI," *Journal of Magnetic Resonance Imaging*, vol. 21, pp. 383–390, Mar. 2005.

[22] H. Faas, G. S. Hebbard, C. Feinle, P. Kunz, J. G. Brasseur, K. Indireshkumar, J. Dent, P. Boesiger, M. Thumshirn, M. Fried, and W. Schwizer, "Pressure-geometry relationship in the antroduodenal region in humans," *American Journal of Physiology-Gastrointestinal and Liver Physiology*, vol. 281, pp. G1214–G1220, Nov. 2001.

[23] W. Schwizer, R. Fraser, J. Borovicka, G. Crelier, P. Boesiger, and M. Fried, "Measurement of gastric emptying and gastric motility by magnetic resonance imaging (MRI)," *Digestive Diseases and Sciences*, vol. 39, pp. 101S–103S, Dec. 1994.

[24] T. Baumann, S. Kuesters, J. Grueneberger, G. Marjanovic, L. Zimmermann, A.-O. Schaefer, U. T. Hopt, M. Langer, and W. K. Karcz, "Time-resolved MRI after ingestion of liquids reveals motility changes after laparoscopic sleeve gastrectomy—preliminary results," *Obesity Surgery*, vol. 21, pp. 95–101, Nov. 2010.

[25] R. Schoonjans, B. V. Vlem, N. V. Heddeghem, W. Vandamme, R. Vanholder, N. Lameire, R. Lefebvre, and M. D. Vos, "The 13c-octanoic acid breath test: validation of a new noninvasive method of measuring gastric emptying in rats," *Neurogastroenterology and Motility*, vol. 14, pp. 287–293, June 2002.

[26] S. T. Odunsi, M. Camilleri, L. A. Szarka, and A. R. Zinsmeister, "Optimizing analysis of stable isotope breath tests to estimate gastric emptying of solids," *Neurogastroenterology & Motility*, vol. 21, pp. 706–e38, July 2009.

[27] Y. F. Ghoos, B. D. Maes, B. J. Geypens, G. Mys, M. I. Hiele, P. J. Rutgeerts, and G. Vantrappen, "Measurement of gastric emptying rate of solids by means of a carbon-labeled octanoic acid breath test," *Gastroenterology*, vol. 104, pp. 1640–1647, June 1993.

[28] M.-G. Choi, M. Camilleri, D. D. Burton, A. R. Zinsmeister, L. A. Forstrom, and S. K. Nair, "Reproducibility and simplification of 13c-octanoic acid breath test for gastric emptying of solids," *American Journal of Gastroenterology*, vol. 93, pp. 92–98, Jan. 1998.

[29] M. Q. Bromer, S. B. Kantor, D. A. Wagner, L. C. Knight, A. H. Maurer, and H. P. Parkman *Digestive Diseases and Sciences*, vol. 47, no. 7, pp. 1657–1663, 2002.

[30] A. D. Farmer, S. M. Scott, and A. R. Hobson, "Gastrointestinal motility revisited: The wireless motility capsule," *United European Gastroenterology Journal*, vol. 1, pp. 413–421, Dec. 2013.

[31] M. Camilleri, A. E. Bharucha, C. di Lorenzo, W. L. Hasler, C. M. Prather, S. S. Rao, and A. Wald, "American neurogastroenterology and motility society consensus statement on intraluminal measurement of gastrointestinal and colonic motility in clinical practice," *Neurogastroenterology & Motility*, vol. 20, pp. 1269–1282, Dec. 2008.

[32] B. Kuo, R. W. McCallum, K. L. Koch, M. D. Sitrin, J. M. Wo, W. D. Chey, W. L. Hasler, J. M. Lackner, L. A. Katz, J. R. Semler, G. E. Wilding, and H. P. Parkman, "Comparison of gastric emptying of a nondigestible capsule to a radio-labelled meal in

healthy and gastroparetic subjects," *Alimentary Pharmacology & Therapeutics*, vol. 27, pp. 186–196, Oct. 2007.

[33] F. de A.A. Gondim, J. da Graça, G. de Oliveira, M. Rêgo, R. Gondim, and F. Rola, "Decreased gastric emptying and gastrointestinal and intestinal transits of liquid after complete spinal cord transection in awake rats," *Brazilian Journal of Medical and Biological Research*, vol. 31, pp. 1605–1610, Dec. 1998.

[34] P. Padmanabhan, J. Grosse, A. B. M. A. Asad, G. K. Radda, and X. Golay, "Gastrointestinal transit measurements in mice with 99mtc-DTPA-labeled activated charcoal using NanoSPECT-CT," *EJNMMI Research*, vol. 3, no. 1, p. 60, 2013.

[35] J. Y. Eor, P. L. Tan, S. M. Lim, D. H. Choi, S. M. Yoon, S. Y. Yang, and S. H. Kim, "Laxative effect of probiotic chocolate on loperamide-induced constipation in rats," *Food Research International*, vol. 116, pp. 1173–1182, Feb. 2019.

[36] Z. Zhou, L. Wang, M. Xu, L. Yin, F. Yang, S. Hui, Y. Yi, P. Feng, J. Wang, Y. Lin, J. Peng, and D. Chen, "Fruit bromelain ameliorates rat constipation induced by loperamide," *RSC Advances*, vol. 7, no. 72, pp. 45252–45259, 2017.

[37] J. D. Chen and R. W. McCallum, "Clinical applications of electrogastrography," *Am J Gastroenterol*, vol. 88, no. 9, pp. 1324–36.

[38] C. Tümer, H. D. Oflazoğlu, B. D. Obay, M. Kelle, and E. Taşdemir, "Effect of ghrelin on gastric myoelectric activity and gastric emptying in rats," *Regulatory Peptides*, vol. 146, pp. 26–32, Feb. 2008.

[39] G. O'Grady, T. R. Angeli, P. Du, C. Lahr, W. J. Lammers, J. A. Windsor, T. L. Abell, G. Farrugia, A. J. Pullan, and L. K. Cheng, "Abnormal initiation and conduction of slow-wave activity in gastroparesis, defined by high-resolution electrical mapping," *Gastroenterology*, vol. 143, pp. 589–598.e3, Sept. 2012.

[40] H. P. Simonian, K. Panganamamula, J. Z. Chen, R. S. Fisher, and H. P. Parkman, "Multichannel electrogastrography (EGG) in symptomatic patients: A single center study," *American Journal of Gastroenterology*, vol. 99, pp. 478–485, Mar. 2004.

[41] R. Berry, L. K. Cheng, P. Du, N. Paskaranandavadivel, T. R. Angeli, T. Mayne, G. Beban, and G. O'Grady, "Patterns of abnormal gastric pacemaking after sleeve gastrectomy defined by laparoscopic high-resolution electrical mapping," *Obesity Surgery*, vol. 27, pp. 1929–1937, Feb. 2017.

[42] J. R. Miranda, O. Baffa, R. B. de Oliveira, and N. M. Matsuda, "An AC biosusceptometer to study gastric emptying," *Medical Physics*, vol. 19, pp. 445–448, Mar. 1992.

[43] C. C. Quini, M. F. Américo, L. A. Corá, M. F. Calabresi, M. Alvarez, R. B. Oliveira, and J. A. Miranda, "Employment of a noninvasive magnetic method for evaluation of gastrointestinal transit in rats," *Journal of Biological Engineering*, vol. 6, Dec. 2012.

[44] O. Baffa, R. B. Oliveira, J. R. A. Miranda, and L. E. A. Troncon, "Analysis and development of AC biosusceptometer for orocaecal transit time measurements," *Medical & Biological Engineering & Computing*, vol. 33, pp. 353–357, May 1995.

[45] M. F. Américo, R. G. Marques, E. A. Zandoná, U. Andreis, M. Stelzer, L. A. Corá, R. B. Oliveira, and J. R. A. Miranda, "Validation of ACB in vitro and in vivo as a biomagnetic method for measuring stomach contraction," *Neurogastroenterology & Motility*, vol. 22, pp. 1340–e374, Sept. 2010.

[46] L. A. Corá, F. G. Romeiro, F. C. Paixão, M. F. Américo, R. B. Oliveira, O. Baffa, and J. R. A. Miranda, "Enteric coated magnetic HPMC capsules evaluated in human gastrointestinal tract by AC biosusceptometry," *Pharmaceutical Research*, vol. 23, pp. 1809–1816, July 2006.

[47] M. F. Calabresi, A. Tanimoto, A. G. Próspero, F. P. Mello, G. Soares, L. C. D. Stasi, and J. R. Miranda, "Changes in colonic contractility in response to inflammatory bowel disease: Long-term assessment in a model of TNBS-induced inflammation in rats," *Life Sciences*, vol. 236, p. 116833, Nov. 2019.

[48] M. F. F. Calabresi, C. C. Quini, J. F. Matos, G. M. Moretto, M. F. Americo, J. R. V. Graça, A. A. Santos, R. B. Oliveira, D. R. Pina, and J. R. A. Miranda, "Alternate current biosusceptometry for the assessment of gastric motility after proximal gastrectomy

in rats: a feasibility study," *Neurogastroenterology & Motility*, vol. 27, pp. 1613–1620, Aug. 2015.

[49] R. G. Marques, M. F. Americo, C. T. Spadella, L. A. Corá, R. B. Oliveira, and J. R. A. Miranda, "Different patterns between mechanical and electrical activities: an approach to investigate gastric motility in a model of long-term diabetic rats," *Physiological Measurement*, vol. 35, pp. 69–81, Dec. 2013.

[50] L. A. Corá, M. F. Américo, R. B. Oliveira, C. H. R. Serra, O. Baffa, R. C. Evangelista, G. F. Oliveira, and J. R. A. Miranda, "Biomagnetic methods: Technologies applied to pharmaceutical research," *Pharmaceutical Research*, vol. 28, pp. 438–455, Oct. 2010.

[51] L. A. Corá, U. Andreis, F. G. Romeiro, M. F. Américo, R. B. Oliveira, O. Baffa, and J. R. A. Miranda, "Magnetic images of the disintegration process of tablets in the human stomach by ac biosusceptometry," *Physics in Medicine and Biology*, vol. 50, pp. 5523–5534, Nov. 2005.

[52] L. A. Pinto, L. A. Corá, G. S. Rodrigues, A. G. Prospero, G. A. Soares, U. de Andreis, and J. R. de Arruda Miranda, "Pharmacomagnetography to evaluate the performance of magnetic enteric-coated tablets in the human gastrointestinal tract," *European Journal of Pharmaceutics and Biopharmaceutics*, vol. 161, pp. 50–55, Apr. 2021.

[53] C. C. Quini, A. G. Próspero, M. F. Calabresi, G. M. Moretto, N. Zufelato, S. Krishnan, D. R. Pina, R. B. Oliveira, O. Baffa, A. F. Bakuzis, and J. R. Miranda, "Real-time liver uptake and biodistribution of magnetic nanoparticles determined by AC biosusceptometry," *Nanomedicine: Nanotechnology, Biology and Medicine*, vol. 13, pp. 1519–1529, May 2017.

[54] A. G. Prospero, P. F. de Oliveira, G. A. Soares, M. F. Miranda, L. A. Pinto, D. C. dos Santos, V. dos S Silva, N. Zufelato, A. F. Bakuzis, and J. R. Miranda, "AC biosusceptometry and magnetic nanoparticles to assess doxorubicin-induced kidney injury in rats," *Nanomedicine*, vol. 15, pp. 511–525, Feb. 2020.

[55] A. G. Próspero, C. C. Quini, A. F. Bakuzis, P. F. de Oliveira, G. M. Moretto, F. P. F. Mello, M. F. F. Calabresi, R. V. R. Matos, E. A. Zandoná, N. Zufelato, R. B. Oliveira, and J. R. A. Miranda, "Real-time in vivo monitoring of magnetic nanoparticles in the bloodstream by AC biosusceptometry," *Journal of Nanobiotechnology*, vol. 15, Mar. 2017.

[56] A. G. Próspero, G. A. Soares, G. M. Moretto, C. C. Quini, A. F. Bakuzis, and J. R. de Arruda Miranda, "Dynamic cerebral perfusion parameters and magnetic nanoparticle accumulation assessed by AC biosusceptometry," *Biomedical Engineering / Biomedizinische Technik*, vol. 65, pp. 343–351, May 2020.

[57] G. A. Soares, A. G. Prospero, M. F. Calabresi, D. S. Rodrigues, L. G. Simoes, C. C. Quini, R. R. Matos, L. A. Pinto, A. A. Sousa-Junior, A. F. Bakuzis, P. A. Mancera, and J. R. A. Miranda, "Multichannel AC biosusceptometry system to map biodistribution and assess the pharmacokinetic profile of magnetic nanoparticles by imaging," *IEEE Transactions on NanoBioscience*, vol. 18, pp. 456–462, July 2019.

Capítulo 2

Sleeve gastrectomy elicits alterations in gastric motility and morphometry in obese rats

Prefácio

Este trabalho teve seu início em 2018, como o principal tópico a ser desenvolvido durante meu doutorado. A ideia inicial do projeto veio após o mestrado do Dr. Marcos Calabresi, orientado do Prof. José Ricardo. Em sua dissertação, o Dr. Marcos Calabresi abordou as alterações provocadas pela cirurgia de fundectomia na motilidade gastrintestinal de ratos através da BAC. O trabalho foi então publicado em 2015 na revista *Neurogastroenterology & Motility*, a qual é a principal revista e referência na área. Entretanto, a cirurgia abordada não é mais comum na rotina clínica.

Portanto, durante a escrita do meu projeto de doutorado, o Dr. Marcos Calabresi e o Prof. José Ricardo tiveram a ideia de abordarmos a cirurgia de gastrectomia vertical, a qual é a mais realizada no mundo para controle da obesidade. Devido ao fato de ter acompanhado diversos projetos relacionados a motilidade gastrintestinal durante minha iniciação científica, aceitei a responsabilidade de desenvolver este projeto como tópico principal no meu doutorado.

Além do fato de trabalhar com ratos, o grande desafio do trabalho foi aprender o procedimento cirúrgico da gastrectomia vertical, o qual é extremamente delicado. Primeiramente, recebi muita ajuda da Dra. Juliana Matos, que no momento era aluna de doutorado do Prof. José Ricardo, e que possuia uma vasta experiência com cirurgia. Além disso, a Profa. Rozemeire Marques foi essencial para me ensinar todos os protocolos e procedimentos cirúrgicos. Para realizar a cirurgia, tive acesso a toda infraestrutura da Unidade de Pesquisa Experimental (UNIPEX) da Faculdade de Medicina de Botucatu, sem a qual eu não teria as melhores condições para desenvolver essa parte tão delicada do projeto.

Por fim, usamos a técnica BAC para avaliar as mudanças na motilidade gastrintestinal de ratos obesos submetidos a cirurgia de gastrectomia vertical. Aqui utilizamos um modelo de obesidade através de ração hipercalórica desenvolvida na UNIPEX, e foram realizadas medidas BAC antes e após a gastrectomia vertical. Foram avaliados parâmetros metabólicos e bioquímicos, esvaziamento gástrico, trânsito orocecal, contratilidade gástrica e análise morfométrica do estômago. Aqui também cabe meu agradecimento a Profa. Madileine Américo, que em conjunto da Dra. Loyane Almeida e da minha grande amiga Msc. Mariana Machado

realizaram as análises histológicas, além de toda contribuição para a redação do manuscrito.

Sleeve gastrectomy elicits alterations in gastric motility and morphometry in obese rats

Leonardo Antonio Pinto[1], André Gonçalves Próspero[1], Mariana Pirani Rocha Machado[1], Loyane Almeida Gama[2], Gabriela Nogueira Bittencourt[1], Guilherme Augusto Soares[1], Michael Almeida[1], Evandro Molinari[1], Rozemeire Garcia Marques[3] Madileine Francely Américo[2], José Ricardo de Arruda Miranda[1]

[1]Institute of Biosciences, Department of Biophysics and Pharmacology, São Paulo State University, UNESP, Botucatu, Brazil.

[2]Institute of Biological Sciences and Health, Federal University of Mato Grosso, UFMT, Barra do Garças, Brazil.

[3] Botucatu School of Medicine, Department of Surgery and Orthopedics, UNESP, Botucatu, Brazil.

Corresponding author

Leonardo Antonio Pinto, +55 14 3880-0285, Instituto de Biociências, UNESP – Rua Prof. Dr. Antonio Celso Wagner Zanin, 18618-689 Botucatu, Brazil.

Email: leonardo.antonio@unesp.br

Abstract

Background: Sleeve gastrectomy (SG) is a bariatric procedure resulting in long-term weight loss, but detailed studies on gastric contractility and gastrointestinal transit in the same subject are absent. This study aimed to evaluate the effects of SG on gastrointestinal motility in rats using alternate current biosusceptometry (ACB).

Methods: Male Wistar rats were fed with a high sugar-fat diet for 12 weeks and randomly assigned to two experimental groups: Sham and SG. A 30-day experimental protocol was carried out in three time points: preoperative, 7, and 30 days after the surgical procedure. GI motility measurements were performed using the ACB technique. Mean gastric emptying time (MGET), mean cecum arrival time (MCAT), and gastric contractility were assessed. Moreover, rats from both groups underwent nutritional, lipid profile, and morphometry analysis.

Key Results: MGET and MCAT were accelerated at 7 and 30 days after SG compared to preoperatively. Gastric dominant frequency was decreased, and the signal presented a non-stationary and non-sinusoidal profile after the SG procedure. Thirty days after SG, gastric morphometry showed a reduced thickness of mucosa and muscularis mucosa layers, while increased leukocyte infiltration indicated inflammation in gastric layers.

Conclusions & Inferences: The resection of the gastric greater curvature induced severe dysmotility. Acceleration of gastric emptying, orocecal transit, impairment of gastric contractile activity, and morphometric alterations persist long after SG.

Keywords: Sleeve gastrectomy, AC Biosusceptometry, gastric emptying, orocecal transit time, gastric contractility

Introduction

The prevalence of obesity and an overweight condition is increasing globally, and the comorbidities associated with obesity, such as hypertension and type 2 *diabetes mellitus*, result in increased mortality and morbidity [1]. Although strategies such as pharmacotherapy and lifestyle changes may temporarily alleviate obesity symptoms [2], still bariatric surgery is the most effective approach, resulting in substantial weight loss with the remission of obesity-related comorbidities [3].

Sleeve gastrectomy (SG) presents long-term effectiveness of weight loss in the treatment of morbid obesity [4, 5]. The procedure involves removing the stomach's fundus and the greater curvature, but the mechanism to achieve consistent weight loss is complex. The excised portions of the stomach play a key role in gastrointestinal (GI) function, where the fundus is responsible for receptive relaxation, and the greater curvature is the dominant site of the interstitial cells of Cajal (ICC) and responsible for producing ghrelin [6, 7]. The remaining narrow sleeve is characterized by lesser distensibility and higher intraluminal pressure, resulting in early satiety [8].

GI motility comprises several processes, including gastric emptying, GI transit, contractile activity (mechanical and myoelectrical), tone, and compliance [9]. Although previous studies conducted in humans showed that SG accelerates gastric emptying and small bowel transit, few studies have investigated the effects of SG on gastric contractility [10]. The lack of studies focusing on the effects of SG on gastric contractility may be related to the high invasiveness and costs associated with the techniques used [11, 12]. The alternate current biosusceptometry (ACB) is a low-cost and noninvasive technique extensively used for GI motility studies in humans and animals [13–18]. ACB enables a real-time assessment of GI transit (*e. g.*, gastric emptying, orocecal transit) and contractility parameters in the same measurement using magnetic tracers. Due to practical and ethical challenges on human subjects, animal models are essential for understanding the effects of SG on the GI tract. The impact of SG in rats' weight loss, food intake, and metabolic parameters have been extensively reported [19–21]; however, the relationship between gastric contractility and emptying associated with morphometry after SG still remain unclear. This study aimed to

compare changes in metabolic parameters, GI motility and gastric morphology following SG in rats.

Materials and Methods

Animals and experimental protocols

The Committee on Animal Research and Ethics approved all the experiments and procedures (CEUA Protocol number 1067) performed following the Ethical Principles in Animal Research adopted by the Brazilian College of Animal Experimentation (COBEA).

Sixteen 45-day-old male Wistar rats were obtained from the ANILAB Laboratory (Paulínia, SP, Brazil) and maintained under controlled temperature (24 ± 2 °C), humidity (60 ± 5%), and a 12 h light/dark cycle. During 12 consecutive weeks, rats were fed ad libitum on a high sugar-fat (HSF) diet containing 53.5% carbohydrates, 18.0% proteins, and 16.5% fats, with an energy density of 4.35 kcal/g. The diet consisted of soybean meal, sorghum, soybean peel, dextrin, sucrose, fructose, lard, vitamins, and minerals. The diet protocol was developed at the São Paulo State University (UNESP), Medical School, Botucatu, Brazil, and was published previously [22].

At the end of the 12^{th} week, the rats were randomly assigned to one of two groups: Sham (n = 8) or SG (n = 8). A 30-day experimental protocol was divided into three distinct time points: preoperative, 7, and 30 days after surgery. The sham group was used only as a control for the nutritional, lipid levels profile, adiposity index, and morphometric analysis so that the SG group was its own control for the GI motility measurements.

Surgical techniques

After 12-hour fasting, the rats were anesthetized with ketamine (30 mg/kg) and xylazine (15 mg/kg) injected intraperitoneally. Subcutaneous administration of enrofloxacin (5 mg/kg) and tramadol (10 mg/kg) were performed immediately before surgery. As postoperative care, the animals received meloxicam (1 mg/kg) and tramadol (10 mg/kg) subcutaneously for three days. After surgery, the rats were fed a liquid diet (HSF diet mixed with

water) for three days and then returned to the same diet as preoperatively [23].

Sleeve gastrectomy

SG was performed as previously described [23]. Briefly, after a midline abdominal incision of 1.5 cm from the xiphoid process down, the stomach was exteriorized, and a 7 FR catheter was passed through the mouth to the duodenum to standardize the size of the gastric sleeve. The stomach's fundus and greater curvature were removed with an electric scalpel while preserving the gastroesophageal junction and the pylorus. The stomach was then closed with a 4-0 polypropylene suture in two layers creating the gastric sleeve. The muscle layer's closure was performed using a 4-0 non-absorbable nylon suture and on the skin with 4-0 silk sutures.

Sham surgery

A midline abdominal incision was performed for the sham group, and the stomach was exposed as in the SG surgery groups. The muscle layer and skin closure were performed as described in the SG surgery. Operative time was prolonged to match the SG surgery time.

Nutritional analysis

Body weight and food consumption were measured 0 (preoperatively) and at 7, 14, 21, and 30 days after SG or sham surgery. The caloric intake (CI) was calculated as follows [24]:

$$\text{CI (kcal/day)} = \text{daily food consumption (g)} \times \text{energy density (kcal)} \tag{1}$$

Gastrointestinal motility measurements

The signal intensity obtained from an ACB measurement is directly proportional to the amount of magnetic material and inversely proportional to the distance between the ACB sensor and the magnetic material. The direct relation between the amount of magnetic material and signal intensity enables the evaluation of GI transit. Furthermore, the contraction of a stomach containing magnetic material increases the distance between the material and

the sensor on the abdominal surface. At the same time, the relaxation of the segment decreases the distance, and therefore increases the signal registered by the ACB sensor. These signal modulations allow the assessment of contractile activity noninvasively using the ACB technique. Details on the instrumentation and working principles are described elsewhere [16, 25, 26].

GI motility measurements were performed only in SG group rats preoperatively, at 7 and 30 days postoperatively (note that each rat was its control). Gastric emptying, orocecal transit, and gastric contractility were recorded during the same day. Rats were fasted for 12 h and fed with a 2 g test meal composed of 0.5 g of magnetic tracers incorporated into 1.5 g of standard rat chow (Presence Nutrição Animal, Paulínia, SP, Brazil). Manganese ferrite ($MnFe_2O_4$) microparticles, with a size between 53 and 75 μm, were used as non-absorbable and inert magnetic tracer at any GI pH [14].

For gastric emptying and orocecal transit measurements, the ACB sensor was placed on the gastric and cecum projections (based on external anatomical references) to measure magnetic signal intensity. Subsequent measurements were performed at these two same points at regular 15 min intervals for 6 h [15].

Thirty minutes after beginning gastric emptying and orocecal transit measurements, the rats were anesthetized with isoflurane (4.0% induction and 1.5% maintenance) for the gastric contractility recordings. The rats were kept in a supine position, and the ACB sensor was positioned in the gastric projection for a 20 min signal recording [15]. The signal was acquired at a sampling rate of 20 Hz and digitized using an A/D board (MP100 System; BIOPAC Inc., Santa Barbara, CA, USA). After the gastric contractility recordings, the gastric emptying and orocecal transit measurements continued with the awake rats.

ACB data analysis

All raw signals were analyzed in MatLab (Mathworks Inc., Natick, USA). Gastric emptying and orocecal transit time: Statistical moments were calculated through the temporal average pondered by magnetic intensity values, normalized by the area under the curve [15, 16, 27]. The following parameters were quantified: mean gastric emptying time (MGET), which was defined as the time t (min) when a mean amount of magnetic tracer was emptied from the

stomach; mean cecum arrival time (MCAT), defined as the time t (min) when occurred an increase occurred in the mean amount of tracer in the cecum.

Gastric contractility: Firstly, the signal was filtered by a bi-directional Butterworth band-pass filter with a cut-off frequency of 1.0 – 9.0 cycles per minute (cpm). Afterward, Fast Fourier transform (FFT) was used, and the highest peak of each FFT was considered the gastric dominant frequency. Gastric contractility signals were also visually analyzed regarding the waveform. Signal waveforms presenting a morphology of irregular peaks (*e. g.*, spikes) were classified as non-sinosoidal. Moreover, Running Spectral Analysis (RSA) was used to identify frequency variations over time. In this case, signals were classified as non-stationary [28]. The percentage of time in which the gastric dominant frequency was outside the normal frequency range was determined as the abnormal rhythmic index (ARI). The normal frequency range was the mean $\pm$ 2 $\times$ SD of the gastric dominant frequency obtained preoperatively [29, 30].

Lipid profile and body fat analyses

On the 31st day after surgery, the sham and SG group rats were killed by decapitation under deep anesthesia with ketamine. Blood samples were collected in non-additive tubes, and a laparotomy was performed to collect fat pads. The serum was separated by centrifugation at 1,490 g for 15 min at 4 °C and stored at -80 °C to assess serum parameters. Serum levels of total cholesterol (TC), triglycerides (TG), and high-density lipoproteins (HDL-C) were measured by the enzymatic methodology [31]. Values of very-low-density lipoprotein (VLDL-C) were estimated according to the calculation proposed by Knopfholz *et al.* [32].

Fat pads of adipose tissue were dissected, dipped in saline, and after the excess was removed tissues were weighted. The total body fat was measured from the sum of the individual fat pad weights: visceral, retroperitoneal, and epididymal fat. The adiposity index (%) was calculated as follows [33]:

$$\text{Adiposity index (\%)} = \frac{\text{Total body fat}}{\text{Body weight}} \times 100 \tag{2}$$

Gastric morphometry analysis

Tissue samples from the gastric body were fixed in 10% neutral buffered formalin for 24 hours, dehydrated with serial alcohol and xylol solutions. Samples were included in paraffin, and histological cuts were performed with 4 μm thickness, stained with hematoxylin and eosin (HE). Images were acquired using an Eclipse E200-Nikon optical microscope (Nikon), in objective x10, equipped with a 5.0 MP digital camera system (model ISH 500, Opton), and connected to a computer with an image capture program (TCapture). All analyses were performed using ImageJ software (NIH). The morphometric analysis was carried out by measuring the gastric mucosa, muscularis mucosa, and submucosa thickness. Furthermore, histopathological examination was performed using a graded assessment of leukocyte infiltration (Table 1) [34, 35].

Table 1. Histopathological scoring criteria. HPF: high power field.

Pathological state	Score	
Leukocyte infiltration	0	Absent
	1	2 - 10/HPF
	2	11 - 20/HPF
	3	21 - 30/HPF
	4	>31/HPF

Statistical analysis

All parameters were tested for normality using the Shapiro-Wilk test, and results were expressed as mean ± SD or median (interquartile range). A comparison of nutritional analysis, lipid profile, body fat, gastric morphometry, and histopathology between the sham and SG group was carried out by the unpaired Student's t-test (normal distribution) or Mann-Whitney test (non-normal distribution). The difference between GI parameters for the same animal during the three distinct measurements was determined by one-way analysis of variance (ANOVA) followed by the post hoc Tukey's test (normal distribution) or by the Friedman test followed by post hoc Dunn's test (non-normal distribution). Values of $p <$

0.05 were considered statistically significant. All statistical analyses were performed using GraphPad Prism 6 software (GraphPad Software, La Jolla, USA).

Results

Gastrointestinal motility

Figure 1 shows an example of the gastric emptying and orocecal transit curve profile, respectively, obtained after ingesting test meal for the same rat preoperatively (day 0), at 7 and 30 days after SG.

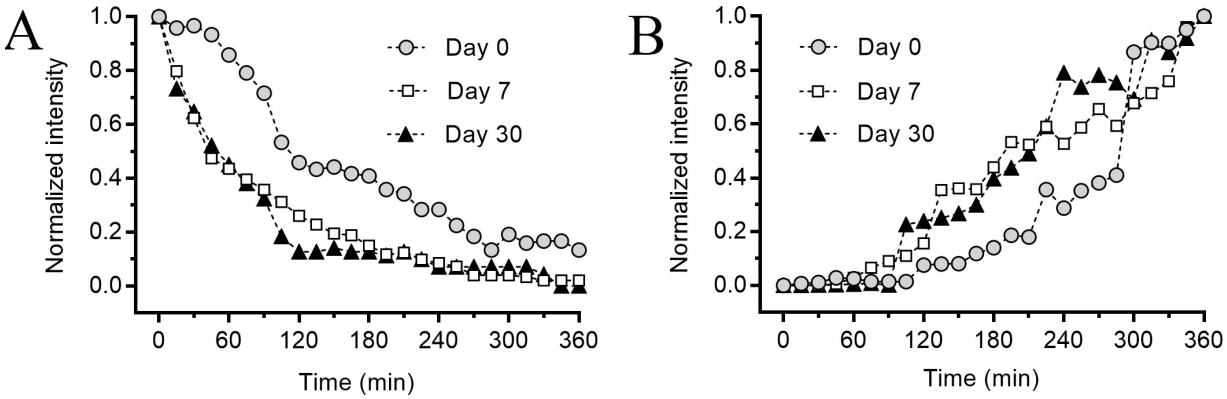

Figure 1. Example of individual curves of (A) gastric emptying and (B) orocecal transit preoperatively (day 0) and at 7 and 30 days postoperatively.

The MGET (Figure 2A) was significantly decreased on the 7th (83.2 $\pm$ 13.3 min, $p < 0.001$) and 30th (88.3 $\pm$ 8.5 min, $p < 0.0001$) postoperatively day compared to preoperatively (113.9 $\pm$ 3.7 min). The MCAT decreased from 259.6 $\pm$ 16.1 min preoperatively to 236.0 $\pm$ 17.6 min ($p < 0.05$) and 230.0 $\pm$ 6.2 min ($p < 0.05$) at 7 and 30 days after SG, respectively (Figure 2B).

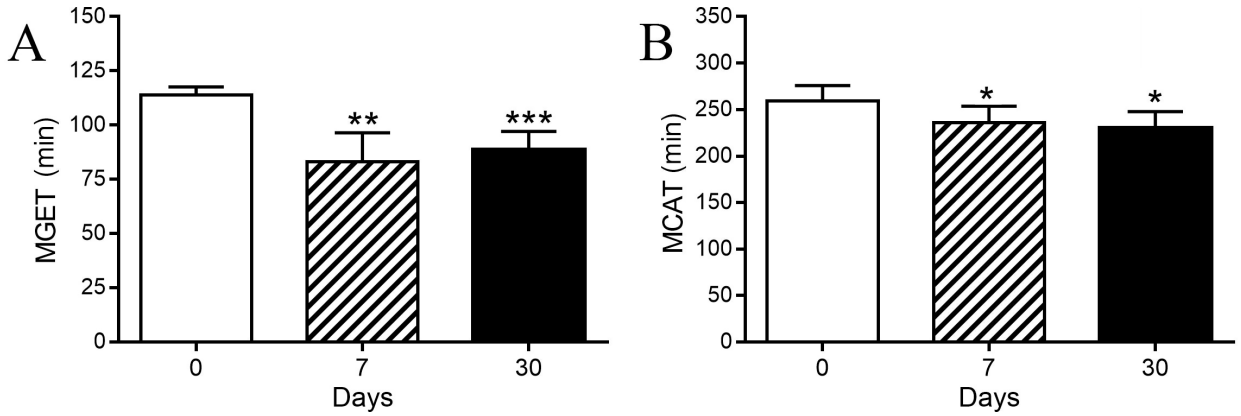

Figure 2. Gastric emptying and orocecal transit results before and after SG. (A) Mean gastric emptying time (MGET) and (B) Mean cecum arrival time (MCAT) preoperatively (day 0), and at 7 and 30 days after surgery. Data are presented as mean ± SD. *$p < 0.05$, **$p < 0.001$, and ***$p < 0.0001$ vs. day 0.

Figure 3 shows a 10-min signal excerpt and the respective RSA of each gastric activity acquisition (preoperatively and at 7 and 30 days postoperatively) for the same rat. Before surgery, the gastric activity had a sinusoidal waveform and a narrow band of frequency (Figure 3A). However, the postoperatively measurements presented significant differences in gastric dominant frequency of contraction and signal waveform. Figure 3B shows a non-stationary signal related to gastric contractility 7 days after SG. Furthermore, Figure 3C shows the gastric contractility 30 days after SG, which can be observed that the signal morphology is non-sinusoidal. The RSA after 30 days shows a relatively narrow frequency range, and bradygastria compared to before SG. Overall, 7 days after SG, we found non-stationary or non-sinusoidal waveform in 87.5% (7 out of 8 rats) of the signals. Considering 30 days after SG, 6 out of 8 rats presented abnormal gastric contractility patterns, with 75.0% and 62.5% of non-sinusoidal and non-stationary signals, respectively.

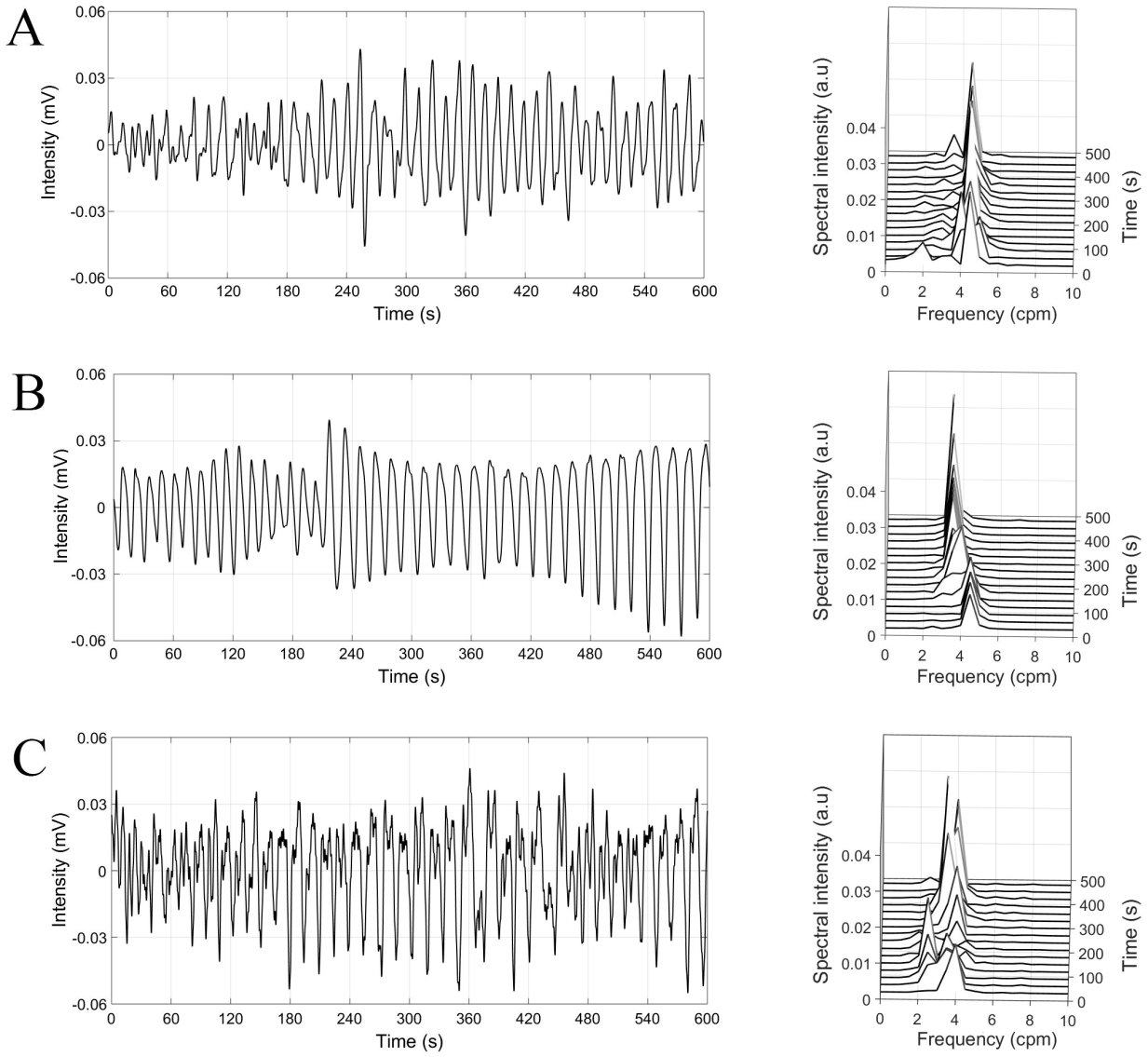

Figure 3 Example of mechanical gastric contractility signals (left panel) and their respective RSA (right panel) obtained (A) preoperatively and at (B) 7 and (C) 30 days after SG in the same animal.

Figure 4 shows the quantification of the gastric contractility measurements. The gastric dominant frequency at 7 (3.7 ± 0.2 cpm) and 30 (3.6 ± 0.5 cpm) days postoperatively were significantly decreased compared to preoperatively (4.5 ± 0.4 cpm) ($p < 0.01$). As a result of the lower frequencies and the non-stationary characteristics of the signals postoperatively, the ARI was significantly increased from 2% (0 – 48.9) preoperatively to 95% (52.1 – 100)

at 30 days after SG ($p < 0.05$).

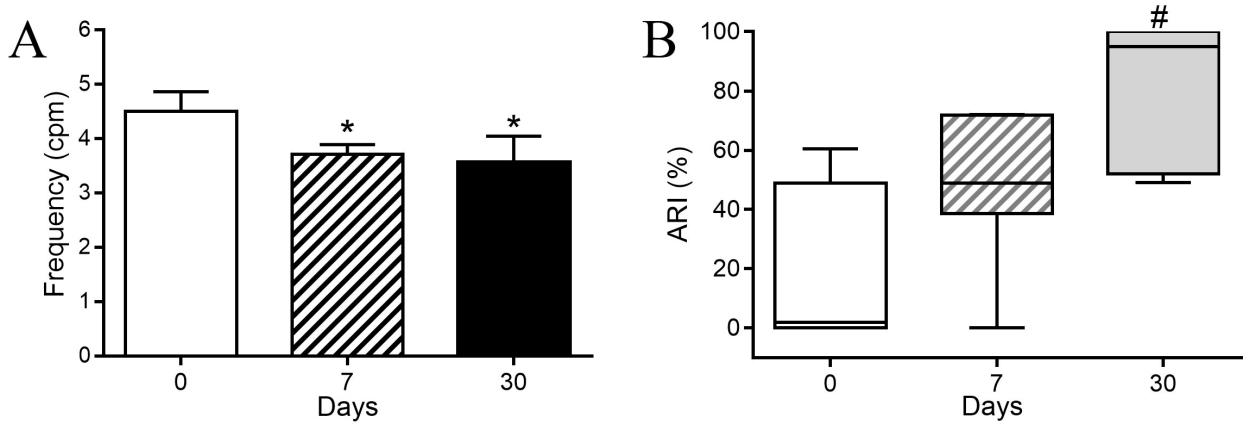

Figure 4. Gastric contractility parameters before and at 7 and 30 days after SG. (A) Gastric dominant frequency and (B) abnormal rhythmic index (ARI). Frequency results are expressed as the mean ± SD, and ARI results are expressed as (medians; interquartile intervals). *$p < 0.05$ vs. day 0 (ANOVA followed by Tukey multiple comparison test) and #$p < 0.05$ vs. day 0 (Friedman test followed by the Dunn multiple comparison test).

Nutritional analysis

Figure 5A shows the animal's body weight during the 30-day experimental protocol. From day 0 to day 30, the sham rats' mean body weight increased 8.7%, while the SG rats' mean body weight decreased 10.6%. As a result, on day 30, the SG rats' mean body weight was approximately 16.9% lower than the sham rats' mean body weight (423.4 ± 42.9 g SG, 509.4 ± 19.5 g sham, $p < 0.01$). After SG, rats displayed an initial decrease in daily caloric mean intake at 7 ($p = 0.17$) and 14 days ($p = 0.27$) after surgery, but no significant differences were found between the groups (Figure 5B).

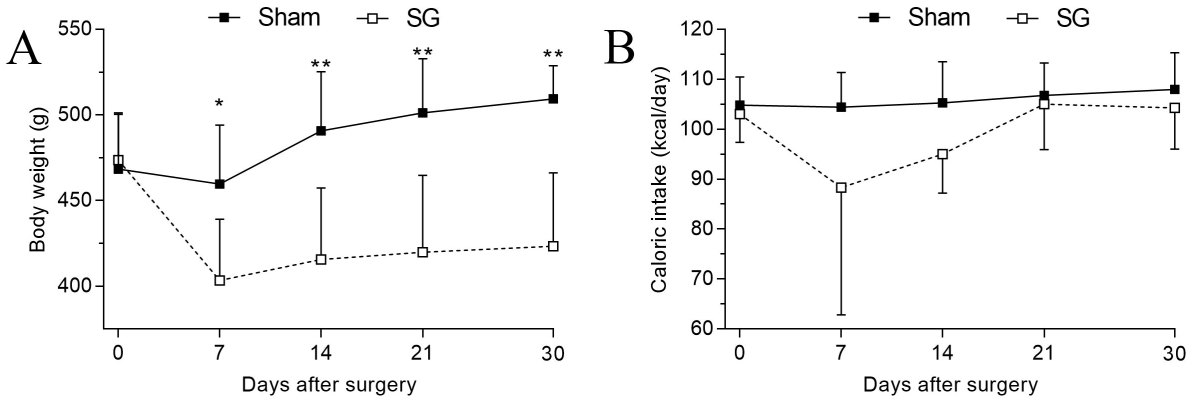

Figure 5. Nutritional analysis. (A) Body weight and (B) caloric intake of sham and SG rats throughout the 30 days of study. Data expressed as mean ± SD. *p < 0.05 and **p < 0.01 represents difference between the Sham and SG groups for the same time point (unpaired Student's t-test).

Lipid profile and body fat analyses

Serum levels of lipids and body fat results are shown in Table 2. Rats submitted to SG presented a mean adiposity index 53.7% lower than the sham group rats ($p < 0.001$). However, no significant differences were found for TC, TG, HDL-C, and VLDL-C levels between the sham and SG rats.

Table 2. Serum levels of lipids and adiposity index of sham and SG groups. Data are presented as mean ± SD.

Parameters	Sham (n = 8)	SG (n = 8)
Adiposity index (%)	5.4 ± 1.7	2.9 ± 0.9**
TC (mg/dl)	106.5 ± 24.6	94.0 ± 22.4
TG (mg/dl)	68.0 ± 28.0	51.8 ± 13.8
HDL-C (mg/dl)	29.0 ± 3.3	28.6 ± 3.8
VLDL-C (mg/dl)	13.3 ± 5.9	9.2 ± 2.5

**p < 0.001 vs. Sham (unpaired Student's t-test).

Gastric morphometry analysis

Gastric morphometry and histopathological analyses are presented in Figure 6. The stomach of the sham group (Figure 6A) showed a typical histological structure of the gastric muscular layer, and no leukocyte infiltration was observed (Figure 6B). In contrast, tissue remodeling was observed in SG rats (Figure 6C), showing multiple leukocyte infiltration in muscularis mucosa, submucosal, and mucosa layers of gastric body (Figure 6D). Gastric tissue alterations were evaluated using a pathological score (Figure 6E) and were associated with significantly higher leukocyte infiltration in SG rats compared to sham rats ($p < 0.0001$). Inflammatory cell infiltration was observed in the muscular, submucosa, and mucosa layers after 30 days of SG. In morphometry analysis, SG rats had a lower thickness in both the gastric mucosa and muscularis mucosa layers compared to the sham rats ($p < 0.0001$, Figure 6F). No difference was observed in the thickness of the submucosa layer between the groups.

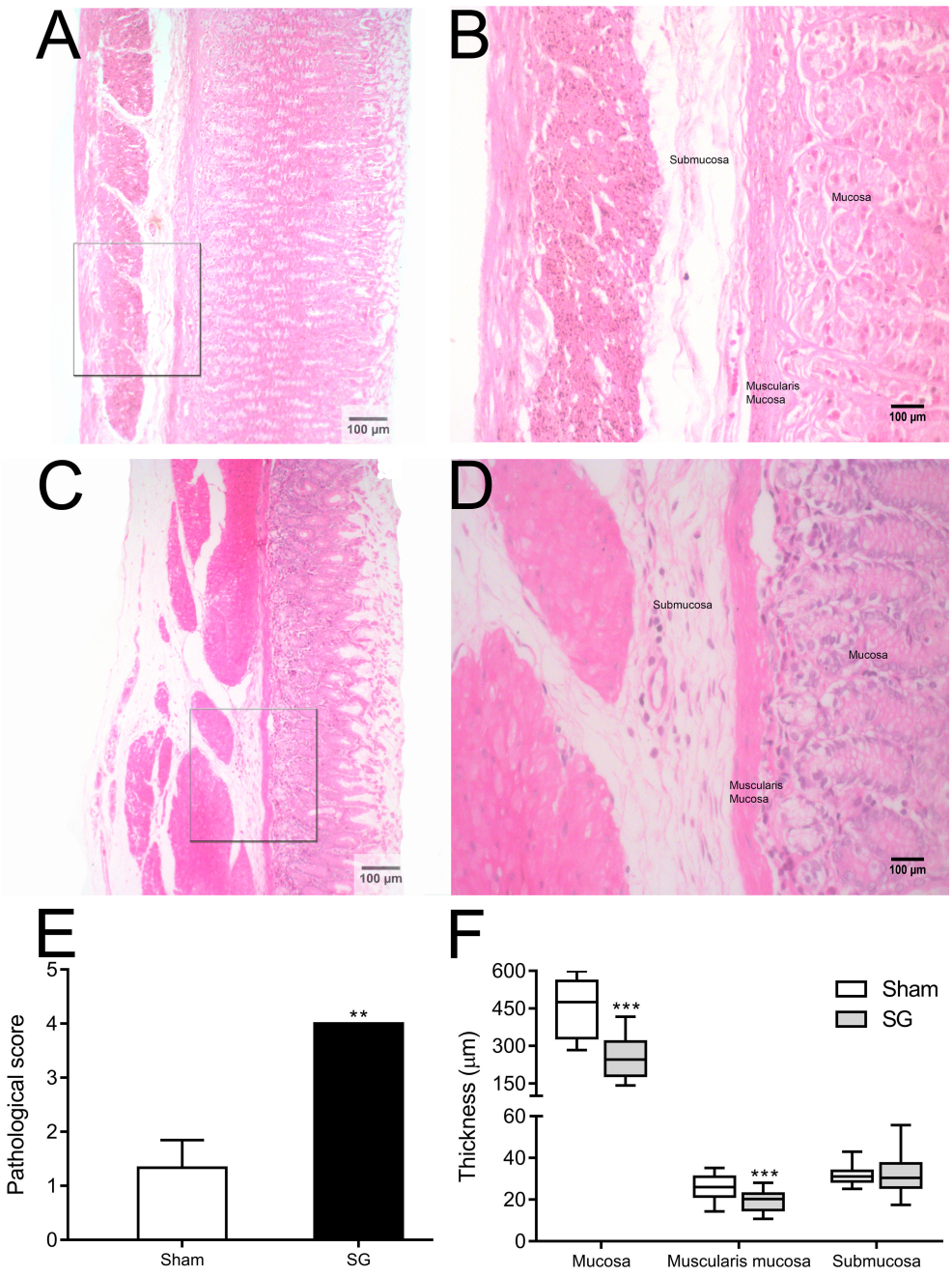

Figure 6 Effect of SG on gastric body samples. Histological photomicrographs using HE stain of Sham (× 10 objective [A] and × 40 objective [B]) and SG rats (× 10 objective [C] and × 40 objective [D]), Leukocyte infiltration score (E) and gastric morphometry analysis (F). ** $p < 0.001$ and *** $p < 0.0001$ vs. sham.

Discussion and Conclusion

Our study reported significant alterations after SG surgery in gastric emptying, orocecal transit time, gastric mechanical activity, and gastric morphometry.

The rats' body weight results showed an initial decrease 7 days after the surgical procedure for the sham and SG groups, presumably an acute reflex of the liquid diet after the procedure. Until the end of the experimental period, the rats' body weight increased as expected, but the SG group presented a significantly lower body weight growth than the sham group. Even though not statistically significant, our results showed an initial decrease in daily caloric intake of SG rats for the first 14 days after surgery, followed by a gradual increase up to the baseline caloric intake until the end of the experimental protocol. This unexpected behavior of caloric intake may be related to the loss of the restrictive gastric capacity due to restrictive enlargement or dilatation observed. Similarly to Guimarães et al. [19], we observed a considerable gastric dilatation post mortem in rats submitted to SG, which might explain the lack of a reduced caloric intake in SG rats. Sleeve dilatation was also reported in humans, but it was not necessarily related to the procedure success in achieving weight loss [36]. In addition, the SG rats' weight loss without reducing caloric intake may also result from an accelerated GI transit or malabsorption of nutrients after the procedure, which was also reported in humans [37].

The preoperative gastric emptying curve profile was characterized by an initial test meal retention, representing the accommodation reflex. In contrast, the gastric emptying curve profile after SG showed an exponential decay with the accommodation reflex absence. As a result, the MGET was significantly accelerated at both 7 and 30 days after SG. Chambers et al. [20] also reported a greatly accelerated gastric emptying using scintigraphy in a rodent SG model, which was connected to impaired inhibitory feedback from the intestine and increased gastric intraluminal pressure. Fundus, which is the distensible region of the stomach and responsible for the accommodation reflex and controlling the gastric intraluminal pressure, when removed, promotes an increased gastric intraluminal pressure that accelerates gastric emptying [8, 38]. Although the gastric intraluminal pressure and impaired responses at the intestine level were not assessed in our study, the alterations in gastric contractility and

tissue remodeling of the gastric muscular layer found may have contributed to the accelerated gastric emptying.

In our results, signals before SG were characterized by stationary and sinusoidal waveforms with a narrow band of frequencies, as expected [15, 39]. However, the signal's waveform after SG showed distinct characteristics. For instance, the presence of irregular peaks (non-sinusoidal waveform) and frequency drifts (non-stationary waveform) during the gastric contractility acquisition. Furthermore, bradygastria was observed after SG. All these findings suggest a difficulty for the stomach muscles to contract properly after the excision of the greater curvature. It is worth noting that gastric contractility was still erratic 30 days after SG, and further studies may focus on whether these alterations can persist long after SG.

The mechanical gastric contractility results from gastric slow waves originated from electrical activity in the ICCs [40, 41]. The ICCs along the stomach show efficient entrainment, and the highest slow wave frequency, which is present in the greater curvature, controls all sites simultaneously, resulting in a gastric dominant frequency [42–45]. In mice studies, separating the antrum from the corpus caused a significant decrease in the antrum slow wave dominant frequency [45]. Furthermore, in a proximal gastrectomy model in rats, the excision of the upper corpus region resulted in bradygastria [15]. In our study, SG removed the greater curvature of the stomach, which presumably interferes with the ICCs network, and there was a decrease in the gastric dominant frequency and severe alterations in the gastric contractility waveform. There are no gastric contractility studies using a rodent model of SG in the literature, to the best of our knowledge. In humans, SG significantly increased the propagation velocity of slow waves and antral propulsions, but no changes were documented in gastric dominant frequency [11, 12].

Our gastric morphometry results showed a morphological remodeling of the gastric muscular layer after SG. The thickness of the mucosa and muscularis mucosa were decreased compared to sham rats. Furthermore, histopathological analysis revealed that SG induced leukocyte infiltration in the muscular, submucosa, and mucosa layers, indicating inflammation [46, 47]. Inflammation has a remarkable impact on smooth muscle function, which plays a key role in gastric contractility. For instance, inflammation may modulate the activity or

number of ion channels, intracellular signaling molecules, or transcription factors, resulting in gastric contractility alterations [48]. Moreover, inflammation in the small intestine of rats has been linked with alterations in the network of ICCs, resulting in uncoupling between ICCs and smooth muscle cells and consequently impaired contractility [49], which is flagged in our study by significantly decreased gastric dominant frequency and abnormal waveform after SG. Nevertheless, further studies are required to specify other possible mechanisms involved in gastric contractility alterations, such as assessing the ICCs network and its connection to morphological alterations.

Although only the stomach is resected during SG, motility alterations in the GI tract beyond the stomach may arise. Our results demonstrate that the orocecal transit curves presented the same pattern before and after SG, but the magnetic tracer arrived earlier to the cecum after SG, resulting in a faster MCAT postoperatively. Other studies also observed an accelerated intestinal transit after SG in both rat model and human subjects, presumably occurring regardless of the faster gastric emptying [20, 50, 51]. The earlier nutrient arrival into the distal intestine resulting from the acceleration of both gastric emptying and intestinal transit has been suggested as a key factor to the improved glucose homeostasis and enhanced release of glucagon-like peptide-1 (GLP-1) after SG [20, 51–53].

In rats, dye techniques such as phenol red recovery are considered the gold standard for the assessment of GI transit. However, the phenol red technique requires the sacrifice of the animal, and therefore a large number of animals is needed to obtain enough data [54–56]. Other methods such as scintigraphy, ^{13}C breath test, and radiopaque tracers have been used to assess GI transit in rats. Still, these methods present several drawbacks, including ionizing radiation and high implementation cost, hindering their use in research [57, 58]. On the other hand, methods to assess the mechanical gastric contractility in rats are scarce. While the current gold standard method manometry is highly invasive, magnetic resonance imaging presents a high complexity to obtain and quantify the data [57, 59]. In this context, ACB is a noninvasive and low-cost technique to assess GI parameters through easy implementation and low complexity. A related point to consider is that ACB enables the simultaneous measurement of distinct GI motility parameters in a single method, which reduces the necessity of multi-instrumental approaches.

In summary, this study described the alterations in metabolic parameters, GI motility, and gastric morphology in rats submitted to SG. MGET and MCAT were accelerated after SG, presumably as a response to the increased intragastric pressure. The excision of the greater curvature of the stomach evoked alterations in the gastric contractile activity, such as bradygastria with non-stationary signals and non-sinusoidal waveforms. Considerable gastric tissue remodeling was found after SG, with a reduced thickness of the mucosa and muscularis mucosa layer, in addition to inflammation in the muscular, submucosa, and mucosa layers determined by leukocyte infiltration, which probably also affected the gastric contractile activity. The observed GI dysmotility persisted until the end of the 30-day experimental protocol, indicating that extended follow-up studies are necessary to show evidence of possible permanent GI motility outcomes after sleeve gastrectomy in rats. Therefore, non-invasive and reproducible approaches, such as ACB are desirable to perform a long-term follow-up in the same animal.

Acknowledgments

This work was supported by the São Paulo Research Foundation (FAPESP - grant no. 2015/14923-9), the National Council for Scientific and Technological Development (CNPq), and the Coordination for the Improvement of Higher Education Personnel (CAPES – Finance code 001). We would like to thank the São Paulo State University Medical School for the technical support with the surgical procedures and diets.

Disclosure

All the authors declare that there are no conflicts of interest.

References

[1] A. Must, "The disease burden associated with overweight and obesity," *JAMA*, vol. 282, p. 1523, Oct. 1999.

[2] G. A. Bray and L. A. Tartaglia, "Medicinal strategies in the treatment of obesity," *Nature*, vol. 404, pp. 672–677, Apr. 2000.

[3] H. Buchwald, Y. Avidor, E. Braunwald, M. D. Jensen, W. Pories, K. Fahrbach, and K. Schoelles, "Bariatric surgery," *JAMA*, vol. 292, p. 1724, Oct. 2004.

[4] T. Diamantis, K. G. Apostolou, A. Alexandrou, J. Griniatsos, E. Felekouras, and C. Tsigris, "Review of long-term weight loss results after laparoscopic sleeve gastrectomy," *Surgery for Obesity and Related Diseases*, vol. 10, pp. 177–183, Jan. 2014.

[5] L. Angrisani, A. Santonicola, P. Iovino, G. Formisano, H. Buchwald, and N. Scopinaro, "Bariatric surgery worldwide 2013," *Obesity Surgery*, vol. 25, pp. 1822–1832, Apr. 2015.

[6] I. Quercia, R. Dutia, D. Kotler, S. Belsley, and B. Laferrère, "Gastrointestinal changes after bariatric surgery," *Diabetes & Metabolism*, vol. 40, pp. 87–94, Apr. 2014.

[7] K.-J. Won, K. M. Sanders, and S. M. Ward, "Interstitial cells of cajal mediate mechanosensitive responses in the stomach," *Proceedings of the National Academy of Sciences*, vol. 102, pp. 14913–14918, Oct. 2005.

[8] R. T. Yehoshua, L. A. Eidelman, M. Stein, S. Fichman, A. Mazor, J. Chen, H. Bernstine, P. Singer, R. Dickman, S. A. Shikora, R. J. Rosenthal, and M. Rubin, "Laparoscopic sleeve gastrectomy—volume and pressure assessment," *Obesity Surgery*, vol. 18, June 2008.

[9] M. B. Hansen, "Neurohumoral control of gastrointestinal motility," *Physiological research*, vol. 52, pp. 1–30, 2003.

[10] E. Sioka, G. Tzovaras, K. Perivoliotis, V. Bakalis, E. Zachari, D. Magouliotis, V. Tassiopoulou, S. Potamianos, A. Kapsoritakis, A. Poultsidi, K. Tepetes, C. Chatzitheofilou, and D. Zacharoulis, "Impact of laparoscopic sleeve gastrectomy on gastrointestinal motility," *Gastroenterology Research and Practice*, vol. 2018, pp. 1–17, 2018.

[11] R. Berry, L. K. Cheng, P. Du, N. Paskaranandavadivel, T. R. Angeli, T. Mayne, G. Beban, and G. O'Grady, "Patterns of abnormal gastric pacemaking after sleeve gas-

trectomy defined by laparoscopic high-resolution electrical mapping," *Obesity Surgery*, vol. 27, pp. 1929–1937, Feb. 2017.

[12] T. Baumann, S. Kuesters, J. Grueneberger, G. Marjanovic, L. Zimmermann, A.-O. Schaefer, U. T. Hopt, M. Langer, and W. K. Karcz, "Time-resolved MRI after ingestion of liquids reveals motility changes after laparoscopic sleeve gastrectomy—preliminary results," *Obesity Surgery*, vol. 21, pp. 95–101, Nov. 2010.

[13] J. R. A. Miranda, R. B. Oliveira, P. L. Sousa, F. J. H. Braga, and O. Baffa, "A novel biomagnetic method to study gastric antral contractions," *Physics in Medicine and Biology*, vol. 42, pp. 1791–1799, Sept. 1997.

[14] M. F. Américo, R. G. Marques, E. A. Zandoná, U. Andreis, M. Stelzer, L. A. Corá, R. B. Oliveira, and J. R. A. Miranda, "Validation of ACB in vitro and in vivo as a biomagnetic method for measuring stomach contraction," *Neurogastroenterology & Motility*, vol. 22, pp. 1340–e374, Sept. 2010.

[15] M. F. F. Calabresi, C. C. Quini, J. F. Matos, G. M. Moretto, M. F. Americo, J. R. V. Graça, A. A. Santos, R. B. Oliveira, D. R. Pina, and J. R. A. Miranda, "Alternate current biosusceptometry for the assessment of gastric motility after proximal gastrectomy in rats: a feasibility study," *Neurogastroenterology & Motility*, vol. 27, pp. 1613–1620, Aug. 2015.

[16] C. C. Quini, M. F. Américo, L. A. Corá, M. F. Calabresi, M. Alvarez, R. B. Oliveira, and J. A. Miranda, "Employment of a noninvasive magnetic method for evaluation of gastrointestinal transit in rats," *Journal of Biological Engineering*, vol. 6, Dec. 2012.

[17] A. G. Prospero, L. A. Pinto, R. V. R. Matos, G. A. Soares, R. B. Oliveira, S. Mascarenhas, and J. R. de Arruda Miranda, "New device for active gastric mechanical stimulation," *Neurogastroenterology & Motility*, May 2021.

[18] L. Pinto, G. Soares, A. Próspero, E. Stoppa, G. Biasotti, F. Paixão, A. Santos, R. Oliveira, and J. Miranda, "An easy and low-cost biomagnetic methodology to study regio-

nal gastrointestinal transit in rats," *Biomedical Engineering / Biomedizinische Technik*, vol. 0, Feb. 2021.

[19] M. Guimarães, M. Nora, T. Ferreira, S. Andrade, A. M. Ribeiro, V. Oliveira, M. C. Carreira, F. F. Casanueva, and M. P. Monteiro, "Sleeve gastrectomy and gastric plication in the rat result in weight loss with different endocrine profiles," *Obesity Surgery*, vol. 23, pp. 710–717, Mar. 2013.

[20] A. P. Chambers, E. P. Smith, D. P. Begg, B. E. Grayson, S. Sisley, T. Greer, J. Sorrell, L. Lemmen, K. LaSance, S. C. Woods, R. J. Seeley, D. A. D'Alessio, and D. A. Sandoval, "Regulation of gastric emptying rate and its role in nutrient-induced GLP-1 secretion in rats after vertical sleeve gastrectomy," *American Journal of Physiology-Endocrinology and Metabolism*, vol. 306, pp. E424–E432, Feb. 2014.

[21] A. Cabrera, M. Vives, A. Molina, M. París, E. Raga, A. Sánchez, F. Sabench, and D. D. Castillo, "Gastric plication and sleeve gastrectomy in an experimental model of obesity: New insights into weight loss, intake and metabolic results," *Obesity Surgery*, vol. 28, pp. 3259–3267, June 2018.

[22] F. Francisqueti, I. Minatel, A. Ferron, S. Bazan, V. Silva, J. Garcia, D. de Campos, A. Ferreira, F. Moreto, A. Cicogna, and C. Corrêa, "Effect of gamma-oryzanol as therapeutic agent to prevent cardiorenal metabolic syndrome in animals submitted to high sugar-fat diet," *Nutrients*, vol. 9, p. 1299, Nov. 2017.

[23] B. G. Bruinsma, K. Uygun, M. L. Yarmush, and N. Saeidi, "Surgical models of roux-en-y gastric bypass surgery and sleeve gastrectomy in rats and mice," *Nature Protocols*, vol. 10, pp. 495–507, Feb. 2015.

[24] Y. S. Diniz, L. A. Faine, C. M. Galhardi, H. G. Rodrigues, G. X. Ebaid, R. C. Burneiko, A. C. Cicogna, and E. L. Novelli, "Monosodium glutamate in standard and high-fiber diets: metabolic syndrome and oxidative stress in rats," *Nutrition*, vol. 21, pp. 749–755, June 2005.

[25] O. Baffa, R. B. Oliveira, J. R. A. Miranda, and L. E. A. Troncon, "Analysis and development of AC biosusceptometer for orocaecal transit time measurements," *Medical & Biological Engineering & Computing*, vol. 33, pp. 353–357, May 1995.

[26] L. A. Corá, U. Andreis, F. G. Romeiro, M. F. Américo, R. B. Oliveira, O. Baffa, and J. R. A. Miranda, "Magnetic images of the disintegration process of tablets in the human stomach by ac biosusceptometry," *Physics in Medicine and Biology*, vol. 50, pp. 5523–5534, Nov. 2005.

[27] F. Podczeck, J. M. Newton, and K.-H. Yuen *Pharmaceutical Research*, vol. 12, no. 3, pp. 376–379, 1995.

[28] J. Chen, "A computerized data analysis system for electrogastrogram," *Computers in Biology and Medicine*, vol. 22, pp. 45–57, Jan. 1992.

[29] S. Cucchiara, A. Franzese, G. Salvia, L. Alfonsi, V. D. Iula, A. Montisci, and F. L. Moreira, "Gastric emptying delay and gastric electrical derangement in IDDM," *Diabetes Care*, vol. 21, pp. 438–443, Mar. 1998.

[30] Q.-L. Long, D.-C. Fang, H.-T. Shi, and Y.-H. Luo, "Gastro-electric dysrhythm and lack of gastric interstitial cells of cajal," *World Journal of Gastroenterology*, vol. 10, no. 8, p. 1227, 2004.

[31] R. B. Friedman, R. E. Anderson, S. M. Entine, and S. B. Hirshberg, "Effects of diseases on clinical laboratory tests," *Clin Chem*, vol. 26, pp. 1D–476D, 1980.

[32] J. Knopfholz, C. C. D. Disserol, A. J. Pierin, F. L. Schirr, L. Streisky, L. L. Takito, P. M. Ledesma, J. R. Faria-Neto, M. Olandoski, C. L. P. da Cunha, and A. M. Bandeira, "Validation of the friedewald formula in patients with metabolic syndrome," *Cholesterol*, vol. 2014, pp. 1–5, Feb. 2014.

[33] A. S. Leopoldo, A. P. Lima-Leopoldo, M. M. Sugizaki, A. F. do Nascimento, D. H. S. de Campos, R. de Azevedo Melo Luvizotto, E. Castardeli, C. A. B. Alves, P. C. Brum, and A. C. Cicogna, "Involvement of l-type calcium channel and serca2a in myocardial

dysfunction induced by obesity," *Journal of Cellular Physiology*, vol. 226, pp. 2934–2942, Aug. 2011.

[34] N. N. Shahin, N. F. Abdelkader, and M. M. Safar, "A novel role of irbesartan in gastroprotection against indomethacin-induced gastric injury in rats: Targeting DDAH/ADMA and EGFR/ERK signaling," *Scientific Reports*, vol. 8, Mar. 2018.

[35] J. Liu, F. Wang, H. Luo, A. Liu, K. Li, C. Li, and Y. Jiang, "Protective effect of butyrate against ethanol-induced gastric ulcers in mice by promoting the anti-inflammatory, anti-oxidant and mucosal defense mechanisms," *International Immunopharmacology*, vol. 30, pp. 179–187, Jan. 2016.

[36] E. Disse, A. Pasquer, E. Pelascini, P.-J. Valette, C. Betry, M. Laville, C. Gouillat, and M. Robert, "Dilatation of sleeve gastrectomy: Myth or reality?," *Obesity Surgery*, vol. 27, pp. 30–37, June 2016.

[37] N. Pech, F. Meyer, H. Lippert, T. Manger, and C. Stroh, "Complications and nutrient deficiencies two years after sleeve gastrectomy," *BMC Surgery*, vol. 12, July 2012.

[38] K. Indireshkumar, J. G. Brasseur, H. Faas, G. S. Hebbard, P. Kunz, J. Dent, C. Feinle, M. Li, P. Boesiger, M. Fried, and W. Schwizer, "Relative contributions of "pressure pump" and "peristaltic pump" to gastric emptying," *American Journal of Physiology-Gastrointestinal and Liver Physiology*, vol. 278, pp. G604–G616, Apr. 2000.

[39] R. G. Marques, M. F. Americo, C. T. Spadella, L. A. Corá, R. B. Oliveira, and J. R. A. Miranda, "Different patterns between mechanical and electrical activities: an approach to investigate gastric motility in a model of long-term diabetic rats," *Physiological Measurement*, vol. 35, pp. 69–81, Dec. 2013.

[40] G. D. S. Hirst and S. M. Ward, "Interstitial cells: involvement in rhythmicity and neural control of gut smooth muscle," *The Journal of Physiology*, vol. 550, pp. 337–346, July 2003.

[41] K. Sanders, "A case for interstitial cells of cajal as pacemakers and mediators of neurotransmission in the gastrointestinal tract," *Gastroenterology*, vol. 111, pp. 492–515, Aug. 1996.

[42] K. Kelly and C. Code, "Canine gastric pacemaker," *American Journal of Physiology-Legacy Content*, vol. 220, pp. 112–118, Jan. 1971.

[43] J. D. Z. Chen, X. Zou, X. Lin, S. Ouyang, and J. Liang, "Detection of gastric slow wave propagation from the cutaneous electrogastrogram," *American Journal of Physiology-Gastrointestinal and Liver Physiology*, vol. 277, pp. G424–G430, Aug. 1999.

[44] H. Hashitani, A. P. Garcia-Londoño, G. D. S. Hirst, and F. R. Edwards, "Atypical slow waves generated in gastric corpus provide dominant pacemaker activity in guinea pig stomach," *The Journal of Physiology*, vol. 569, pp. 459–465, Nov. 2005.

[45] T. Ördög, M. Baldo, R. Danko, and K. M. Sanders, "Plasticity of electrical pacemaking by interstitial cells of cajal and gastric dysrhythmias in w/wv mutant mice," *Gastroenterology*, vol. 123, pp. 2028–2040, Dec. 2002.

[46] Y. I. Mahmoud and E. A. A. El-Ghffar, "Spirulina ameliorates aspirin-induced gastric ulcer in albino mice by alleviating oxidative stress and inflammation," *Biomedicine & Pharmacotherapy*, vol. 109, pp. 314–321, Jan. 2019.

[47] K. Sagun, V. K. Roy, R. S. Kumar, K. S. Ibrahim, T. Parimelazhagan, N. S. Kumar, and G. Gurusubramanian, "Antioxidant potential, anti-inflammatory activity and gastroprotective mechanisms of mallotus roxburghianus (muell.) against ethanol-induced gastric ulcers in wistar albino rats," *Journal of Functional Foods*, vol. 36, pp. 448–458, Sept. 2017.

[48] T. Shea-Donohue, L. Notari, R. Sun, and A. Zhao, "Mechanisms of smooth muscle responses to inflammation," *Neurogastroenterology & Motility*, vol. 24, pp. 802–811, Aug. 2012.

[49] T. Der, P. Bercik, G. Donnelly, T. Jackson, I. Berezin, S. M. Collins, and J. D. Huizinga,

"Interstitial cells of cajal and inflammation-induced motor dysfunction in the mouse small intestine," *Gastroenterology*, vol. 119, pp. 1590–1599, Dec. 2000.

[50] J. Melissas, A. Leventi, I. Klinaki, K. Perisinakis, S. Koukouraki, E. de Bree, and N. Karkavitsas, "Alterations of global gastrointestinal motility after sleeve gastrectomy," *Annals of Surgery*, vol. 258, pp. 976–982, Dec. 2013.

[51] S. Shah, P. Shah, J. Todkar, M. Gagner, S. Sonar, and S. Solav, "Prospective controlled study of effect of laparoscopic sleeve gastrectomy on small bowel transit time and gastric emptying half-time in morbidly obese patients with type 2 diabetes mellitus," *Surgery for Obesity and Related Diseases*, vol. 6, pp. 152–157, Mar. 2010.

[52] T. Masuda, M. Ohta, T. Hirashita, Y. Kawano, H. Eguchi, K. Yada, Y. Iwashita, and S. Kitano, "A comparative study of gastric banding and sleeve gastrectomy in an obese diabetic rat model," *Obesity Surgery*, vol. 21, pp. 1774–1780, Aug. 2011.

[53] F. Sista, V. Abruzzese, M. Clementi, S. Carandina, M. Cecilia, and G. Amicucci, "The effect of sleeve gastrectomy on GLP-1 secretion and gastric emptying: a prospective study," *Surgery for Obesity and Related Diseases*, vol. 13, pp. 7–14, Jan. 2017.

[54] R. J. Bennink, W. J. D. Jonge, E. L. Symonds, A. L. S. Rene M van den Wijngaard, M. A. Benninga, and G. E. Boeckxstaens, "Validation of gastric-emptying scintigraphy of solids and liquids in mice using dedicated animal pinhole scintigraphy," *Journal of Nuclear Medicine*, vol. 44, pp. 1099–104, July 2003.

[55] M. A. N. Souza, M. H. L. P. Souza, R. C. Palheta, P. R. M. Cruz, B. A. Medeiros, F. H. Rola, P. J. C. Magalhães, L. E. A. Troncon, and A. A. Santos, "Evaluation of gastrointestinal motility in awake rats: a learning exercise for undergraduate biomedical students," *Advances in Physiology Education*, vol. 33, pp. 343–348, Dec. 2009.

[56] F. de Assis Aquino Gondim, C. L. Rodrigues, J. R. V. da Graça, F. D. Camurça, H. M. P. de Alencar, A. A. dos Santos, and F. H. Rola, "Neural mechanisms involved in the delay of gastric emptying and gastrointestinal transit of liquid after thoracic spinal cord transection in awake rats," *Autonomic Neuroscience*, vol. 87, pp. 52–58, Feb. 2001.

[57] L. A. Szarka and M. Camilleri, "Methods for measurement of gastric motility," *American Journal of Physiology-Gastrointestinal and Liver Physiology*, vol. 296, pp. G461–G475, Mar. 2009.

[58] M. Camilleri, W. L. Hasler, H. P. Parkman, E. M. Quigley, and E. Soffer, "Measurement of gastrointestinal motility in the GI laboratory," *Gastroenterology*, vol. 115, pp. 747–762, Sept. 1998.

[59] K.-H. Lu, J. Cao, S. T. Oleson, T. L. Powley, and Z. Liu, "Contrast-enhanced magnetic resonance imaging of gastric emptying and motility in rats," *IEEE Transactions on Biomedical Engineering*, vol. 64, pp. 2546–2554, Nov. 2017.

Capítulo 3

An easy and low-cost biomagnetic methodology to study regional gastrointestinal transit in rats

Prefácio

Este trabalho foi idealizado originalmente pelo Prof. José Ricardo em colaboração com o Prof. Ricardo Brandt. Apesar de ser da área de Clínica Médica, o Prof. Ricardo Brandt sempre demonstrou muito entusiasmo em conciliar seus conhecimentos em gastroenterologia com pesquisa na área de biomagnetismo. Desta maneira, suas visitas ao Laboratório de Biomagnetismo sempre foram muito proveitosas para pensarmos em colaborações e pesquisas futuras.

Dessa forma, a ideia inicial desse projeto era aplicar a BAC para estudar o trânsito gastrintestinal regional através de imagens. Utilizando uma metodologia relativamente simples, a proposta possuia como inovação o fato de a BAC possibilitar a visualização da distribuição intrasegmentar de alimentos, tópico pouco explorado na literatura.

A princípio, quem iniciou a execução desse projeto foi o Dr. Fabiano Carlos Paixão (na época aluno de doutorado), entretanto, ao final do doutorado o projeto foi descontinuado. Desde o meu início no Laboratório de Biomagnetismo, em meados de 2016, acompanhei o Dr. Ronaldo Matos em seus projetos sobre imagens utilizando o sistema BAC. Desta forma, recebi a proposta do Prof. José Ricardo de dar continuidade e finalizar este projeto. Fizemos uma reavaliação dos dados obtidos até então, e realizamos mais uma série de experimentos para complementar o trabalho.

Este trabalho compreende a validação da BAC para avaliar, através de imagens, o trânsito gastrintestinal regional em ratos *ex vivo*. Para isso, utilizamos também a técnica de vermelho de fenol, a qual é considerada padrão ouro para este tipo de análise. A validação da BAC se mostrou interessante no que concerne o uso de imagens para estudar o trânsito gastrintestinal, fato que nunca havia sido alcançado em nosso laboratório. Além disso, esse trabalho serviu como base para otimizações no sistema BAC, as quais serão exploradas no próximo capítulo.

O resultado final desse projeto foi publicado na revista Biomedical Engineering/ Biomedizinische Technik.

DE GRUYTER Biomed. Eng.-Biomed. Tech. 2020; ■■■(■■■): 1–8

Leonardo Pinto*, Guilherme Soares, André Próspero, Erick Stoppa, Gabriel Biasotti, Fabiano Paixão, Armênio Santos, Ricardo Oliveira and José Miranda

An easy and low-cost biomagnetic methodology to study regional gastrointestinal transit in rats

https://doi.org/10.1515/bmt-2020-0202
Received August 3, 2020; accepted January 19, 2021; published online ■■■

Abstract: The identification of gastrointestinal (GI) motility disorders requires the evaluation of regional GI transit, and the development of alternative methodologies in animals has a significant impact on translational approaches. Therefore, the purpose of this study was to validate an easy and low-cost methodology (alternate current biosusceptometry – ACB) for the assessment of regional GI transit in rats through images. Rats were fed a test meal containing magnetic tracer and phenol red, and GI segments (stomach, proximal, medial and distal small intestine, and cecum) were collected to assess tracer's retention at distinct times after ingestion (0, 60, 120, 240, and 360 min). Images were obtained by scanning the segments, and phenol red concentration was determined by the sample's absorbance. The temporal retention profile, geometric center, gastric emptying, and cecum arrival were evaluated. The correlation coefficient between methods was 0.802, and the temporal retention of each segment was successfully assessed. GI parameters yielded comparable results between methods, and ACB images presented advantages as the possibility to visualize intrasegmental tracer distribution and the automated scan of the segments. The imaging approach provided a reliable assessment of several parameters simultaneously and may serve as an accurate and sensitive approach for regional GI research in rats.

Keywords: alternate current biosusceptometry; magnetic imaging; phenol red

***Corresponding author: Leonardo Pinto**, Department of Biophysics and Pharmacology, São Paulo State University, Biosciences Institute of Botucatu, Prof. Antonio Celso Wagner Zanin Street, 18618-689 Botucatu, Brazil, E-mail: leonardo.antonio@unesp.br. https://orcid.org/0000-0002-6037-6064
Guilherme Soares, André Próspero, Erick Stoppa, Gabriel Biasotti and José Miranda, Department of Biophysics and Pharmacology, São Paulo State University, Biosciences Institute of Botucatu, Botucatu, Brazil. https://orcid.org/0000-0002-4723-466X (G. Soares). https://orcid.org/0000-0001-5163-8280 (A. Próspero). https://orcid.org/0000-0002-8306-8056 (J. Miranda)
Fabiano Paixão, Science and Technology Institute, Federal University of São Paulo, São José dos Campos, Brazil
Armênio Santos, Department of Physiology and Pharmacology, Federal University of Ceará, Fortaleza, Brazil. https://orcid.org/0000-0003-4098-5652
Ricardo Oliveira, Ribeirão Preto Medical School, São Paulo University, Ribeirão Preto, Brazil

Introduction

Evaluation of gastrointestinal (GI) transit time is useful for identifying motility disorders. Gastroparesis, irritable bowel syndrome, diabetes, and other diseases are associated with GI motility disorders. Symptoms from distinct segments of the GI tract may overlap in clinical practice; therefore, the assessment of regional GI transit (gastric, small bowel, and colon) is appropriate [1–3]. Despite the importance of regional GI transit evaluation, studying meal distribution throughout the animal's GI tract is useful. It has been applied in a wide range of pharmacological and physiological studies, which may significantly impact translational approaches. More specifically, this methodology was employed to elucidate the role of several molecules in the GI transit (aiming both the study of established drugs side effects [4] and the development of new ones for dysmotility treatments [5, 6]), neural mechanisms involved with GI dysmotility [7, 8], prediction of plasma concentration of drugs [9], and influence of hormones [10], aging [11], and injuries [12] in GI function. Therefore, studies of meal distribution in animals allow us to perform a careful evaluation of regional GI transit, resulting in essential information about the dynamics of GI distribution of tracers segmentally. It is worth to point out that, remarkably, the assessment of food distribution within a specific GI segment remains challenging in laboratory and pre-clinical conditions.

Among the tracers used for studying meal distribution (radiolabeled, radiopaque, and colorimetric tracers), phenol red is the gold standard [7, 13, 14]. The technique is based upon the measurement of light absorbance in processed samples containing phenol red. Therefore, the division of the GI tract into different segments enables the quantification of phenol red retention in a specific region of the GI tract. However, phenol red analysis presents some drawbacks. There is no information about the distribution of phenol red within the segment, and the samples need to be

processed. Hence, the development of new methods to provide a detailed evaluation of the regional GI transit without sample processing is essential.

The alternate current biosusceptometry (ACB) is a biomagnetic technique that allows the detection and monitoring of magnetic tracers in biological systems [15]. ACB was validated in humans for gastric motor function analysis with scintigraphy and intestinal transit time using breath hydrogen test [16, 17]. In dogs, ACB demonstrated a strong correlation with manometry, electromyography, and electrogastrography [18–20]. In rats, the methodology was validated for gastric motor function analysis with strain-gauge [21], and recently several GI motility studies employing ACB were carried out in rats [22–24].

In a previous feasibility study, the ACB system was successfully employed to obtain *in vitro* images of magnetic powder distribution by scanning the samples. Furthermore, the tracers' signal was proportional to the tracer amount in each pixel of the image [25]. Even though it was noticed the potential of ACB to study the GI transit using images until now, there are no reports of a reliable methodology to perform such tasks in animal experiments. In this present study, we developed and validated an easy and low-cost methodology based on the ACB imaging technique, with ferrite microparticles as tracer, to evaluate the regional GI transit in rats *ex vivo*.

Materials and methods

Magnetic microparticles

As a magnetic tracer, we employed manganese ferrite ($MnFe_2O_4$) microparticles (Ferroxcube, El Paso, USA) with a relative magnetic permeability (μ_r) of 3,000 [15] and sizes between 53 and 75 μm. The magnetic material and its size were chosen because it is non-absorbable and also inert at any pH [21].

AC biosusceptometry fundamentals and imaging methodology

The single-channel ACB is composed of two coaxial pairs of coils; one pair is the reference system, and the other is the measurement system. Each pair consists of an induction and a detection coil. The reference and measurement systems are connected in a gradiometric configuration to minimize the background signal and increase the signal-to-noise ratio. An alternate current is applied to the induction coils, generating a magnetic flux in the detection coils. The presence of magnetic materials near the detection coil disbalances the system's total magnetic flux, thus generating a voltage [26]. The system's working principle can be modeled, as shown in Eq. (1) [15, 27]:

$$V_m = \frac{d}{dt}\left[\left(\frac{1}{\mu_0 I_r}\right)\int B_a(r)\cdot B_r(r)\chi(r,\omega)dV\right] \quad (1)$$

Where V_m is the measured voltage in the detection coils, μ_0 is the vacuum magnetic permeability, I_r is the reciprocal current, from the reciprocal principle where the $B_r(r)$ is the reciprocal field produced by this current, $B_a(r)$ is the induction coil applied field and $\chi(r,\omega)$ is the magnetic susceptibility in the volume for a given induction field frequency. Note that this equation is valid for any geometry and can be solved numerically. Also, assuming symmetric geometries for each GI segment and that the magnetic field produced by the magnetic material magnetization is uniform in the detection coil cross-section, this equation can be solved straightforward.

Figure 1 shows a schematic of the ACB imaging methodology. A lock-in amplifier (SR830, Stanford Research Systems, Sunnyvale, USA) generates a signal of 0.7 V at 10 kHz, which is amplified to 40 V by a power amplifier (TIP 800, Ciclotron, Barra Bonita, Brazil) and applied to the inductor coils. The electrical signal generated in the detection coils returns to the lock-in amplifier, which processes the output signal to acquire the 10 kHz component and converts it to a DC signal. The signal is recorded online (LabVIEW 2010, National Instruments, Austin, USA), digitized by an A/D card (DAQ-Pad-6015, National Instruments, Austin, USA), and stored in a computer.

We attached the samples into a CNC XYZ-stage with a precision of 0.1 mm, controlled using specific software (MachMill, Newfangled Solutions LLC, Livermore Falls, USA), and connected with LabVIEW for data recording. The measurement of each position consists of 1s acquisition with the sample still, and the mean value of each measurement point is used to reconstruct the image. Each signal intensity was related to a pixel value proportional to the concentration of magnetic tracer in the measurement position. Raw images were processed (MatLab, Mathworks Inc., Natick, USA) with background correction and spline interpolation.

ACB characterization

A cylindrical phantom with 1.3 mm diameter and 2 mm height, containing 4.4 mg of magnetic microparticles, was used for the sensitivity tests. For the axial sensitivity tests, the phantom was moved at fixed distances from 2 to 20 mm. The phantom was moved laterally at 25 mm of distance from the detection coil for the transversal sensitivity test, with a fixed distance of 2 mm.

A 30 × 200 mm phantom was constructed to simulate a rat small intestine, which consisted of seven cylindrical holes (1.3 mm diameter and 2 mm height) at distinct distances (40, 30, 20, 15, and 10 mm) containing 5 mg of magnetic microparticles. The phantom was positioned at 2 mm from the detection coil and scanned in a 50 × 220 mm array with a step of 5 mm. The scanning was repeated in 10 different days at distinct times, and the area under the curve for each image was calculated. The dispersion of the results was expressed in terms of the *coefficient of variation* (CV) using Eq. (2):

$$CV = \frac{\sigma}{|\mu|}\times 100 \quad (2)$$

Where σ is the standard deviation to the mean μ of the 10 measurements.

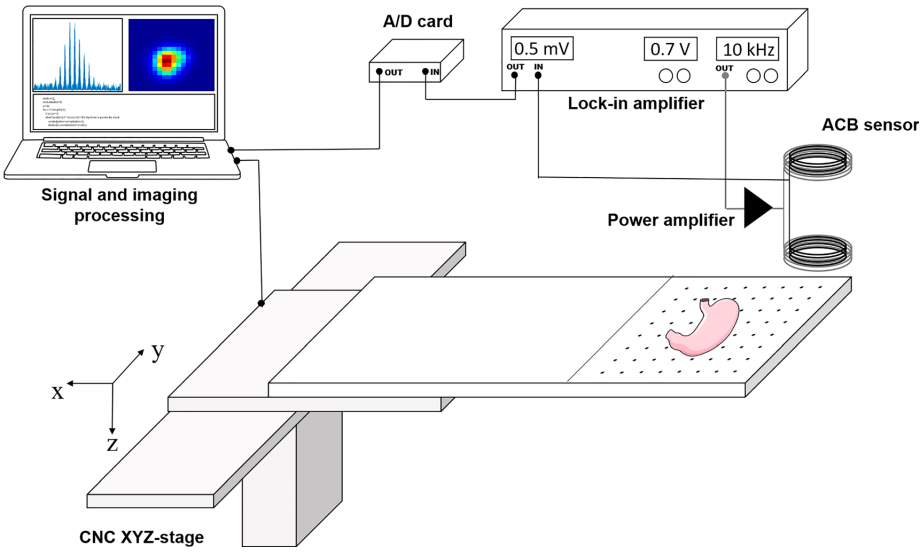

Figure 1: Experimental setup of ACB imaging. The sample is attached to a computer-controlled CNC XYZ-state, which is scanned using a fixed ACB sensor. The lock-in amplifier generates a signal, which is amplified and delivered to the inductor coils (black lines). The electrical signal from the samples returns from the detector coils (gray lines) to the lock-in amplifier is digitized by an A/D card and stored in a computer for signal and imaging processing.

Animals and experimental design

We used 25 male Wistar rats (250–300 g) from the Animal Laboratory (ANILAB, Paulínia, SP, Brazil), housed under controlled temperature (24 ± 2 °C), humidity (60 ± 5%) and a 12 h light/dark cycle with *ad libitum* access to chow (Presence Nutrição Animal, Paulínia, SP, Brazil) and tap water. The animals were handled according to the Ethical Principles in Animal Research of the Brazilian College of Animal Experimentation and the Bioscience Institute/UNESP Ethics on the Use of Animals (protocol number 1032).

We divided the rats into five distinct groups (0, 60, 120, 240, and 360 min), according to the time after test meal ingestion in which they were euthanized. Rats were fasted for 12 h and fed with a 3.015 g test meal composed of 0.5 g of magnetic microparticles and 0.015 g of phenol red (Merck, Darmstadt, Germany), incorporated into chow (2.5 g). It is worth pointing out that the 0 min group was performed 10 min after the feeding interval, as with all the other groups. We euthanized the rats by cervical dislocation, and a midline laparotomy was performed. The gut was carefully removed and stretched, then excised to obtain five consecutive segments: stomach, proximal (~40%), medial (~30%), and distal small intestine (~30%), and cecum.

To obtain the ACB images, we scanned the stomach and cecum in an 85 × 85 mm array; proximal small intestine in a 50 × 720 mm array; and medial and distal small intestine in a 50 × 480 mm array. All the scans were performed with a step of 5 and 2 mm distance between the detection coil and the samples. After background correction and interpolation, images were segmented with a 30% threshold of the maximum pixel value, and the area under curve normalized by the number of non-zero value pixels was calculated.

The methodology to quantify the amount of phenol red is widely described in the literature [7, 14, 28]. Briefly, we added the segments into 100 mL of 0.1 N NaOH solution. Next, homogenized the segments using an electric mixer for 30 s. After 20 min, we centrifuged 10 mL of the supernatant for 10 min (2,800 rpm). We precipitated the proteins in 5 mL of the homogenate with 0.5 mL of trichloroacetic acid (20% wt vol^{-1}), and then the solution was centrifuged again for 20 min. Finally, we added 3 mL from the supernatant to 4 mL of 0.5 N NaOH, and the absorbance of the samples was read by an Ultrospec 2,000 Spectrophotometer (Pharmacia Biotech, USA) at 560 nm.

Data and statistical analysis

Using Eq. (3), we calculated the ACB imaging and phenol red retention (%) in each GI segment:

$$R_x = \frac{TR_x}{TR_t} \tag{3}$$

Where R_x is the retention in segment x, TR_x is the tracer recovered in segment x, and TR_t is the total tracer recovered. Retention values for each segment were used to calculate the geometric center of GI transit [29, 30], a quantitative evaluation of the distribution and progression of the tracer along the GI tract, accordingly to Eq. (4):

$$\mathrm{GC} = \sum_{n=1}^{5} \frac{R_n \times n}{R_t} \tag{4}$$

Where GC is the geometric center, R_n is the tracer retention in segment number n, and R_t is the total retention. The geometric center ranges from 1 to 5, which means that a value of 1 indicates maximal retention in the stomach, and 5 indicates maximum retention in the cecum.

We obtained the GI transit statistical moment through the temporal average pondered by retention value curves, normalized by the area under the curve [31]. The following parameters were calculated: Mean Gastric Emptying Time (MGET), defined as the time t (min) when a mean amount of tracer is emptied from the stomach; Mean Cecum Arrival Time (MCAT), defined as the time t (min) when occurred an increase in the mean amount of tracer in the cecum. We used the Pearson correlation to determine the correlation between the methodologies.

Statistical differences between ACB image and phenol red were determined with Student's t-test for paired means. Values of $p<0.05$ were considered statistically significant. We performed all analyses and figures using GraphPad Prism 7.05 (GraphPad Software, La Jolla, California, USA). All of the results are presented as mean ± standard deviation.

Results

Figure 2A shows the axial sensitivity of ACB. Figure 2B shows the ACB signal when the phantom was moved laterally from the detection coil. The spatial resolution was 13.8 mm, measured as the full width at the half maximum (FWHM) of the curve. The image of the phantom (Figure 2C) shows that ACB imaging was able to solve two distinct structures with a distance of 15 mm. Still, when the distance decreases to 10 mm, the separate structures were not differentiated, which confirms the FWHM result. Furthermore, a CV of 1.89% was obtained from 10 repeated measurements, reinforcing the low dispersion and inter-day variability of the methodology.

Figure 3 shows examples of *ex vivo* ACB images acquired at different time points. Figure 3A shows the images for all segments at 60 min after test meal ingestion, while Figure 3C shows the images for all segments at 360 min. Figure 3B, D are the local distribution of pixels intensity along each segment length for 60 and 360 min, respectively.

Geometric center values are shown in Figure 4. The tracers GC increased with time, ranging from 1.18 ± 0.12 to 3.81 ± 0.51 for ACB images and from 1.14 ± 0.06 to 3.94 ± 0.51 for phenol red.

Figure 5 shows the temporal retention profile of each segment for the ACB images and phenol red. Initially, the tracers were found in the stomach and were progressively emptied to the small intestine, representing the gastric emptying process. Gastric retention values ranged from 89.87 ± 7.78% to 18.50 ± 10.47% for ACB images, and from 90.51 ± 6.49% to 15.50 ± 13.53% to phenol red. The small intestine segment retention profile was similar for both methods. Proximal small intestine showed the lowest mean retention values compared to all other segments, which reached the maximum retention of 2.87 ± 1.64% for ACB image (60 min) and 5.87 ± 4.03% for phenol red (120 min). Differently from the proximal segment, medial and distal segments retention values were increased over time, suggesting that the intestinal transit is slower in these segments. Medial small intestine mean retention was maximum for ACB images at 240 min (22.88 ± 14.54%), while for phenol red, the maximum mean retention was at

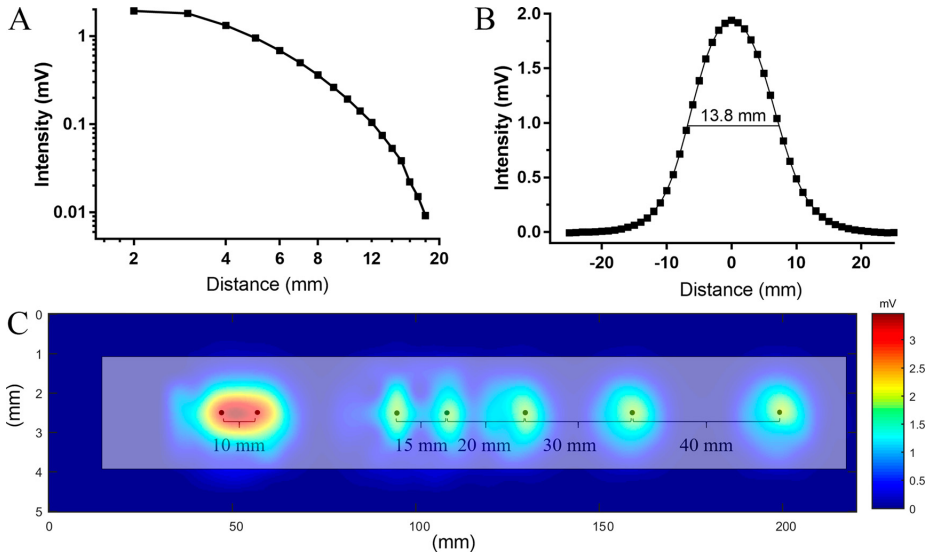

Figure 2: ACB characterization. The intensity of the signal detected as a function of the axial (A) and transversal (B) distance for a cylindrical phantom containing 4.4 mg of magnetic tracers; (C) reconstructed image of the small intestine phantom.

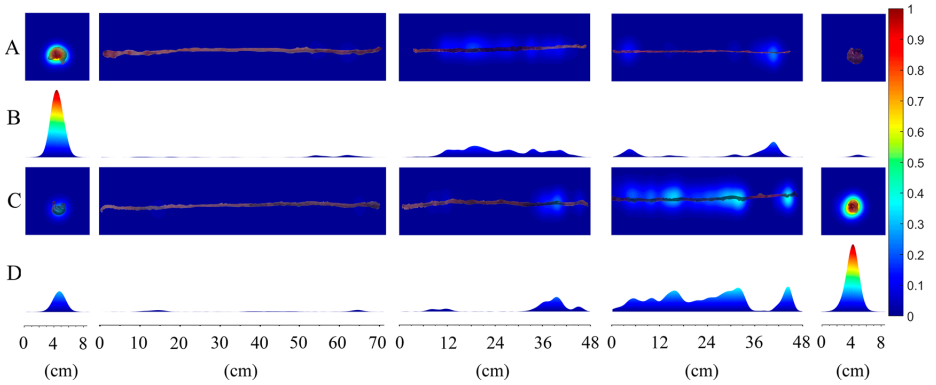

Figure 3: Representative example of normalized ACB images and local distribution of pixels intensity for 60 (A and B) and 360 min (C and D) after test meal ingestion. Images show the following segments from left to right: stomach, proximal, medial, and distal small intestine, and cecum.

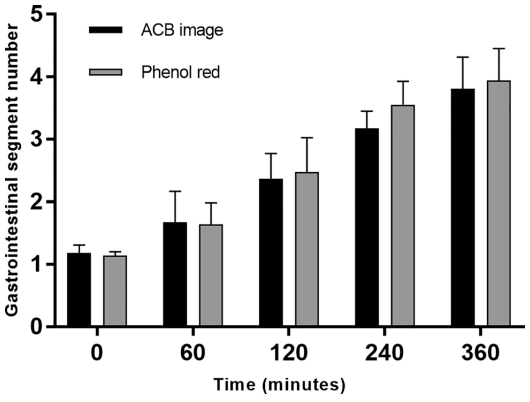

Figure 4: Geometric center values representing the progression of tracers from the stomach (segment number 1) to the cecum (segment number 5).

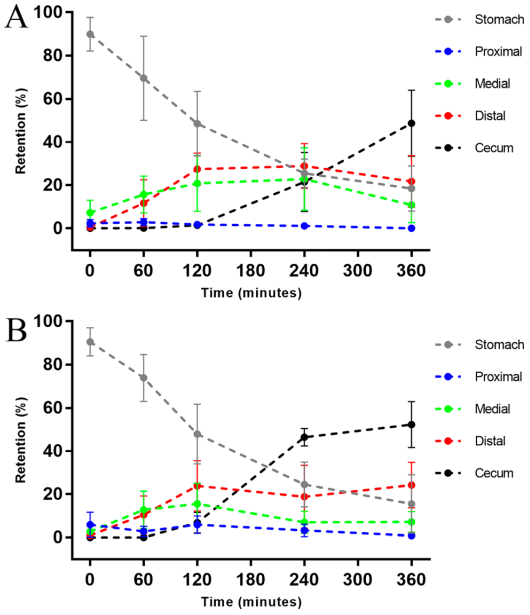

Figure 5: Temporal variation of retention values (%) in each segment obtained from (A) ACB images and (B) phenol red data.

120 min (15.54 ± 9.51%). For the distal segment, the maximum mean retention was 28.93 ± 10.41 (240 min) for the ACB image and 24.21 ± 10.56 (360 min) for phenol red. For the first two moments (0 and 60 min), the cecum retention values were negligible, attesting that the tracers were still in transit, which started to reach the cecum after 120 min. The mean retention values of the 240 min group showed a significant difference between the methods ($p<0.01$), suggesting that the phenol red arrived at the segment faster than the magnetic tracer.

We also quantified GI transit parameters by statistical moments. MGET values were 128.84 ± 29.63 min and 125.51 ± 30.83 min for ACB images and phenol red, respectively. MCAT values were 279.31 ± 21.16 min for ACB image and 260.43 ± 24.26 min for phenol red. No statistical difference was found in the parameters between the methods.

The Pearson correlation coefficient between the methods was $R=0.802$ with $p<0.001$ (Figure 6), which represents a strong correlation and low dispersion.

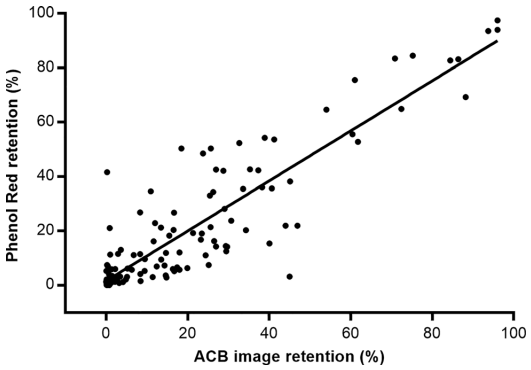

Figure 6: Pearson correlation between ACB image and phenol red retention values.

Discussion

The ACB imaging methodology was able to acquire images from the magnetic microparticles incorporated in the test meal for the assessment of regional GI transit in rats, showing the potential of ACB imaging as an alternative tool for these analyzes. Methods that apply radioactive markers to assess the GI transit require a high implementation cost, the necessity of specific equipment and installations, and the use of ionizing radiation, which makes phenol red and ACB imaging more suitable for the use in laboratories. Even though, ACB imaging presented several advantages in comparison to phenol red: the automatic scan of the segment, which does not require sample processing; the possibility of tracer distribution visualization by images; and a more precise data quantification, once that it takes into account the tracer distribution within a given segment, which makes ACB imaging suitable for studies of injuries or diseases that affect the food distribution in a specific segment.

Geometric center quantification showed that both methods were able to detect tracers' progression, once that the GC was shifted through the segments as the time after the test meal increased (Figure 4). The GI transit parameters (MGET and MCAT) were comparable to the ones found in the literature for *in vivo* measurements [22, 24, 32], which reinforces our results' reliability.

The temporal data showed the dynamics of the tracers through the GI tract (Figure 5). It was possible to observe the gastric emptying and cecal filling for both tracers. As for the small intestine, a gradient of propagation velocities of contraction that decreases aborally has been reported in dogs [33]. In rats, by using phenol red as a tracer, Sawamoto et al. [9] estimated the GI transit profile of different segments. The paper shows that the small intestine's transit rate constant was maximum at the duodenum (proximal segment) and minimum at the ileum (distal segment). These previous studies corroborated our results once we found a retention gradient for the different small intestine segments. The proximal small intestine had the lowest mean retention compared to other small intestine segments, while the distal segment showed the highest values. Moreover, the increased mean retention values in the distal segment may be a consequence of the ileocecal valve, which separates the small intestine and cecum and consequently accumulates the tracers. We observed this accumulation in Figure 3A, C, where the local distribution of pixels intensity shows a peak at the end of the distal small intestine segment; therefore, the magnetic tracer is concentrated in the ileocecal valve.

Another finding was that the phenol red was delivered to the cecum faster than the magnetic tracer (Figure 5). This difference is probably because phenol red is part of chime's liquid phase, while the magnetic tracer is a non-digestible solid [15]. Therefore, the magnetic microparticles may be more reliable than phenol red for solid meal studies in the small intestine and cecum.

The study of regional GI transit in laboratory animals is essential, once that is the first step to achieve clinical trials of drugs or diseases. In this present work, we used rats to validate the ACB imaging, since phenol red requires the euthanasia of the animals, and that the spatial resolution of ACB limit its application to *ex vivo* images (for small animals – it is worth to point out that for humans the system might be able to solve different segments and even intrasegmental distributions). Even though improvements in the methodology or the system's characteristics may result in a spatial resolution that enables *in vivo* images in rats, in the current state of the art, further studies may address the effects of drug, diets, or diseases, specifically on each region of the GI tract in rats.

Research funding: The São Paulo Research Foundation supported this work (FAPESP – grant no. 2015/14923-9), Coordenação de Aperfeiçoamento de Pessoa de Nível Superior – Brasil (CAPES – Financial code 001) and Conselho Nacional de Desenvolvimento Científico e Tecnológico (CNPq).
Author contributions: All authors have accepted responsibility for the entire content of this manuscript and approved its submission.
Competing interests: Authors state no conflict of interest.

Ethical approval: The animals were handled according to the Ethical Principles in Animal Research of the Brazilian College of Animal Experimentation and the Bioscience Institute/UNESP Ethics on the Use of Animals (protocol number 1032).

References

1. Sarosiek I, Selover KH, Katz LA, Semler JR, Wilding GE, Lackner JM, et al. The assessment of regional gut transit times in healthy controls and patients with gastroparesis using wireless motility technology. Aliment Pharmacol Ther 2010;312:313–22.
2. Sfarti C, Trifan A, Hutanasu C, Cojocariu C, Singeap AM, Stanciu C. Prevalence of delayed gastric emptying of solids in functional dyspepsia and its relationship to symptoms. Rev Med Chir Soc Med Nat Iasi 2009;113:1040–7.
3. Serra J, Azpiroz F, Malagelada JR. Impaired transit and tolerance of intestinal gas in the irritable bowel syndrome. Gut 2001;48:14–9.
4. Wu C-L, Hung C-R, Chang F-Y, Lin L-C, Pau K-YF, Wang PS. Effects of evodiamine on gastrointestinal motility in male rats. Eur J Pharmacol 2002;457:169–76.
5. Bajad S, Bedi K, Singla A, Johri R. Piperine inhibits gastric emptying and gastrointestinal transit in rats and mice. Planta Med 2001;67:176–9.
6. Qiu W-C, Wang Z-G, Lv R, Wang W-G, Han X-D, Yan J, et al. Ghrelin improves delayed gastrointestinal transit in alloxan-induced diabetic mice. World J Gastroenterol 2008;14:2572.
7. Gondim FA, da-Graca JR, de-Oliveira GR, Rego MC, Gondim RB, Rola FH. Decreased gastric emptying and gastrointestinal and intestinal transits of liquid after complete spinal cord transection in awake rats. Braz J Med Biol Res 1998;31:1605–10.
8. Gondim FdAA, Rodrigues CL, da Graça JRV, Camurça FD, de Alencar HMP, dos Santos AA, et al. Neural mechanisms involved in the delay of gastric emptying and gastrointestinal transit of liquid after thoracic spinal cord transection in awake rats. Auton Neurosci 2001;87:52–8.
9. Sawamoto T, Haruta S, Kurosaki Y, Higaki K, Kimura T. Prediction of the plasma concentration profiles of orally administered drugs in rats on the basis of gastrointestinal transit kinetics and absorbability. J Pharm Pharmacol 1997;49:450–7.
10. Wu C-L, Chang F-Y, Pau K-YF, Wang PS. Pharmacological effects of oxytocin on gastric emptying and intestinal transit of a non-nutritive liquid meal in female rats. Naunyn Schmiedebergs Arch Pharmacol 2003;367:406–13.
11. Smits GJ, Lefebvre RA. Influence of aging on gastric emptying of liquids, small intestine transit, and fecal output in rats. Exp Gerontol 1996;31:589–96.
12. Gondim F, Rodrigues C, Lopes A, Leal P, Camurca F, Freire C, et al. Effect of preinjury large bowel emptying on the inhibition of upper gastrointestinal motility after spinal cord injury in rats. Dig Dis Sci 2003;48:1713–8.
13. Padmanabhan P, Grosse J, Asad AB, Radda GK, Golay X. Gastrointestinal transit measurements in mice with 99mTc-DTPA-labeled activated charcoal using NanoSPECT-CT. EJNMMI Res 2013;3:60.
14. Souza MA, Souza MH, Palheta RC Jr., Cruz PR, Medeiros BA, Rola FH, et al. Evaluation of gastrointestinal motility in awake rats: a learning exercise for undergraduate biomedical students. Adv Physiol Educ 2009;33:343–8.
15. Baffa O, Oliveira RB, Miranda JR, Troncon LE. Analysis and development of AC biosusceptometer for orocaecal transit time measurements. Med Biol Eng Comput 1995;33:353–7.
16. Americo MF, Oliveira RB, Romeiro FG, Baffa O, Cora LA, Miranda JR. Scintigraphic validation of AC Biosusceptometry to study the gastric motor activity and the intragastric distribution of food in humans. Neuro Gastroenterol Motil 2007;19:804–11.
17. Oliveira RB, Baffa O, Troncon LE, Miranda JR, Cambrea CR. Evaluation of a biomagnetic technique for measurement of orocaecal transit time. Eur J Gastroenterol Hepatol 1996;8:491–5.
18. Americo MF, Ietsugu MV, Romeiro FG, Cora LA, Oliveira RB, Miranda JR. Effects of meal size and proximal-distal segmentation on gastric activity. World J Gastroenterol 2010;16:5861–8.
19. Moraes R, Cora LA, Americo MF, Oliveira RB, Baffa O, Miranda JR. Measurement of gastric contraction activity in dogs by means of AC biosusceptometry. Physiol Meas 2003;24:337–45.
20. Andreis U, Americo MF, Cora LA, Oliveira RB, Baffa O, Miranda JR. Gastric motility evaluated by electrogastrography and alternating current biosusceptometry in dogs. Physiol Meas 2008;29:1023–31.
21. Americo MF, Marques RG, Zandona EA, Andreis U, Stelzer M, Cora LA, et al. Validation of ACB *in vitro* and *in vivo* as a biomagnetic method for measuring stomach contraction. Neuro Gastroenterol Motil 2010;22:1340–4.
22. Quini CC, Americo MF, Cora LA, Calabresi MF, Alvarez M, Oliveira RB, et al. Employment of a noninvasive magnetic method for evaluation of gastrointestinal transit in rats. J Biol Eng 2012;6:6.
23. Matos JF, Americo MF, Sinzato YK, Volpato GT, Cora LA, Calabresi MF, et al. Role of sex hormones in gastrointestinal motility in pregnant and non-pregnant rats. World J Gastroenterol 2016;22:5761–8.
24. Calabresi MF, Quini CC, Matos JF, Moretto GM, Americo MF, Graca JR, et al. Alternate current biosusceptometry for the assessment of gastric motility after proximal gastrectomy in rats: a feasibility study. Neuro Gastroenterol Motil 2015;27:1613–20.
25. Moreira M, Murta LO, Baffa O. Imaging ferromagnetic tracers with an ac biosusceptometer. Rev Sci Instrum 2000;71:2532–8.
26. Miranda JR, Baffa O, de Oliveira RB, Matsuda NM. An AC biosusceptometer to study gastric emptying. Med Phys 1992;19:445–8.
27. Bastuscheck C, Williamson S. Technique for measuring the ac susceptibility of portions of the human body or other large objects. J Appl Phys 1985;58:3896–906.
28. Bennink RJ, De Jonge WJ, Symonds EL, van den Wijngaard RM, Spijkerboer AL, Benninga MA, et al. Validation of gastric-emptying scintigraphy of solids and liquids in mice using dedicated animal pinhole scintigraphy. J Nucl Med 2003;44:1099–104.
29. Williams CL, Villar RG, Peterson JM, Burks TF. Stress-induced changes in intestinal transit in the rat: a model for irritable bowel syndrome. Gastroenterology 1988;94:611–21.

30. Troncon LE, Santos AA, Garbacio VL, Secaf M, Verceze AV, Cunha-Melo JR. Inhibition of gastric emptying and intestinal transit in anesthetized rats by a Tityus serrulatus scorpion toxin. Braz J Med Biol Res 2000;33:1053–8.
31. Podczeck F, Newton JM, Yuen KH. The description of the gastrointestinal transit of pellets assessed by gamma scintigraphy using statistical moments. Pharm Res 1995;12:376–9.
32. de Lima MB, Gama LA, Hauschildt AT, Dall'Agnol DJR, Cora LA, Americo MF. Gastrointestinal motility, mucosal mast cell, and intestinal histology in rats: effect of prednisone. Biomed Res Int 2017;2017:4637621.
33. Siegle ML, Buhner S, Schemann M, Schmid HR, Ehrlein HJ. Propagation velocities and frequencies of contractions along canine small intestine. Am J Physiol 1990;258:G738–44.

Capítulo 4

Single-channel and multi-channel AC Biosusceptometry systems to reconstruct quantitative images of magnetic nanoparticles

Prefácio

No início de 2019, nosso laboratório escreveu um projeto em parceria com o Prof. Oswaldo Baffa Filho (USP Ribeirão Preto) e o Prof. Andris Figueiroa Bakuzis (UFG) para o programa Probral, fruto da parceria entre a CAPES e o Serviço Alemão de Intercâmbio Acadêmico (DAAD) para fomento de projeto de pesquisa em parceria ao Physikalisch-Technische Bundesanstalt (PTB).

O PTB é o instituto nacional de metrologia da Alemanha, o qual possui sua sede em Berlin. Dentro de inúmeras linhas de pesquisa, o PTB é referência mundial no estudo de nanopartículas magnéticas, área que nosso laboratório iniciou os estudos recentemente. Felizmente, o projeto foi aceito, o qual resultou na oportunidade para alunos das três universidades do Brasil (UNESP, USP e UFG) irem para Alemanha, além da visita de pesquisadores do PTB ao Brasil. Em Outubro de 2019, tive a oportunidade de viajar para Alemanha, e permanecer durante seis meses como pesquisador visitante no PTB em Berlin. O objetivo da minha visita foi primeiramente aprender as técnicas utilizadas no PTB, as quais são praticamente únicas no mundo, e além disso, os pesquisadores do PTB nos ajudaram a aprimorar a técnica BAC, mais especificamente em relação ao problema inverso, o qual sempre foi um tópico almejado pelo Prof José Ricardo, desde seu mestrado.

Como resultado, houve uma extraordinária troca de conhecimento entre todos os laboratórios, o qual culminou no desenvolvimento de inúmeros projetos. Entre tais projetos desenvolvidos, este trabalho consiste na resolução do problema inverso para os sistemas mono e multi canal da BAC. Através do problema inverso, as imagens obtidas apresentam como unidade massa de partículas, e não mais a unidade de tensão. Devido a essa implementação, a BAC pode ser utilizada como técnica alternativa para diversos estudos na área de nanopartículas magnéticas.

Portanto, este trabalho é apenas um projeto inicial de vários que foram e estão sendo desenvolvidos. Neste capítulo o enfoque foi dado a resolução do problema inverso para estudo futuros envolvendo o trânsito gastrintestinal.

Single-channel and multi-channel AC Biosusceptometry systems to reconstruct quantitative images of magnetic nanoparticles

Leonardo A. Pinto[1], Gabriel G. Biasotti[1], André G. Próspero[1], Guilherme A. Soares[1], Gustavo S. Rodrigues[1], Erick G. Stoppa[1], Maik Liebl[2], Frank Wiekhorst[2], José R. Miranda[1]

[1]Institute of Biosciences, Department of Biophysics and Pharmacology, São Paulo State University, UNESP, Botucatu, Brazil.

[2]PTB – Physikalisch-Technische Bundesanstalt, 10587 Berlin, Charlottenburg, Germany

Corresponding author

Leonardo Antonio Pinto, +55 14 3880-0285, Instituto de Biociências, UNESP – Rua Prof. Dr. Antonio Celso Wagner Zanin, 18618-689 Botucatu, Brazil.

Email: leonardo.antonio@unesp.br

Abstract

Non-invasive magnetic imaging techniques are necessary to assist biomedical applications of magnetic nanoparticles by detecting their distribution. In alternate current biosusceptometry systems, an alternate magnetic field is applied to magnetize the magnetic nanoparticles through excitation coils, and pick-up coils acquire its response. In this present work, we compared the single- and multi-channel alternate current biosusceptometry systems to reconstruct quantitative images of magnetic nanoparticles by solving the inverse problem. The magnetic nanoparticle type Perimag was used to prepare a total of 12 cubic phantoms and two phantoms designed with the shape of a rat's stomach. The single-channel system presented a sensitivity of 0.76 mg, while for the multi-channel system, a value of 1.01 mg was found. Furthermore, the single-channel system distinguished between the different stomach phantom sizes, while for the multi-channel, the images were very similar. We presented two alternate current biosusceptometry systems to reconstruct quantitative images of magnetic nanoparticles. Our results demonstrate that both systems showed sensitivity in the milligram scale and may be used as a tool for magnetic nanoparticles and gastroenterology studies with a low cost and portability.

Keywords: alternate current biosusceptometry, inverse problem, magnetic nanoparticles

Introduction

Magnetic nanoparticles (MNPs) present great versatility due to their physical and chemical characteristics such as reduced size, composition, and magnetic properties, enabling several biomedical applications as a cancer treatment by hyperthermia and controlled drug delivery [1].Thus, techniques capable of detecting, locating, and quantifying MNPs in the biological environment are indispensable to assist biomedical applications [2, 3]. For this purpose, different techniques were developed to reconstruct MNPs spatial distributions based on the MNPs magnetic properties. The highly sensitive Magnetorelaxometry (MRX), Magnetic Particle Imaging (MPI), and Magnetic Susceptibility Imaging (MSI) have been used in MNPs studies [4–6]. Despite the fact that each of these techniques employs distinct physic properties of the MNPs, all of them use magnetic field sensors to detect the MNPs response after or during exposure to a magnetizing field. To reconstruct quantitative spatial MNP distributions, an ill-posed inverse problem must be solved, and distinct strategies have been adopted (e.g., multiple magnetizing fields and magnetic field sensor, magnetic field gradients, and frequency decodification) [5, 7].

The Alternate Current Biosusceptometry (ACB) is a coil-based magnetic technique that detects magnetic materials through a lower instrumental and operational cost and less technical effort than MRX, MPI, and MSI [8, 9]. Although ACB imaging approaches have been recently applied to study the regional gastrointestinal transit in rats *ex vivo* [10] and to map the biodistribution of MNPs in rats *in vivo* [11], there is currently no quantitative ACB imaging.

In the current state of the art, there are two methodologies to reconstruct MNPs spatial distributions using ACB: a scanning approach employing a single-channel system or multiple detection coils. The scanning approach consists of moving a single-channel ACB system to register the MNPs signal in a predetermined number of spatial points [10, 12]. The multi-channel ACB system uses multiple distinct detection coils to simultaneously record the MNPs signal in multiples space points. The images are reconstructed in a field-of-view (FOV) determined by the system's geometric and acquisition characteristics [11].

In this comparison study, we used the single- and multi-channel ACB systems to re-

construct 2D quantitative imaging of MNPs distribution. Twelve gypsum cubes and two phantoms simulating a rat's stomach containing different MNPs mass were used to evaluate both ACB system's precision to reconstruct and quantify MNPs distributions. We compared both systems for solving the inverse problem to reconstruct the phantoms distributions, aiming for future applications in *in vivo* MNPs biodistribution and gastrointestinal transit studies.

Material and Methods

ACB system and instrumentation

The ACB system works as a double flux transformer with an air core and is composed of a sensor and electronic devices. The sensor consists of one pair of excitation coil, while the number of detection coil pairs depends on the system adopted (*e.g.*, one pair for the single-channel and multiple pairs for the multi-channel system). Each pair of excitation and detection coils can be divided into two sub-systems: the reference and the measurement system. The reference system is placed far from the sample to subtract the environmental noise, while the measurement system is used to detect the samples' signal. The electronic devices include a lock-in amplifier (SR830, Stanford Research Systems, USA), an audio amplifier (TIP 800, Ciclotron, Brazil), and an A/D board (DAQPad 6015, National Instruments, USA). The lock-in is used to generate an AC voltage with a specific phase and frequency, amplified by the audio amplifier to feed the excitation coils, resulting in an AC magnetic field for the sample's magnetizing. When a magnetic material is near the sensor, there is an imbalance in the measurement system's magnetic flux. The electric signal difference between measurement and reference system is the ACB signal due to material magnetization. The signals are read-out as a voltage by the lock-in amplifier, which is then acquired at a 20 Hz sampling rate using the A/D board and LabView software (National Instruments, USA). In this present work, we used the single- and multi-channel ACB systems described in the following sections.

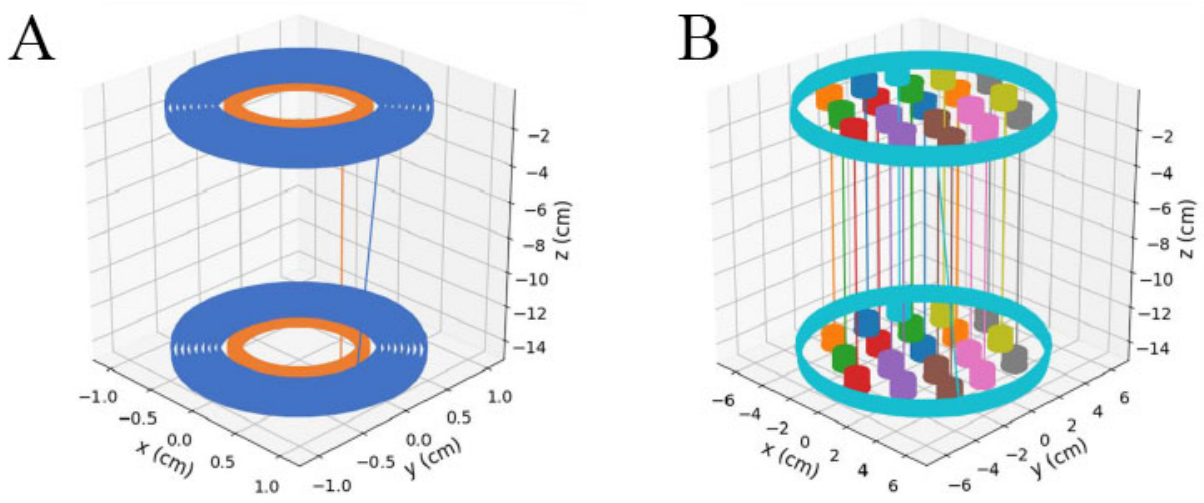

Figure 1. Representation of the single- (A) and multi-channel (B) ACB systems. The inner coils act as detection coils, and the outer coils act as excitation coils.

Single-channel ACB system

The single-channel ACB sensor is composed of one pair of excitations and one pair of detection coils, with 137 mm of distance between each coil of the same pair, as shown in Figure 1A. The sensor was developed with the excitation coils with a radius of 8.36 mm (AWG 24) and 150 turns, while the detection coils with a radius of 10.34 mm (AWG 36) and 450 turns.

Multi-channel ACB system

The multi-channel ACB sensor consists of one pair of excitations and nineteen pairs of detection coils (Figure 1B). A baseline of 137 mm separates the coils. The excitation coils present a radius of 62.43 mm (AWG 20) with 135 turns, while each detection coils were developed with a radius of 8.36 mm (AWG 32) with 1200 turns.

ACB forward model and inverse problem

The magnetic flux generated in the ACB detection coils by an extensive magnetized source can be described as [13]:

$$\phi_m = \frac{1}{\mu_0 I_r} \int_V \chi_v(V)(B_a(V) \cdot B_r(V))dV \tag{1}$$

where ϕ_m is the magnetic flux in the detection coil, μ_0 is the magnetic permeability in vacuum, I_r is the reciprocal current, χ_v is the volumetric magnetic susceptibility of the material, B_a is the excitation field, and B_r the reciprocal field. This continuous forward model was built considering the reciprocal principle by interchanging the detection and sample position to compute the generated signal [13].

However, for quantitative imaging, a discrete forward model is necessary. Therefore, we discretize the problem, dividing a field-of-view (FOV) in k voxels. Thus, the voltage generated in a single detection coil by an MNPs mass ($X_{MNP,k}$) in the k-th voxel is calculated by Faraday's law:

$$V_k = -\frac{d\phi_k}{dt} = -\frac{d}{dt}\left[\frac{\mu_0}{I_r} \cdot (\boldsymbol{H_{r,k}} \cdot \boldsymbol{H_{e,k}}) \cdot \boldsymbol{\chi(\omega)} \cdot \boldsymbol{X}_{MNP,k}\right] \tag{2}$$

where V_k is the voltage induced in the detection coil, $\boldsymbol{H_{r,k}}$ and $\boldsymbol{H_{e,k}}$ are the reciprocal and the excitation field, respectively, in the k-th voxel, and $\boldsymbol{\chi(\omega)}$ is the frequency-dependent mass susceptibility due to the presence of $\boldsymbol{X}_{MNP,k}$ MNPs mass in the k-th voxel. When considering distinct ACB systems, Equation 2 can be extended to M sensor positions (single-channel scanning) or N detection coils (multi-channel). The separation of geometric parameters and material properties of the MNPs from the MNPs mass inside the k-th voxel in Equation 2 can be written as [14]:

$$\boldsymbol{V} = \sum_k \boldsymbol{L} \cdot X_{MNP,k} = \boldsymbol{L} \cdot \boldsymbol{X}_{MNP,k} \tag{3}$$

where $\boldsymbol{V}$ is a vector containing the induced voltage in each detection coil, $\boldsymbol{L}$ is the sensitivity matrix of the system (system transfer function), which includes both the geometric parameters of the system and MNPs properties, and $\boldsymbol{X}_{MNP,k}$ is the MNPs distribution vector that represents the MNPs mass in each voxel. The L possesses the dimensions of $(N \cdot M) \times k$,

where M is the number of points in which the sensor is translated during signal acquisition, and N is the number of detection coils. Note that the sensitivity matrix can be determined a priori either by simulations or experimentally.

Equation (3) may be solved by employing the Moore-Penrose pseudo-inverse matrix ($\boldsymbol{L}^{+} = (\boldsymbol{L}^{\boldsymbol{T}}\boldsymbol{L})^{-1}\boldsymbol{L}^{\boldsymbol{T}}$), which is a minimum norm estimation obtained by a truncated singular value decomposition (TSVD). This approach has shown to be feasible for similar MNPs imaging problems with other magnetic techniques [15, 16]:

$$\boldsymbol{X}_{MNP,est} = \boldsymbol{L}^{+} \cdot \boldsymbol{V} \tag{4}$$

where $\boldsymbol{X}_{MNP,est}$ is the estimated MNPs distribution.

MNPs phantoms

The MNP type Perimag® plain (micromod, Rostock, Germany) was immobilized in gypsum for phantoms production. A total of 12 cubic phantoms ($1.2 \times 1.2 \times 1.2$ cm^3) with an MNPs mass ranging from 0.04 to 4.81 mg was prepared. Two phantoms were designed with the shape of a rat's stomach with different dimensions, aiming to simulate a normal rat's stomach and a resected stomach due to a surgical procedure (*e.g.*, sleeve gastrectomy). Both stomach phantoms were prepared using the same MNPs concentration, resulting in an MNPs mass of 4.50 mg for the normal stomach and 2.38 mg for the resected stomach. Figure 2 shows a single cube and the stomach-shaped phantoms used.

Measurements and imaging quality parameters

During all signal acquisition, the phantoms were positioned at a 1 mm distance from the detection coils' surface. A current of 500 mA and 180 mA was applied to the single- and multi-channel ACB systems, respectively. The single-channel ACB measurements were carried out by a scanning approach, performed using a 2D CNC stage with a precision of 0.1 mm. Each phantom was positioned in the center of a 110×50 mm^2 FOV, and the sensor was moved with a step of 5 mm, stopping 1 s for the signal acquisition in each

position. Furthermore, multi-channel ACB measurements were performed by positioning each phantom in the center of the system's FOV and acquiring the signal for 30 s.

We established two parameters to assess the reconstructed image quality. The Pearson Correlation Coefficient (R) was used to determine the linearity between the nominal ($\boldsymbol{X}_{MNP,nom}$) and the estimated ($\boldsymbol{X}_{MNP,est}$) MNPs distributions [17]. Furthermore, the quantification accuracy was evaluated by the absolute relative percentual difference ($X_{MNP,diff}$) between ($\boldsymbol{X}_{MNP,nom}$) and ($\boldsymbol{X}_{MNP,est}$). The sensitivity of each system was defined as the lower MNPs amount in which primarily result in ($X_{MNP,diff}$) $\leq 20\%$.

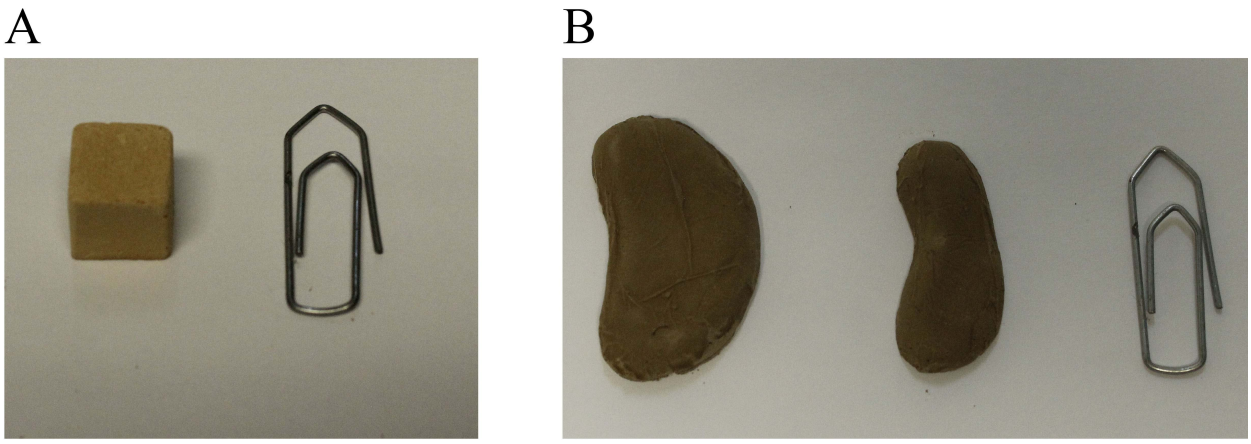

Figure 2. Phantoms produced for the ACB measurements: (A) gypsum cube and (B) normal and resected stomach-shaped phantoms.

Results and Discussion

The sensitivity matrices' singular values may be used to evaluate the inverse solution's stability [18]. The TSVD method used to calculate the pseudo-inverse matrix $\boldsymbol{L}^{+}$ has the truncated singular values of the sensitivity matrix $\boldsymbol{L}$ as parameters. As a result, the maximum number of voxels containing MNPs, which can be simultaneously reconstructed, is determined by the number of not null singular values above the truncation threshold. Therefore, the obtained normalized singular values for both ACB systems using a voxel of 5×5×12 mm^3 are shown in Figure 3. The sensitivity matrix $\boldsymbol{L_m}$ for the multi-channel ACB system is of dimensions ($[19 \cdot 1] \times 220$), and the optimal truncation threshold value (based on

$X_{MNP,diff}$ found was 10%. The fast decay is resulted from the system of equations, which provides only 19 equation to solve a FOV containing 220 voxels. This situation is referred to as an ill-conditioned problem. The sensitivity matrix $\boldsymbol{L_s}$ for the single-channel ACB system is of dimensions ([1 ·288] × 220) with truncation threshold of 2%, showing a significantly slower decay of singular values.

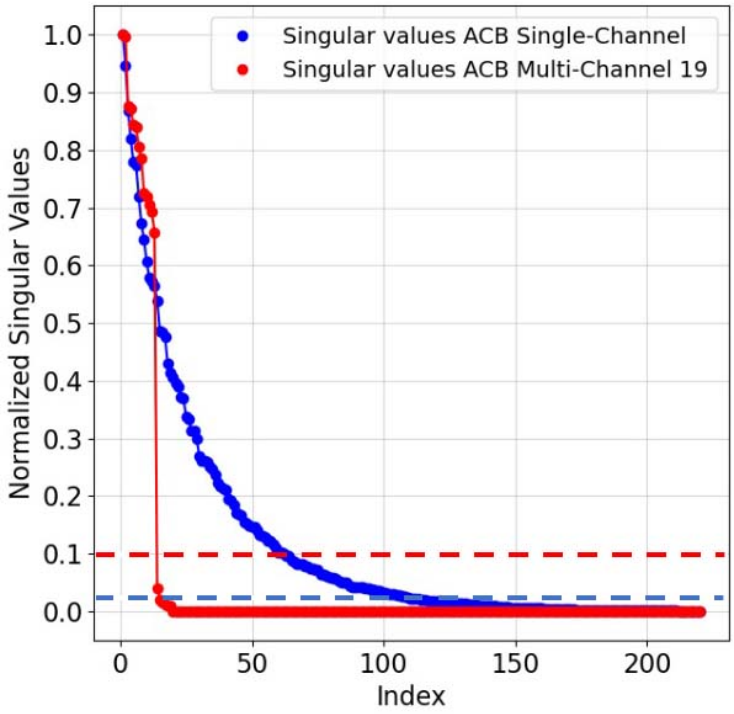

Figure 3. Normalized singular values for the single- and multi-channel ACB systems with the truncation threshold used (dashed lines) in TSVD for model inversion.

Figure 4 shows the nominal distribution and the quantitative reconstruction of a single gypsum cube containing MNPs for both systems in a FOV of 110 × 50 × 12 mm^3. Figure 5 shows the correlation coefficient and $X_{MNP,diff}$ profiles obtained by measuring 12 cubes with different concentrations of MNP using the single and multi-channel ACB systems. Both systems presented a high correlation coefficient (R > 0.7) for cubes with an MNPs mass above 0.28 mg (Figure 5A). However, for lower concentrations, the R values decrease exponentially. Furthermore, the multi-channel ACB system R values presented a faster decay compared to the single-channel system. The $X_{MNP,diff}$ results are shown in Figure 5B. For better visualization, we used a $X_{MNP,diff}$ threshold of 150%. As in the correlation coefficient

results, both systems presented a similar profile. Considering the condition adopted to determine each system's sensitivity, the single-channel presented a sensitivity of 0.76 mg, while for the multi-channel system, a value of 1.01 mg was found.

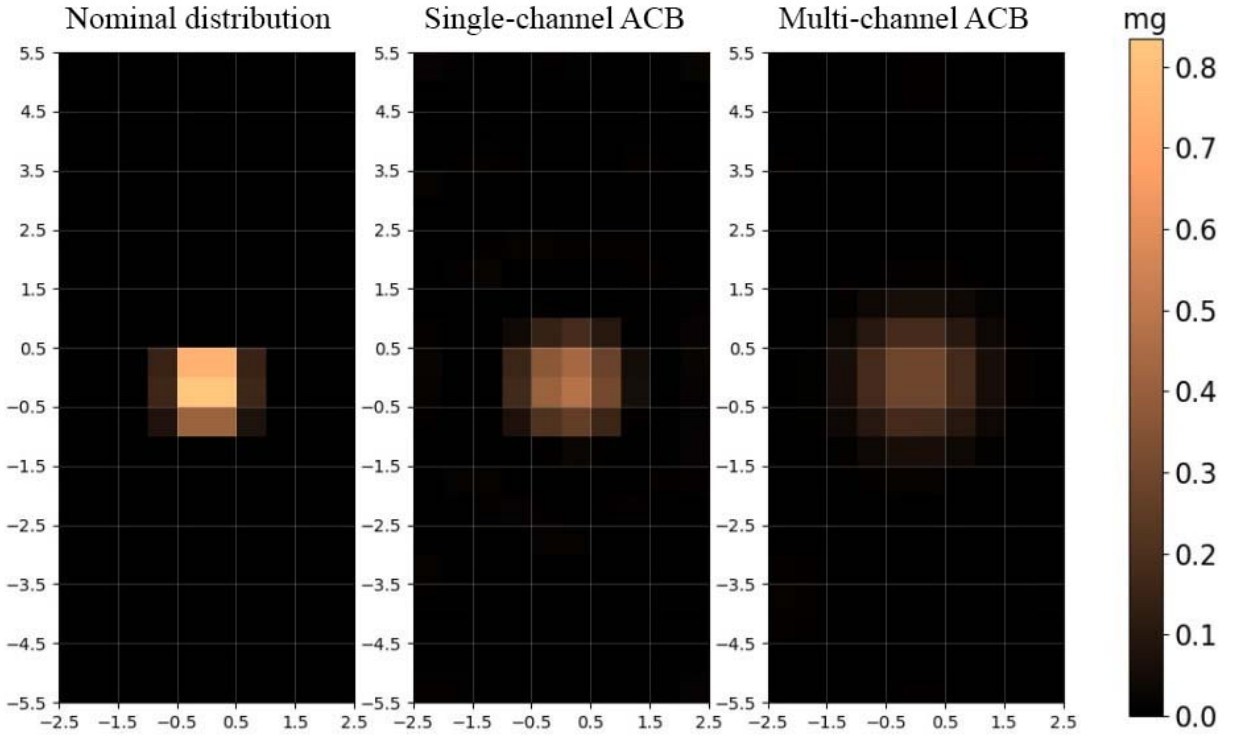

Figure 4. Nominal distribution and quantitative reconstruction of a single gypsum cube containing MNPs for the single- and multi-channel ACB systems.

Figure 6 shows the nominal distribution and the reconstructed quantitative images of the stomach-shaped phantoms. For the normal stomach phantom, the single-channel ACB reconstructed yielded a correlation coefficient of 0.94 and a $X_{MNP,diff}$ of 0.39%, while the multi-channel ACB reconstruction presented a correlation coefficient and $X_{MNP,diff}$ values of 0.77 and 10.50%, respectively. Regarding the resected stomach phantom, the image obtained with the single-channel ACB resulted in a correlation coefficient of 0.94 and a $X_{MNP,diff}$ of 0.11%. The multi-channel ACB image presented a correlation coefficient of 0.76 and a $X_{MNP,diff}$ of 11.32%. These results indicate that the single-channel ACB reconstructed images presented an increased quality compared to the multi-channel ACB. While the first system distinguished between the different phantom sizes, both multi-channel ACB images

were very similar, corroborated by the lower values of the correlation coefficient.

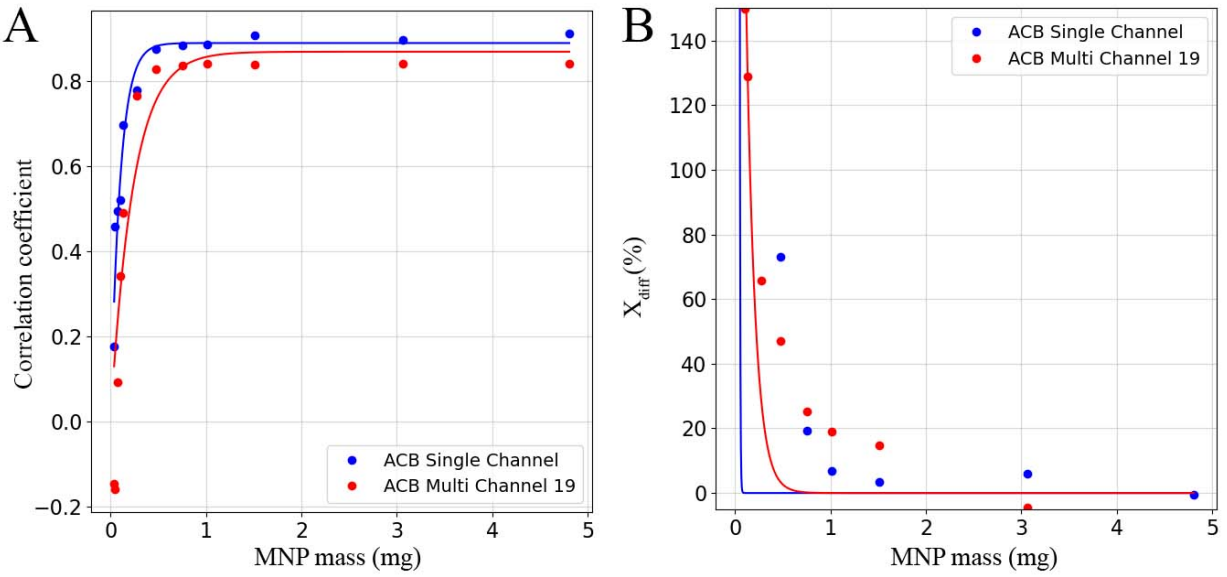

Figure 5. Imaging quality parameters: (A) correlation coefficient and (B) $X_{MNP,diff}$ of the quantitative reconstruction of gypsum cubes containing MNPs for the single- and multi-channel ACB systems. $X_{MNP,diff}$ values were truncated with a threshold of 150% for better visualization.

In previous studies from our group, the single-channel ACB system was used to detect manganese ferrite nanoparticles coated with citrate (Cit-$MnFe_2O_4$) in a mass range between 10.0-30.0 mg [9, 19, 20]. Even though the MNP type was different from the one used in this work, according to our results, both single- and multi-channel ACB systems present enough sensitivity to be used for *in vivo* MNP studies in rats. Although the reconstructions' imaging quality obtained using the single-channel ACB system was superior to the multi-channel, some considerations must be performed regarding *in vivo* experiments. The single-channel scanning approach to get the data takes about 6 minutes, while the multi-channel works in real-time at a 20 Hz sampling rate. Therefore, we consider the multi-channel the best option for biodistribution studies of MNP since the system acquires the signals in real-time, enabling longer measurement times [11]. However, for *in vitro* and *ex vivo* applications, the single-channel ACB system provides a better quantification quality. It is worth pointing out that based on other techniques, such as MRX, MPI, and MSI, the ACB system can be

considerably improved in terms of sensitivity and spatial resolution, which may be addressed in further studies.

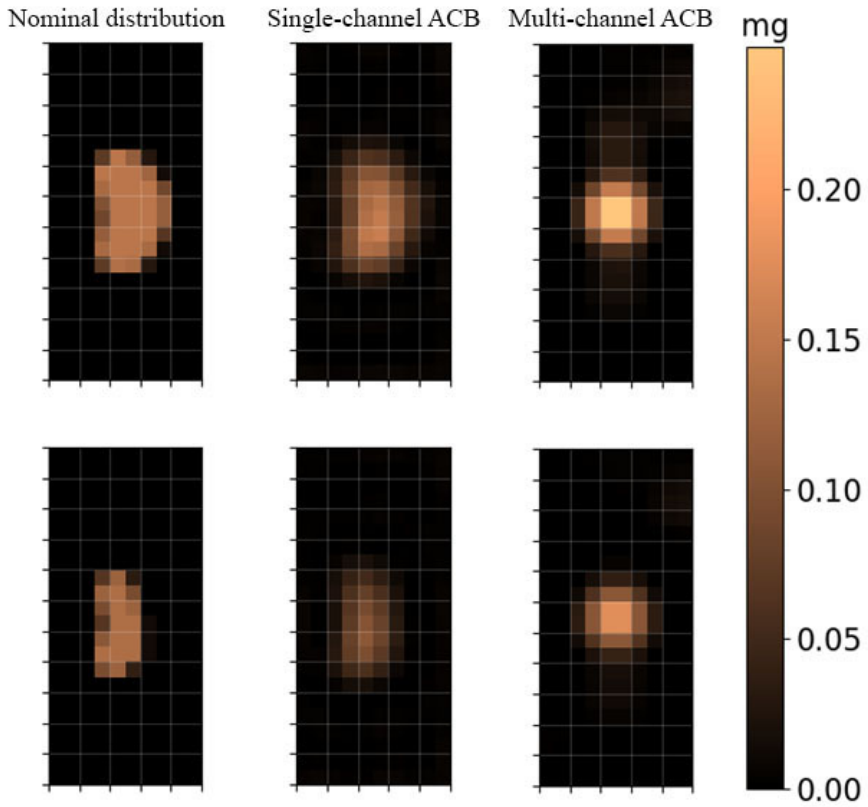

Figure 6. Nominal distribution and quantitative reconstruction of the normal (first line) and resected (second line) shaped phantoms a single gypsum cube containing MNPs for the single- and multi-channel ACB systems.

Aiming for future applications in gastroenterology, both systems' sensitivity suggests that gastric emptying measurements in vivo using rats is feasible since the variation of MNP mass due to the gastric emptying can be quantified as we obtained using cubes with different concentrations of MNP. Although scintigraphy and magnetic resonance imaging techniques use reconstructed images to evaluate gastric emptying [21], to the best of our knowledge, quantitative images have never been used to assess gastric emptying in vivo. To achieve this, rats may be fed with a test meal containing either solid (*e.g.*, manganese ferrite microparticles) or fluid (*e.g.*, MNPs) particles, then anesthetized using an inhalational anesthetic as isoflurane in predetermined times, as it's adopted in scintigraphy studies [22]. Even though

a multi-channel ACB measurement is performed in real-time, we consider that the scanning approach using the single-channel ACB is preferable since it presents an increased sensitivity and better reconstruction quality of the image. However, a multi-channel ACB measurement of a few minutes would yield to gastric emptying and gastric contractility simultaneously, which must be considered depending on the objectives.

Conclusions

In this work, we presented two ACB systems and they forward model and an inverse problem solution that enabled quantitative imaging of MNPs. The results demonstrated that both systems presented a sensitivity in the mg scale, although the single-channel ACB system yielded better reconstruction quality results. Also, the ACB systems provide quantitative data, which can be employed as a tool for MNPs and gastroenterology studies with a low cost, high versatility, and portability.

Funding

This work was supported by the German Academic Exchange Service (DAAD), São Paulo Research Foundation (FAPESP), National Council for Scientific and Technological Development (CNPq), and Coordination for the Improvement of Higher Education Personnel (CAPES).

References

[1] Q. A. Pankhurst, J. Connolly, S. K. Jones, and J. Dobson, "Applications of magnetic nanoparticles in biomedicine," *Journal of Physics D: Applied Physics*, vol. 36, pp. R167–R181, June 2003.

[2] T. Vangijzegem, D. Stanicki, and S. Laurent, "Magnetic iron oxide nanoparticles for drug delivery: applications and characteristics," *Expert Opinion on Drug Delivery*, vol. 16, pp. 69–78, Dec. 2018.

[3] H. Richter, M. Kettering, F. Wiekhorst, U. Steinhoff, I. Hilger, and L. Trahms, "Magnetorelaxometry for localization and quantification of magnetic nanoparticles for thermal ablation studies," *Physics in Medicine and Biology*, vol. 55, pp. 623–633, Jan. 2010.

[4] J. Weizenecker, B. Gleich, J. Rahmer, H. Dahnke, and J. Borgert, "Three-dimensional real-timein vivomagnetic particle imaging," *Physics in Medicine and Biology*, vol. 54, pp. L1–L10, Feb. 2009.

[5] F. Wiekhorst, U. Steinhoff, D. Eberbeck, and L. Trahms, "Magnetorelaxometry assisting biomedical applications of magnetic nanoparticles," *Pharmaceutical Research*, vol. 29, pp. 1189–1202, Dec. 2011.

[6] B. W. Ficko, P. M. Nadar, P. J. Hoopes, and S. G. Diamond, "Development of a magnetic nanoparticle susceptibility magnitude imaging array," *Physics in Medicine and Biology*, vol. 59, pp. 1047–1071, Feb. 2014.

[7] B. Gleich and J. Weizenecker, "Tomographic imaging using the nonlinear response of magnetic particles," *Nature*, vol. 435, pp. 1214–1217, June 2005.

[8] J. R. A. Miranda, R. B. Oliveira, P. L. Sousa, F. J. H. Braga, and O. Baffa, "A novel biomagnetic method to study gastric antral contractions," *Physics in Medicine and Biology*, vol. 42, pp. 1791–1799, Sept. 1997.

[9] A. G. Prospero, P. F. de Oliveira, G. A. Soares, M. F. Miranda, L. A. Pinto, D. C. dos Santos, V. dos S Silva, N. Zufelato, A. F. Bakuzis, and J. R. Miranda, "AC biosusceptometry and magnetic nanoparticles to assess doxorubicin-induced kidney injury in rats," *Nanomedicine*, vol. 15, pp. 511–525, Feb. 2020.

[10] L. Pinto, G. Soares, A. Próspero, E. Stoppa, G. Biasotti, F. Paixão, A. Santos, R. Oliveira, and J. Miranda, "An easy and low-cost biomagnetic methodology to study regional gastrointestinal transit in rats," *Biomedical Engineering / Biomedizinische Technik*, vol. 0, Feb. 2021.

[11] G. A. Soares, A. G. Prospero, M. F. Calabresi, D. S. Rodrigues, L. G. Simoes, C. C. Quini, R. R. Matos, L. A. Pinto, A. A. Sousa-Junior, A. F. Bakuzis, P. A. Mancera, and

J. R. A. Miranda, "Multichannel AC biosusceptometry system to map biodistribution and assess the pharmacokinetic profile of magnetic nanoparticles by imaging," *IEEE Transactions on NanoBioscience*, vol. 18, pp. 456–462, July 2019.

[12] M. Moreira, L. O. Murta, and O. Baffa, "Imaging ferromagnetic tracers with an ac biosusceptometer," *Review of Scientific Instruments*, vol. 71, pp. 2532–2538, June 2000.

[13] C. M. Bastuscheck and S. J. Williamson, "Technique for measuring the ac susceptibility of portions of the human body or other large objects," *Journal of Applied Physics*, vol. 58, pp. 3896–3906, Nov. 1985.

[14] M. Liebl, U. Steinhoff, F. Wiekhorst, J. Haueisen, and L. Trahms, "Quantitative imaging of magnetic nanoparticles by magnetorelaxometry with multiple excitation coils," *Physics in Medicine and Biology*, vol. 59, pp. 6607–6620, Oct. 2014.

[15] D. Baumgarten, M. Liehr, F. Wiekhorst, U. Steinhoff, P. Münster, P. Miethe, L. Trahms, and J. Haueisen, "Magnetic nanoparticle imaging by means of minimum norm estimates from remanence measurements," *Medical & Biological Engineering & Computing*, vol. 46, pp. 1177–1185, Oct. 2008.

[16] G. Crevecoeur, D. Baumgarten, U. Steinhoff, J. Haueisen, L. Trahms, and L. Dupre, "Advancements in magnetic nanoparticle reconstruction using sequential activation of excitation coil arrays using magnetorelaxometry," *IEEE Transactions on Magnetics*, vol. 48, pp. 1313–1316, Apr. 2012.

[17] P. Schier, M. Liebl, U. Steinhoff, M. Handler, F. Wiekhorst, and D. Baumgarten, "Optimizing excitation coil currents for advanced magnetorelaxometry imaging," *Journal of Mathematical Imaging and Vision*, vol. 62, pp. 238–252, Dec. 2019.

[18] T. Knopp, S. Biederer, T. Sattel, and T. M. Buzug, "Singular value analysis for magnetic particle imaging," in *2008 IEEE Nuclear Science Symposium Conference Record*, IEEE, Oct. 2008.

[19] A. G. Próspero, C. C. Quini, A. F. Bakuzis, P. F. de Oliveira, G. M. Moretto, F. P. F. Mello, M. F. F. Calabresi, R. V. R. Matos, E. A. Zandoná, N. Zufelato, R. B. Oliveira,

and J. R. A. Miranda, "Real-time in vivo monitoring of magnetic nanoparticles in the bloodstream by AC biosusceptometry," *Journal of Nanobiotechnology*, vol. 15, Mar. 2017.

[20] C. C. Quini, A. G. Próspero, M. F. Calabresi, G. M. Moretto, N. Zufelato, S. Krishnan, D. R. Pina, R. B. Oliveira, O. Baffa, A. F. Bakuzis, and J. R. Miranda, "Real-time liver uptake and biodistribution of magnetic nanoparticles determined by AC biosusceptometry," *Nanomedicine: Nanotechnology, Biology and Medicine*, vol. 13, pp. 1519–1529, May 2017.

[21] L. A. Szarka and M. Camilleri, "Methods for measurement of gastric motility," *American Journal of Physiology-Gastrointestinal and Liver Physiology*, vol. 296, pp. G461–G475, Mar. 2009.

[22] G. Tougas, E. Y. Eaker, T. L. Abell, H. Abrahamsson, M. Boivin, J. Chen, M. P. Hocking, E. M. Quigley, K. L. Koch, A. Z. Tokayer, V. Stanghellini, Y. Chen, J. D. Huizinga, J. Ryden, I. Bourgeois, and R. W. McCallum, "Assessment of gastric emptying using a low fat meal: establishment of international control values," *The American Journal of Gastroenterology*, vol. 95, pp. 1456–1462, June 2000.

Capítulo 5

Conclusão geral

Conclusão geral

A presente tese de doutorado apresenta a aplicação da técnica de Biosusceptometria de Corrente Alternada (BAC) em estudos envolvendo a motilidade gastrintestinal de ratos, além do desenvolvimento de modelos matemáticos e computacionais para a resolução do problema inverso, com o intuito de reconstruir imagens quantitativas de nanopartículas magnéticas (MNPs).

No primeiro capítulo, ratos foram submetidos a cirurgia de gastrectomia vertical, e pudemos analisar seus efeitos em diversos parâmetros da motilidade gastrintestinal. Os resultados obtidos demonstram que a cirurgia resultou em uma aceleração do esvaziamento gástrico e trânsito orocecal, além da diminuição da frequência dominante de contração gástrica e alterações no perfil de contratilidade gástrica. Mudanças na morfometria do estômago e também a presença de inflamação em diferentes camadas do tecido gástrico fortalecem as alterações encontradas na motilidade gástrica. Em comparação com as técnicas comumente utilizadas no estudo da motilidade gastrintestinal em ratos, a BAC apresenta diversas vantagens, como a ausência de radiação ionizante, fácil manuseio e baixo custo.

Além disso, desenvolvemos uma metodologia para reconstruir imagens do trânsito gastrintestinal regional em ratos, através do escaneamento de diferentes segmentos do trato. A metodologia proposta foi validada com a técnica de vermelho de fenol, considerada padrão ouro para tais estudos em ratos. Nesse contexto, a BAC apresenta como vantagens a possibilidade da visualização intrasegmentar de traçadores magnéticos, além de não necessitar o processamento das amostras para análise.

Por fim, o terceiro capítulo demonstra a resolução do problema inverso para a reconstrução de imagens quantitativas de MNPs utilizando sistemas BAC contendo uma e múltiplas bobinas detectoras. Para tal, foram construídos fantomas contendo MNPs em diversas concentrações, além de fantomas simulando o estômago de ratos. Imagens quantitativas são de extrema importância, pois apresentam os pixels com unidade de massa de MNPs. Tal característica das imagens permite o uso da BAC em diversas aplicações biomédicas, como hipertermia magnética e drug delivery, com o intuito de se saber precisamente a quantidade de MNPs entregue ao tecido alvo. Além disso, tal metodologia pode ser empregada no futuro

para a análise do trânsito gastrointestinal de ratos através de imagens quantitativas.

Acreditamos que os dados resultantes deste trabalho possam auxiliar no desenvolvimento de futuras aplicações da técnica BAC, fornecendo uma metodologia versátil e de baixo custo para estudos envolvendo a motilidade gastrintestinal e MNPs.

Apêndice A

Pharmacomagnetography to evaluate the performance of magnetic enteric-coated tablets in the human gastrointestinal tract

Prefácio

Este trabalho consiste no resultado final da tese de doutorado do Dr. Uilian de Andreis. Uma vez que o Dr. Uilian de Andreis não seguiu na carreira acadêmica após o término do doutorado, sua tese não foi publicada de imediato.

No início de 2020 aceitei a proposta do Prof. José Ricardo em resgatar esse trabalho, que fora concluído em 2010. Portanto, revisei toda a tese do Dr. Uilian de Andreis, e com a ajuda de outros alunos do Prof. José Ricardo (André Póspero, Gustavo Serafim e Guilherme Soares) e da Profa. Luciana Corá, finalizamos a escrita desse importante trabalho para o nosso laboratório.

Este trabalho demonstra a primeira utilização da BAC em conjunto com parâmetros farmacocinéticos (análise denominada farmacomagnetografia) para o estudo da performance de comprimidos entéricos no trato gastrintestinal. Apesar de eu não ter contribuído na parte experimental do trabalho (afinal, ainda estava no início do ensino médio), sei da dificuldade que é realizar pesquisa com humanos, e admiro o trabalho realizado pelo Dr. Uiliam de Andreis e todos que participaram de seu doutorado. Como resultado final, este trabalho foi publicado na revista *European Journal of Pharmaceutics and Biopharmaceutics*.

European Journal of Pharmaceutics and Biopharmaceutics 161 (2021) 50–55

Contents lists available at ScienceDirect

European Journal of Pharmaceutics and Biopharmaceutics

journal homepage: www.elsevier.com/locate/ejpb

Pharmacomagnetography to evaluate the performance of magnetic enteric-coated tablets in the human gastrointestinal tract

Leonardo Antonio Pinto [a,1], Luciana Aparecida Corá [b,1], Gustavo Serafim Rodrigues [a], Andre Gonçalves Prospero [a], Guilherme Augusto Soares [a], Uilian de Andreis [a], José Ricardo de Arruda Miranda [a,*]

[a] São Paulo State University – UNESP, Department of Biophysics and Pharmacology, Institute of Biosciences, Botucatu, São Paulo 18618-689, Brazil
[b] Alagoas State University of Health Sciences- UNCISAL, Center of Integrative Sciences, Maceio, Alagoas 57010-382, Brazil

ARTICLE INFO

Keywords:
Drug delivery
Disintegration process
Enteric coating
Gastrointestinal motility
Magnetic monitoring
Pharmacokinetics analysis
AC Biosusceptometry

ABSTRACT

A magnetic enteric-coated tablet containing diclofenac sodium was produced, and its performance under physiological and disturbed gastrointestinal motility was assessed through pharmacomagnetography analysis. *In vitro* studies were performed using conventional methods and *in vivo* studies were conducted on healthy volunteers before (control) and after domperidone administration. The magnetic tablet's gastrointestinal (GI) transit and disintegration process were monitored using the Alternating Current Biosusceptometry sensors combined with drug plasmatic concentration. The Gastric Residence Time, Colon Arrival Time, Small Bowel Transit Time, Disintegration Time and the pharmacokinetics parameters were calculated. The pH-dependent polymers used to coat the magnetic tablets were able to avoid the premature drug release on gastric or small intestine simulated medium. Gastric Residence Time was accelerated compared with the control group ($p < 0.01$). No significant differences were found regarding small bowel transit, colon arrival, disintegration process, or pharmacokinetics parameters. A strong correlation between magnetic monitoring and pharmacokinetics parameters analysis was determinant to evaluate the efficiency in the drug delivery at a specific site in the human gastrointestinal tract. In addition, a tablet with a damaged coating was used as a proof of concept to show the suitability of our methodology to evaluate the tablet. Our study showed that pharmacomagnetography is a multi-instrumental approach towards assessing drug delivery and bioavailability.

1. Introduction

Colon-specific drug delivery systems have broadly been developed for local treatment drugs [1,2]. However, colonic delivery systems must overcome the gastrointestinal (GI) tract physiological variables, including pH, fluid volume and composition, motility, and transit patterns [3,4].

Moreover, disturbances in normal gastric emptying or small bowel movements provoked by the drugs, local or systemic disease also contribute to wide variability in oral drug absorption and bioavailability [5].

Over the past few decades, pharmaceutical technology has succeeded in exploring different approaches to enhance colon-target drug delivery systems [1,6]. Particularly, pH-dependent copolymers of methacrylic acid and methyl methacrylate (Eudragit®) have been widely used to achieve such colon-specific drug delivery [7]. These copolymers have a pH-dependent dissolution and are used as enteric coating agents towards protecting the drug core from gastric and small intestinal contents and allowing them to deliver the drug specifically in the colonic region [8]. However, pH-dependent delivery systems could be unpredictable since the GI environment can be influenced by different intrinsic and extrinsic factors as well [9].

In the attempt to develop a more reliable formulation, the strategies include a combination of pH-dependent systems with time-dependent systems, enzyme-triggered systems, and multiple-layer coating, to prevent earlier drug release [1]. Besides, *in vitro* testing has also been

* Corresponding author.
E-mail addresses: leonardo.antonio@unesp.br (L.A. Pinto), luciana.cora@uncisal.edu.br (L.A. Corá), gustavo.serafim@unesp.br (G.S. Rodrigues), andre.prospero@unesp.br (A.G. Prospero), guilherme.soares@unesp.br (G.A. Soares), jose.r.miranda@unesp.br (J.R. de Arruda Miranda).
[1] These authors contributed equally to this work.

https://doi.org/10.1016/j.ejpb.2021.02.006
Received 2 September 2020; Received in revised form 5 February 2021; Accepted 8 February 2021
Available online 13 February 2021

improved to predict the most relevant GI variables that impact drug delivery [10]. Indeed, *in vitro* tests guide the pharmaceutical development of drug delivery systems. However, *in vivo* studies are imperative to evaluate the performance of the dosage forms and the influence of GI variables on drug release and bioavailability. Hence, non-invasive technologies that can monitor the dosage form along the GI segments in association with pharmacokinetics analyses are attractive.

Alternating Current Biosusceptometry (ACB) is a biomagnetic technique that suits a wide range of biological applications [11–15]. Single sensor ACB may be used to monitor solid dosage forms in distinct GI segments [16,17]. This approach enables the determination of the gastric residence time, small intestine transit time, and orocaecal transit time. In addition, single-sensor ACB can be used to scan a delimited area and thus obtain magnetic images of the disintegration process of solid dosage forms, which is quantified by the image area variation. This methodology was adopted to assess the floating lag time and tablet hydration rate of floating tablets *in vitro* [18], *in vivo* images of the disintegration of enteric coated magnetic tablets [16,17], and the influence of immunosuppressive therapy on GI transit [19]. Furthermore, the multi-sensor ACB system may be used to simultaneously acquire signals from different points simultaneously, and obtain magnetic images in real time without the need for scanning. This approach was used to study the effect of different compression force levels on tablet disintegration *in vitro* [20], both stomach and colonic contractility *in vivo* [17], and also the colonic motor activity in response to a meal [21]. Therefore, the ACB system has been proven to be a reliable tool for assessing the interplay between GI motility and drug release.

The simultaneous assessment of a solid dosage form location in the GI tract and the drug plasmatic concentration is a pharmacomagnetography analysis [22]. A magnetic technique very suitable for locating solid dosage forms *in vivo* is the Magnetic Marker Monitoring (MMM), which uses multichannel superconducting interference devices (SQUIDs) to measure the magnetic field of magnetized tablets [23,24]. Recent applications of pharmacomagnetography employing the MMM consisted of investigating the bioavailability of extended release tablets under fasting and fed conditions [25], and also the interplay between drug bioavailability and intragastric tablet deposition [26], but no studies about the effects of a disturbed GI transit were found. However, MMM presents several disadvantages, such as the high cost of implementation and the necessity of a magnetically shielded room, limiting its use on a large scale. In contrast, ACB is a low cost and versatile technique, which does not require a magnetically shielded environment and can be easily employed in both clinics and laboratories.

This work aimed to use the pharmacomagnetography to evaluate the GI transit and pharmacokinetics profile of a magnetic enteric-coated tablet administered to healthy volunteers under physiological and disturbed GI motility. Therefore, a two-phase clinical study was performed using domperidone as a prokinetic drug to provoke GI peristalsis increase, which presumably accelerates the GI transit. In addition, a damaged tablet was used as a proof of concept to highlight the main advantages of pharmacomagnetography.

2. Materials and methods

2.1. Materials

All the materials used in this study were of analytical grade. Black manganese ferrite ($MnZnFe_2O_3$; diameter of $50 < \varphi < 75$ μm) was purchased from Ferroxcube, El Paso, USA. Diclofenac sodium (DS), isopropyl alcohol (IPA), acetonitrile (ACN), magnesium stearate, and talc were purchased from Sigma–Aldrich, Brazil. Blanver, Brazil, kindly supplied microcrystalline cellulose (Microcel®) and sodium starch glycolate (Explosol®). Triethyl citrate (Scandinol®) was provided by Scandiflex, Brazil. Colorcon, Brazil, kindly supplied Acryl-EZE®. Almapal Tecnologia Validada, Brazil supplied Eudragit®S100 (Degussa, Rohm Pharma Polymers).

2.2. Magnetic enteric-coated tablets

Magnetic tablets were obtained manually by direct compression in a single-punch die set machine (Marconi MA098/C, Piracicaba, Brazil) using a matrix of 12 mm in diameter. The tablets are composed of 100 mg diclofenac sodium as a model drug, 800 mg ferrite, 300 mg of microcrystalline cellulose, and 50 mg sodium starch glycolate. The drug and excipients were mixed, and the mixture was compressed (30 kN).

The tablets consisted of three layers with distinct functions: (1) Acryl-EZE sub-coat to promote adhesion and prevent interactions between the core tablet's and Eudragit S-100 [27]; (2) Eudragit S-100 as a pH dependent coating to be dissolved in the colon; (3) Acryl-EZE top-coat to increase the tablets' stability and protect the Eudragit S-100 from the pH variations along the GI tract. The tablets were coated by spray-drying using a bench pan-coating machine (LEMAQ, São Paulo, Brazil). For the sub-coat layer, Acryl-EZE (20%, w/w) was dispersed in water (80%, w/w) and the solution was applied to the tablets to obtain 0.5% weight gain. For the second layer, a coat solution was prepared by dissolving Eudragit S-100 dry polymer (17%, w/w) in isopropyl alcohol (83%, w/w). A mixture of talc (6%, w/w) as a glidant, titanium dioxide (13%, w/w) as a pigment, magnesium stearate (6%, w/w) as a lubricant, and triethyl citrate (15%, w/w) as a plasticizer were dissolved in isopropyl alcohol (60%, w/w), and added to the coat solution, which was applied to the tablets to obtain 3% weight gain. Afterward, a top-coat solution was prepared with Acryl-EZE as described above, and then applied to obtain a 6% weight gain. During the coating procedures, the spray rate, inlet temperature, and rotating speed were maintained in accordance with the manufacturer's guidelines [28,29].

2.3. In vitro drug release study

The *in vitro* drug release study was performed using conventional USP apparatus II (299/3 Ethik Technology, Brazil) based on previous works [30,31]. It was performed in triplicate, at different pH dissolution media under paddle agitation at 50 rpm and 37 °C ± 0.5. Firstly, the magnetic enteric-coated tablets were placed in vessels containing 900 ml of hydrochloric acid, 0.1 N, pH 1.2 for 2 h. The dissolution media was replaced with a phosphate buffer, pH 6.8, for 3 h. Afterward, the dissolution medium's pH was adjusted to pH 7.4, maintaining the drug release for 3 more hours. Aliquots of 5 ml were taken at 30-minute intervals, filtered through 0.22 μm membranes, and analyzed by UV spectrophotometry (Ultrospec 2000 Pharmacia Biotech, Brazil) at 280 nm to determine the % of drug release.

2.4. Alternating current Biosusceptometry (ACB)

The ACB technique (Br4Science®, Botucatu, Brazil) was used to evaluate the gastrointestinal transit and the drug release on healthy volunteers. ACB sensors consist of induction and excitation coils for non-invasive monitoring of magnetic signals [32]. For pharmaceutical applications, solid dosage forms are prepared with ferrite powder (granulometry $50 < \varphi < 75$ μm), a non-toxic, insoluble, and non absorbable magnetic material. After swallowing the tablet, the ACB sensor was positioned on the abdominal surface and the magnetic signals, generated by the magnetic dosage form in response to the applied magnetic field, were detected as a magnetic flux in the detection coils. Detailed technical information was reported earlier [33].

2.5. Ethics and participants

This study was approved by the Institutional Ethics Committee at the São Paulo State University (protocol number 195/2015) and was conducted following the Declaration of Helsinki and its revisions. All participants gave informed consent before entering the study.

Eight healthy volunteers (3 male, 5 female, aged between 20 and 40 years, body weight between 50 and 80 kg, and body mass index < 22 kg/

m^2) were enrolled in the study. General exclusion criteria included pregnancy, smoking, abdominal surgery, diabetes, and other chronic endocrine disorders affecting GI motility, as well as treatment with prokinetics, anticholinergics, opiates, or macrolide drugs.

2.6. Study protocol

This was a single-center, randomized, double-blind, comparative study to evaluate the gastrointestinal transit and the pharmacokinetics of diclofenac sodium before (control) and after domperidone administration. It is important to point out that a 7-day washout period separated the two treatment arms.

After fasting overnight, subjects ingested 40 mg of placebo or 40 mg of an immediate release domperidone tablet with 200 ml water. Thirty minutes later, they received a magnetic enteric-coated tablet with 200 ml of water. They remained in an upright position and the magnetic measurements were started 5 min after the tablet ingestion. Biomagnetic monitoring was performed using single-sensor ACB equipment to monitor gastric and colonic regions (Fig. 1). Each monitoring session lasted 2 min and was repeated every 15 min until the tablet had completely left the stomach. From then on, the measurements were made around the colonic region every 20 min until the magnetic tablet had reached the proximal colon. Blood samples (5 ml) were collected in both treatment periods by indwelling venous catheter at pre-defined time-points: 15 min before dosing to 480 min after magnetic tablet administration. Samples were immediately centrifuged for serum samples collected and stored at – 80 °C for further analysis. Participants remained moderately active during the study day and received standardized meals at 2 h, 4 h, and 6 h post-dose. Post-dose meals consisted of 2 slices of bread (50g), 2 slices of ham, 2 slices of cheese, and 100 ml of orange juice, with a total caloric content of 422.6 Kcal (124.4 Kcal from fat, 210.1 Kcal from carbohydrate, and 88.2 Kcal from protein). Lunch, consisting of lasagna (300g) and 100 ml of orange juice with a caloric content of 483.6 Kcal (157.5 Kcal from fat, 227.2 Kcal from carbohydrate, and 98.9 Kcal from protein), was served 4 h post-dose.

2.7. Proof of concept

To demonstrate the developed dosage form's feasibility, we mechanically damaged a magnetic enteric-coated tablet before administering it to a random volunteer. The measurement followed all the protocols described in the '*Study protocol*' section.

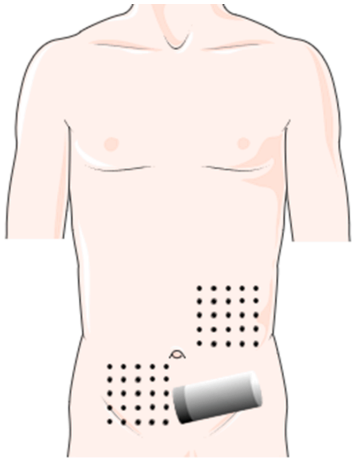

Fig. 1. Colonic region monitored by the ACB mono-channel system. Grey dots represent each position measured in the abdominal surface.

2.8. Magnetic data analysis

Magnetic monitoring was performed to generate time series images used to quantify the disintegration process. The location of the magnetic tablet was obtained by transferring the data to a mathematical coordinate system according to external anatomical references as described by Corá et al. [15,33]. Values for the magnetic imaging area were calculated and expressed graphically as time-intensity curves [16,32].

The following parameters were calculated: Gastric Residence Time (GRT), defined as the time t (min) from the tablet ingestion until its emptying from the stomach; Colon Arrival Time (CAT), defined as the time t (min) it took for the magnetic tablet to enter into the colon; Small Bowel Transit Time (SBTT), defined as the time (min) elapsed between GRT and CAT; Disintegration Time (DT), defined as the time when the spreading of magnetic material promoted a 50% increase in the first imaging area after colon arrival [34]. Magnetic data were processed and analyzed in MatLab (Mathworks, Inc., USA) and Origin (OriginLab, USA).

2.9. Pharmacokinetics analysis

Serum samples were analyzed using a validated high-performance liquid chromatography (HPLC) method [35]. Briefly, 500 µl of serum sample and 2 ml of acetonitrile (ACN) were mixed for 2 min in a 15 ml tube and then centrifuged for 10 min, 4 °C, at 4.000 rpm. The supernatant was evaporated to dryness at 40 °C in a water bath in a dry air stream. Residuals were reconstituted in 200 µl of the mobile phase (ACN/water, 50:50% v/v, pH = 3.3) and centrifuged for 10 min, 4 °C, at 14.000 rpm. Samples of 100 µl were analyzed in an HPLC system (GE Healthcare, Chicago, USA) with a quaternary chromatographic pump, UV detector (λ = 280 nm), a computer interface system controller (UNICORN 5.11), and a 150 mm × 4.6 mm RP-C_8 reversed-phase column.

The following pharmacokinetic parameters were calculated: Tlag, defined as the time at which the first detection of the diclofenac sodium was found in plasma; Cmax, defined as the maximum plasma concentration of diclofenac sodium; Tmax, defined as the time taken to achieve maximum plasma concentration (Cmax); AUC0-480, defined as the area under the plasma concentration curve versus full measurement time (0: 480 min.).

2.10. Statistical analysis

Data are presented as the mean ± standard deviation (SD). Magnetics and pharmacokinetic parameters were compared between both treatments using the paired Student *t*-test. Values of $p < 0.05$ were considered statistically significant. The correlation coefficient was used to compare the magnetic parameter with pharmacokinetics. All data analysis and statistics were performed with GraphPad Prism (GraphPad Software, La Jolla, USA).

3. Results and discussion

Fig. 2 illustrates the diclofenac sodium release profile from the magnetic enteric-coated tablet. It was observed that at pH 1.2, pH 6.8, and pH 7.4 a total of 2.6%, 19.2%, and 71.3% of the drug was released, respectively. Our approach consisted of applying multiple layers by combining copolymers of the methacrylic acid (Eudragit S100 and Acryl-EZE) to protect the dosage form from disintegration and early release in the stomach or small intestine [1]. Overall, according to our *in vitro* assays, the pH-dependent polymers were able to avoid the premature release of the drug. An essential prerequisite for pH-dependent colonic delivery systems is to prevent the immediate release of the drug, and to do it has to overcome the significant inter-subjects' variability of gastric emptying and transit times, in addition to the different pH values in different gastrointestinal segments [8,36].

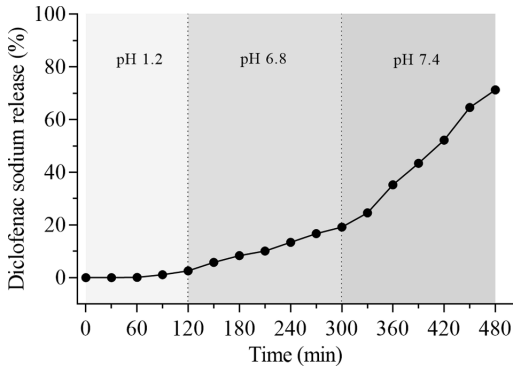

Fig. 2. *In vitro* diclofenac sodium release profile *in vitro* over different pHs related to specific GI tract regions. The study was performed in triplicate. Data are presented as mean ± SD (n = 3).

In terms of oral site-specific solid dosage forms, despite the fact that significant progress has been made in the use of dissolution study for estimating *in vivo* drug release, ongoing efforts are still demanded to improve the accuracy in reproducing the GI environment [10,37]. Indeed, a good *in vitro - in vivo* correlation will be expected if current tests could address all main parameters that can affect the drug release in the human GI tract. However, the significant changes in gastric motility and intestinal transit time, promoted by food, co-administration of drugs, diseases, besides high inter- and intra-individual physiological variability, can impact the extent of drug absorption [8,38,39].

Although our strategy was to demonstrate that the triple layer coating was acceptable in the *in vitro* tests, a proof of concept would be determinant to evaluate the formulation's efficiency in the drug delivery at a specific site in the human GI tract. As such, AC Biosusceptometry combined with pharmacomagnetography analysis, was used to evaluate the GI transit of the magnetic tablets, and drug delivery and absorption processes *in vivo*, ensuring the relation between the release site (magnetic) and absorption (pharmacokinetic).

Similar to pharmacoscintigraphy [40], pharmacomagnetography comprises the association of a noninvasive technique to evaluate the behavior of dosage forms *in vivo* with pharmacokinetics analysis. ACB has been successfully used as a tool for pharmaceutical research. For the first time, we were able to demonstrate that pharmacomagnetography is reliable towards evaluating the gastrointestinal transit of a magnetic enteric-coated tablet, the site-specific disintegration process, and the correlation with the drug absorption.

Fig. 3 shows the pharmacomagnetography monitoring of a magnetic enteric-coated tablet administered to a healthy volunteer before (A) and after a prokinetic drug (C). Magnetic signals and pharmacokinetic profiles (Fig. 3A and C), together with the respective magnetic images (Fig. 3B and D) represent the GI transit of tablets, the disintegration process, and the drug release in the colonic region. Despite variable gastric retention time, it was observed that the tablets only disintegrated and released the drug at the proximal colon, as expected. Moreover, a significant and strong correlation between magnetic monitoring and the pharmacokinetics analysis for the both control ($r = 0.88$; $p = 0.0034$) and domperidone ($r = 0.91$; $p = 0.0014$) was observed showing the magnetic enteric-coated tablet disintegration, the drug release, and the concurrent absorption ratio (Fig. 4).

Table 1 summarizes the gastrointestinal transit and pharmacokinetics parameters calculated for all volunteers before (control) and after domperidone administration. Domperidone is a dopamine-2 receptor antagonist used as a prokinetic drug in the management of dyspepsia [41]. In our study, domperidone was used to disturb the upper gastrointestinal motility and to verify if such alterations could influence

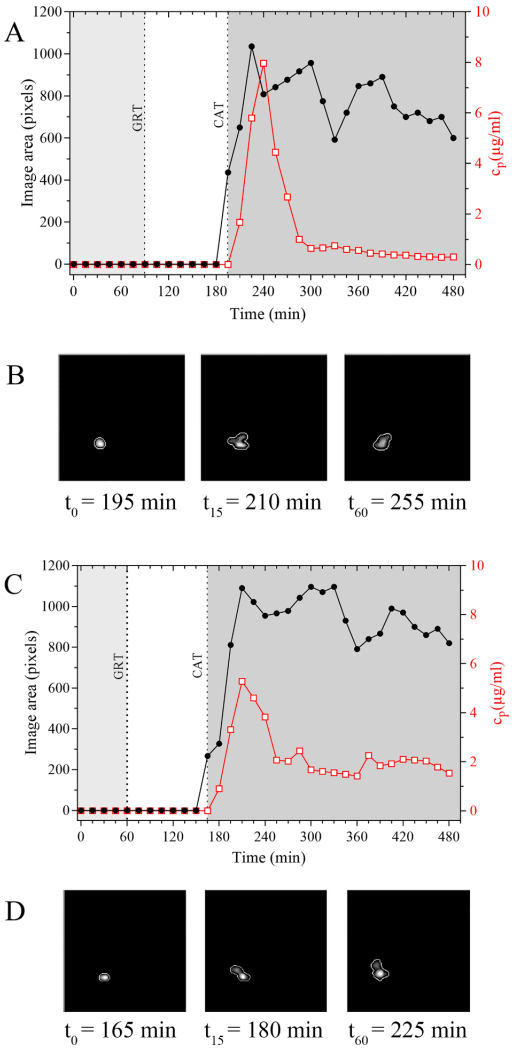

Fig. 3. Pharmacomagnetography monitoring of the magnetic enteric-coated tablets. Magnetic area and diclofenac sodium plasmatic concentration of a healthy volunteer before (A) and after (C) administering a prokinetic drug. Images show the magnetic area increasing over time for a healthy volunteer before the prokinetic drug (B) and after a prokinetic drug (D).

pharmacokinetics. Overall, only GRT was accelerated compared with the control group ($p < 0.01$). No significant differences were found regarding small bowel transit, colon arrival, disintegration process, or pharmacokinetic parameters.

The gastrointestinal tract is a complex environment that offers significant absorption barriers after oral administration [9]. Thus, methodologies that explore the GI physiological variables and their impact on oral drug absorption in both health and in disease conditions could help drug development and analysis. Early studies conducted by our group investigated GI parameters (e.g., gastric retention time, small intestine transit time, and orocecal transit time) and their influence on the biopharmaceutical process related to oral solid dosage forms [16,32,42], However, none had correlated the drug delivery, pharmacokinetic and GI transit. From then on, improvements in the analysis and methods

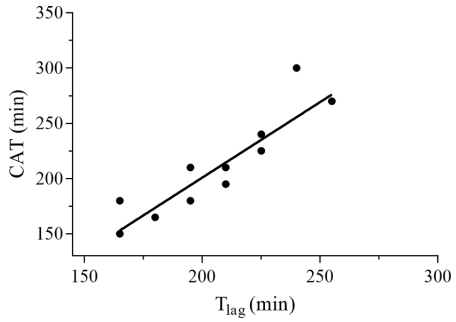

Fig. 4. Correlation between colonic arrival time (CAT) and drug absorption for (A) control and (B) domperidone administration. T_{lag} represents the first plasmatic concentration after magnetic enteric-coated tablets disintegration, and CAT the first detecting the tablet in the colon.

allowed us to propose this new approach. Using the ACB as a non-invasive and radiation-free methodology, pharmacomagnetography can be useful to fill gaps towards understanding how GI physiology or diseases influence the drug delivery and absorption processes reliably.

Interestingly, pharmacomagnetography could also identify when the drug release from the magnetic enteric-coated tablet in the human GI tract was erratic. As a proof of concept, the enteric coating was mechanically damaged before administering to one volunteer. As shown in Fig. 5, plasmatic concentration occurred clearly before the tablet entering in the proximal colon, showing that the damaged coating layer did not allow a site-specific drug release. In terms of pharmaceutical development, such a situation reinforces the need for methodologies able to be applied as proof of concept in human subjects, as inappropriate disintegration of the dosage form or unpredictable drug release may result in therapeutic failure and even unexpected side effect. This example illustrates that only with these two techniques can the *in loco* drug release conditions be verified and used as *in vivo* tablet quality control.

One of the main drawbacks of our methodology is the high amount of ferrite used in the formulation. In the current state of the art of the ACB technique, a high amount of ferrite is needed to achieve an acceptable signal-to-noise ratio. However, in a recent study (data not published) we were able to acquire *in vivo* signals of magnetic tablets in the stomach with formulations containing 500 mg of ferrite, which is a lower value in comparison to the one used in this study (800 mg). We emphasize that ACB systems with improved sensitivity are being developed. Another important recent contribution in studies carried out in our laboratory, which has not yet been published, involves solutions to the inverse problem, that will increase the technique sensitivity and improve the quality of the images. Thus, we aim to perform *in vivo* measurements with 100 mg of ferrite, making tablet size more realistic. Once that the aim of this study was to propose a pharmacomagnetography analysis using the ACB for the first time, the formulation preparation must be improved for further studies.

To sum up, our study presented ACB as an alternative magnetic methodology to locate magnetic-labeled solid dosage forms in the GI tract and assess their disintegration process in human subjects. The pharmacomagnetography analysis performed by the association between GI and pharmacokinetic parameters results in an essential multi-instrumental approach to assessing drug delivery, making it possible to assess motility's interference on the release process and determine the dosage form's disintegration region.

Funding

The Sao Paulo Research Foundation - FAPESP [2015/14923-9], supported this work.

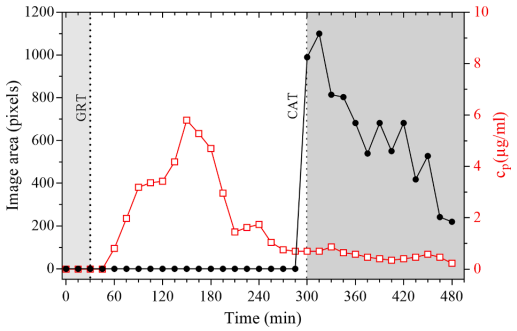

Fig. 5. Example of pharmacomagnetography analysis showing the gastrointestinal transit (black line) and drug release (red line) from a magnetic enteric-coated tablet. In this volunteer, the drug release occurred during the small intestine transit before reaching the proximal colon. (For interpretation of the references to colour in this figure legend, the reader is referred to the web version of this article.)

Table 1
Comparison of the gastrointestinal transit and pharmacokinetic parameters before (control) and after domperidone administration to healthy volunteers. Data are expressed as mean ± SD and median.

Subjects	Control								Domperidone							
	GRT (min)	SBTT (min)	CAT (min)	DT (min)	T_{lag} (min)	T_{max} (min)	C_{max} (µg/ml)	AUC_{0-480} (µg.h/ml)	GRT (min)	SBTT (min)	CAT (min)	DT (min)	T_{lag} (min)	T_{max} (min)	C_{max} (µg/ml)	AUC_{0-480} (µg.h/ml)
1	75	75	150	45	165	300	4.7	484.0	45	165	210	21	195	255	3.5	398.2
2	120	90	210	41	195	360	2.2	316.3	90	90	180	30	195	270	2.8	202.6
3	120	90	210	18	210	240	3.5	542.4	45	150	195	25	210	225	4.5	489.1
4	90	105	195	38	210	240	8.0	735.4	60	105	165	21	180	210	5.3	705.8
5	135	165	300	23	240	315	2.1	918.5	90	90	180	15	165	180	1.8	514.3
6	90	120	210	23	210	240	6.5	634.9	60	180	165	23	180	270	7.9	735.4
7	45	180	225	15	225	240	3.3	637.3	30	240	270	15	255	285	4.2	574.5
8	45	150	195	23	210	240	7.9	735.4	30	135	165	30	180	210	5.2	705.8
Mean	90.0	121.9	211.9	28.3	208.1	271.9	4.8	625.5	56.2	144.4 *	191.3	22.5	195.0	238.1	4.5	540.7
SD	34.0	38.8	42.0	11.3	21.9	47.1	2.4	182.4	23.7	51.3	35.6	5.8	27.8	37.1	1.8	181.9
Median	90.0	112.5	210.0	23.0	210.0	240.0	4.1	636.1	52.5	142.5	180.0	22.0	187.5	240.0	4.3	544.4

* Indicates $p < 0.01$ compared with control (Student's *t*-test). GRT, gastric retention time; SBTT, small bowel transit time; CAT, colon arrival time; DT, disintegration time; T_{lag}, time for the first drug concentration at the plasma; T_{max}, time to peak plasma concentration; C_{max}, peak plasma concentration; AUC_{0-480}, area under the plasma concentration–time curve from time zero to the last quantifiable time point.

Declaration of Competing Interest

The authors declare that they have no known competing financial interests or personal relationships that could have appeared to influence the work reported in this paper.

Acknowledgements

We would like to thank the experts in pharmaceutical formulation and oral delivery Priscileira Ferrari and Cristina Serra for all the support in the revision process. We are grateful to Blanver, Colorcon Brazil, Almapal Tecnologia Validada, and Scandiflex for the pharmaceutical supplies used in this study. We also thankful to the Brazilian agencies FAPESP, CNPq and CAPES for the financial support.

References

[1] S.H. Lee, et al., Strategic approaches for colon targeted drug delivery: an overview of recent advancements, Pharmaceutics 12 (1) (2020).
[2] C. Maderuelo, J.M. Lanao, A. Zarzuelo, Enteric coating of oral solid dosage forms as a tool to improve drug bioavailability, Eur. J. Pharm. Sci. 138 (2019) 105019.
[3] G.B. Hatton, et al., All disease begins in the gut: Influence of gastrointestinal disorders and surgery on oral drug performance, Int. J. Pharm. 548 (1) (2018) 408–422.
[4] M. Pislar, et al., Analysis of small intestinal transit and colon arrival times of non-disintegrating tablets administered in the fasted state, Eur. J. Pharm. Sci. 75 (2015) 131–141.
[5] G.B. Hatton, et al., Gut reaction: impact of systemic diseases on gastrointestinal physiology and drug absorption, Drug Discov. Today 24 (2) (2019) 417–427.
[6] S. Amidon, J.E. Brown, V.S. Dave, Colon-targeted oral drug delivery systems: design trends and approaches, AAPS PharmSciTech 16 (4) (2015) 731–741.
[7] A. Maroni, et al., Enteric coatings for colonic drug delivery: state of the art, Expert Opin. Drug Deliv. 14 (9) (2017) 1027–1029.
[8] V.C. Ibekwe, et al., Interplay between intestinal pH, transit time and feed status on the in vivo performance of pH responsive ileo-colonic release systems, Pharm. Res. 25 (8) (2008) 1828–1835.
[9] B. Hens, et al., Exploring gastrointestinal variables affecting drug and formulation behavior: Methodologies, challenges and opportunities, Int. J. Pharm. 519 (1–2) (2017) 79–97.
[10] S. Silchenko, et al., In vitro dissolution absorption system (IDAS2): Use for the prediction of food viscosity effects on drug dissolution and absorption from oral solid dosage forms, Eur. J. Pharm. Sci. 143 (2020) 105164.
[11] R. Moraes, et al., Measurement of gastric contraction activity in dogs by means of AC biosusceptometry, Physiol. Meas. 24 (2) (2003) 337–345.
[12] C.C. Quini, et al., Employment of a noninvasive magnetic method for evaluation of gastrointestinal transit in rats, J. Biol. Eng. 6 (1) (2012) 6.
[13] G.A. Soares, et al., Multichannel AC biosusceptometry system to map biodistribution and assess the pharmacokinetic profile of magnetic nanoparticles by imaging, IEEE Trans. Nanobiosci. 18 (3) (2019) 456–462.
[14] A.G. Prospero, et al., Real-time in vivo monitoring of magnetic nanoparticles in the bloodstream by AC biosusceptometry, J Nanobiotechnol. 15 (1) (2017) 22.
[15] L.A. Cora, et al., AC biosusceptometry in the study of drug delivery, Adv. Drug Deliv. Rev. 57 (8) (2005) 1223–1241.
[16] L.A. Cora, et al., Enteric coated magnetic HPMC capsules evaluated in human gastrointestinal tract by AC biosusceptometry, Pharm. Res. 23 (8) (2006) 1809–1816.
[17] L.A. Cora, et al., Gastrointestinal transit and disintegration of enteric coated magnetic tablets assessed by ac biosusceptometry, Eur. J. Pharm. Sci. 27 (1) (2006) 1–8.
[18] P.C. Ferrari, et al., A novel automated alternating current biosusceptometry method to characterization of controlled-release magnetic floating tablets of metronidazole, Drug Dev. Ind. Pharm. 40 (8) (2014) 1123–1131.
[19] M. Teixeira, et al., Influence of post-transplant immunosuppressive therapy on gastrointestinal transit using biomagnetic method: A pilot study, Dig. Dis. Sci. 60 (2014).
[20] L.A. Cora, et al., Influence of compression forces on tablets disintegration by AC Biosusceptometry, Eur. J. Pharm. Biopharm. 69 (1) (2008) 372–379.
[21] F.G. Romeiro, et al., A novel biomagnetic approach to study caecocolonic motility in humans, Neurogastroenterol. Motil. 18 (12) (2006) 1078–1083.
[22] W. Weitschies, H. Blume, H. Monnikes, Magnetic marker monitoring: high resolution real-time tracking of oral solid dosage forms in the gastrointestinal tract, Eur. J. Pharm. Biopharm. 74 (1) (2010) 93–101.
[23] M. Bergstrand, et al., Mechanistic modeling of a magnetic marker monitoring study linking gastrointestinal tablet transit, in vivo drug release, and pharmacokinetics, Clin. Pharmacol. Ther. 86 (1) (2009) 77–83.
[24] W. Weitschies, et al., Magnetic markers as a noninvasive tool to monitor gastrointestinal transit, IEEE Trans. Biomed. Eng. 41 (2) (1994) 192–195.
[25] W. Weitschies, et al., Impact of the intragastric location of extended release tablets on food interactions, J. Control. Release 108 (2–3) (2005) 375–385.
[26] W. Weitschies, et al., Bioavailability of amoxicillin and clavulanic acid from extended release tablets depends on intragastric tablet deposition and gastric emptying, Eur. J. Pharm. Biopharm. 70 (2) (2008) 641–648.
[27] D. Sauer, et al., Influence of polymeric subcoats on the drug release properties of tablets powder-coated with pre-plasticized Eudragit L 100–55, Int. J. Pharm. 367 (1–2) (2009) 20–28.
[28] Colorcon. Coating Parameters for the Use of Acryl-EZE®. 2013 January 24, 2021]; Available from: https://www.colorcon.com/products-formulation/all-products/film-coatings/enteric-release/acryl-eze/item/2025-acryl-eze-coating-parameters.
[29] K.M. Lehmann, Practical course in film coating of pharmaceutical dosage forms with EUDRAGIT, Pharma Polymers, Darmstadt, 2001.
[30] F. Liu, et al., Evolution of a physiological pH 6.8 bicarbonate buffer system: application to the dissolution testing of enteric coated products, Eur. J. Pharm. Biopharm. 78 (1) (2011) 151–157.
[31] D.M. Mudie, G.L. Amidon, G.E. Amidon, Physiological parameters for oral delivery and in vitro testing, Mol. Pharm. 7 (5) (2010) 1388–1405.
[32] J.R. Miranda, et al., AC biosusceptometry technique to evaluate the gastrointestinal transit of pellets under influence of prandial state, J. Pharm. Sci. 99 (1) (2010) 317–324.
[33] L.A. Cora, et al., Pharmaceutical applications of AC biosusceptometry, Eur. J. Pharm. Biopharm. 74 (1) (2010) 67–77.
[34] L.A. Cora, et al., Magnetic images of the disintegration process of tablets in the human stomach by ac biosusceptometry, Phys. Med. Biol. 50 (23) (2005) 5523–5534.
[35] Y.M. EL-Sayed, et al., A rapid and sensitive high-performance liquid chromatographic method for the determination of diclofenac sodium in serum and its use in pharmacokinetic studies, J. Pharm. Pharmacol. 40 (10) (1988) 727–729.
[36] F.J. Varum, et al., A novel coating concept for ileo-colonic drug targeting: proof of concept in humans using scintigraphy, Eur. J. Pharm. Biopharm. 84 (3) (2013) 573–577.
[37] P. Schick, et al., Application of the GastroDuo to study the interplay of drug release and gastric emptying in case of immediate release Aspirin formulations, Eur. J. Pharm. Biopharm. 151 (2020) 9–17.
[38] T. Felicijan, et al., The influence of simulated fasted gastrointestinal pH profiles on diclofenac sodium dissolution in a glass-bead flow-through system, AAPS PharmSciTech 19 (7) (2018) 2875–2884.
[39] M. Koziolek, E. Kostewicz, M. Vertzoni, Physiological considerations and in vitro strategies for evaluating the influence of food on drug release from extended-release formulations, AAPS PharmSciTech 19 (7) (2018) 2885–2897.
[40] A. Foppoli, et al., In vitro and human pharmacoscintigraphic evaluation of an oral 5-ASA delivery system for colonic release, Int. J. Pharm. 572 (2019) 118723.
[41] P. Moayyedi, et al., ACG and CAG clinical guideline: management of dyspepsia, Am. J. Gastroenterol. 112 (7) (2017) 988–1013.
[42] L.A. Cora, et al., Disintegration of magnetic tablets in human stomach evaluated by alternate current biosusceptometry, Eur. J. Pharm. Biopharm. 56 (3) (2003) 413–420.